PN-ACP-985

FINAL REPORT

Covering Period: 1.01.1997 - 31.12.2001

Submitted to the Office Agriculture & Food Security
U.S. Agency for International Development

Protection of land and settlements in arid regions from contamination by atmospheric deposition

Principal Investigator: Arieh Singer

Co-Investigators: Yitzhak Mahrer and Amos Banin

Grantee Institution: The Hebrew University of Jerusalem

Collaborators: Dr. L. Poberezsky

Institution: Scientific Research Association
"Waterproject", Victor Malaysov Str. 3
Tashkent 7000, Uzbekistan

Project Number:

Grant Number: **TA-MOV-96-CA16-013**

Grant Project Officer: Mr. David Mulenex
Science Attache, U.S. Embassy
Tel-Aviv, Israel.

Project Duration: January 1, 1997 - December 31, 2001

A

Table of Contents

	Page
Cover Sheet	
Table of Contents	
Executive Summary	1
Research Objectives	4
Methods and Results	
Ground Date by GIS	5
Data Collection	5
Figs. 1-5	6
Tables 1-3	11
GIS map representations	16
Figs. 6-12	23
Meteorological model for dust transfer	35
Figs. 13-21	38
Dust propagation following desiccation:	
Conference presentation	46
Wind erosion potential of the Southern Aral Sea Basin (SASB) soils and sediments	58
General	58
Results	64
Sampling sites	66
Soil crusts in the Amu Darya River Delta: Publication	69
Tables and Figures	81
The Dust Generation Potential of Soils/Sediments: Publication	107
Impact Relevance and Technology Transfer	149

EXECUTIVE SUMMARY

In the first project year (1997) the assemblage, preparation (translation) of various cartographic data and the process of creating a database for GIS were carried out. The Raster Data Model was used for a representative section, covering 44x20 km of the Amu Darya delta basin, with a spatial resolution of 1 km. For this demonstration section, topographic data, soil type and soil use data were used, accompanied by hydrography. From this representation, it can be seen that on a rather level topography, hydromorphic soils, used mainly for pasture, dominate the area. A sizable portion is also taken up by uncultivated areas.

The first project year also dealt with a 3-dimensional atmospheric dust transport model. The model simulates all the major phases of the atmospheric dust life cycle: source and sink processes, vertical turbulent mixing, etc. A preliminary model simulation was performed for the Lake Aral area during the period June 12-16, 1995. During this period, with strong easterly winds, a dust plume was seen to be initiated, to grow, and to be advected west towards the Caspian Sea. This simulation demonstrated the capability of the model to describe and possibly predict dust transport phenomena in the Aral Sea area. This capability will be conducive towards quantifying the process and thus advancing ameliorative measures in the Aral Sea and similar areas.

During the second project year (1998), the cartographic information collected on the Amu Darya delta was transferred into a database for GIS. The database was expanded from the original demonstration section of 44x20 km to the whole of the delta, from the southern Aral Sea shore to south of the city of Nukus.

The work on the 3-dimensional atmospheric dust transport model that was commenced during 1997, was carried on. The model simulates all major phases of an atmospheric dust life cycle: source and sink processes, vertical turbulent mixing, lateral diffusion and horizontal and vertical advection. The numerical simulations were performed for three scenarios: 1. No artificial water bodies; 2. Big artificial water bodies placed in the area; 3. Small artificial water bodies placed in the area. The purpose of these simulations was to examine the ameliorative effect of artificial water bodies on the propagation of dust. The simulations were performed for two storms from 1991 and 1993, and for dust particles the size of 2.5 μm and 15 μm. The major conclusion of these simulations was that only big artificial water bodies reduce the size of the dust cloud.

Also during 1998, an inspection and sampling tour of the Amu Darya delta was carried out. Eight soil samples were brought back to Israel for analysis and examination of deflatability. Results of the analysis showed the soils to be composed mainly of quartzic fine sand. The salt crusts consisted mainly of chlorides and sulfates of sodium and magnesium.

During the third project year (1999), the GIS database, containing information on land use and management, salinity, texture and hydromorphism of the Amu Darya River delta, were used to create superpositions for the purpose of analysis and interpretation of the data. Detailed analysis was carried out for two strategic areas, Chimbay and Kungrad, where urban and industrial development is planned. This work was carried out using the PC that was purchased for the Uzbek partners in 1998.

Using updated data on the wind activity in the Aral Sea region, the Uzbek partners analyzed the wind regime characteristics in the Aral Sea region. This analysis was important for the deflatability studies to be carried out in the wind tunnel in Israel. Also in preparation for these studies, the Uzbek partners prepared an assessment of the soil surfaces that may serve as sources for dust entrainment. In this study, the changes in the moisture regime of Solonchak and Hydromorphic soils throughout the year were detailed. As a result of these studies, recommendations for the management of these lands were formulated.

Prof. Y. Mahrer participated in an international workshop on "Mineral Dust" held in Boulder, Colorado, in June 1999, and presented there a paper on the application of a three-dimensional numerical model to dust generation and transport in the Aral Sea region. Prof. Singer participated in an international workshop on "Desert Ecosystems", held in Germany in May 1999. He presented there a paper on crust formation in the Aral region soils. Contacts with other research groups were established.

The equipment required for the wind tunnel tests to be carried out on soils from the Amu Darya River delta was purchased. Preliminary tests on model soils were carried out.

During the fourth project year (2000), the emphasis was on the determination of the deflatability of the soils and on the ameliorating effect of treatments on the deflatability. The principal soil and wind erosion parameters were determined. Friction velocity and threshold wind velocity determinations were carried out in an open circuit wind tunnel of the suction type. Friction velocities were in the range normal for fine sandy soils. The relatively highest threshold wind velocity was determined for the salt crust of soil No. 1. This indicates that salt crusts are relatively more stable towards wind erosion, i.e. that stronger winds are required to deflate these soils. The most important finding in these experiments was that even low moisture contents (below field capacity) dramatically increase threshold wind velocity, implying that by keeping the surface soil moist, wind erosion can almost completely be avoided. Also soil crusts significantly reduce deflatability. An artificially simulated Takyr soil crust very strongly increased threshold wind velocity.

In a different aspect of studies, soil characteristics that could be used for a prediction of their wind erodibility, were examined. The soil size fraction of <850 eq. diameter is considered as a

measure of the potential for wind erosion. The conclusion of this determination was that all soils examined have a very high potential for wind erosion. Again, the least endangered are soils with a salt crust. An additional characteristic determined was PM 10, i.e. the proportion of particles equal to and smaller than 10 μm, generated by a simulation of a dust storm. This determination, carried out by Dr. T. Zobeck from the USDA in Lubbock, Texas, indicated that the Takyr soil, once the crust was fragmented and shattered, had the highest potential for suspended dust generation.

Research Objectives

The Aral Sea desiccation crisis is an ecological disaster of gigantic proportions. Ultimately, it is severely affecting the health of a population of 3.5 million people. Triggered by the desiccation of the Aral Sea, it has caused the pollution of the atmosphere by immense quantities of contaminated dust. Inhalation of this dust endangers the health of the people. Deposition of this dust salinizes and contaminates water bodies and soils over huge areas. Due to its dimensions, the problem has received wide publicity and been described in detail in both scientific and popular literature, including the internet.

Large efforts are under way to counteract these problems. Some of these efforts are described in: S. Breckle, M.Veste and W. Wucherer (eds.) 2001, Sustainable Land Use in Deserts, Springer. 463 pp.

Considering dust generation as the principal phenomenon setting the chain of processes in motion that are responsible for the disastrous ecological effects, the objectives of the project were to seek ways to reduce the problem, and also to transfer the required technologies to the project partners from Central Asia.

(a) To collect the data essential for an assessment of the phenomenon of atmospheric dust transfer and deposition in the Aral Sea area, and analyze the data using the GIS system.

(b) To assess the rate of mineral (aluminosilicates, soluble salts) matter deflation and deposition taking place in the specified area.

(c) To devise a meteorological model that would describe, quantify, and predict the processes of dust transport and deposition. To establish a salt balance for the region.

(d) To examine methods for the reduction of soil deflation and dust generation by soil surface stabilization, using treatments with soil stabilizers.

(e) To provide recommendations for the establishment of measures aimed at containing the process of dust transfer, propagation and deposition. More specifically: (a) To provide recommendations related to plans for the construction of artificial water bodies/reservoirs, and predict their eventual effects on the process of dust transfer/deposition, using a numerical model; (b) To assess the effect of soil-surface stabilization on regional dust transfer.

METHODS AND RESULTS

Ground data by GIS

Data collection for GIS processing

The purpose of that material was to provide input data for GIS. All that material was cartographic, in the form of various maps.

Twenty-eight maps were obtained: 6 topographic maps at a scale of 1:1,000,000; 9 topographic maps at a scale of 1:500,000. These maps covered a large area south and east of the Aral Sea.

For a much smaller area, including essentially the Amu Darya delta basin and its periphery, 4 soil maps were used, at scales of 1:1,000,000 and 1:200,000, and nine land use maps, at scales of 1:200,000 and 1:500,000. The legends of all these maps were in Russian and had to be translated.

Great difficulties were encountered with the translation of the soil terminology into English. This terminology was according to the Russian taxonomic system, which is very different from the new USDA soil classification system. The USDA equivalents for the Russian soil terms had to be laboriously interpreted, and some of these translations were only finalized after on-site examinations.

The 72 soil types that were marked on the 1:200,000 soil maps were integrated into 35 soil associations (Table 1). Each soil association includes related soil types. The association characteristics follow the characteristics of the dominant (by areal extent) soil type in the association. The legend of the 1:1,000,000 soil map of Karakalpakia contains 25 soil types (Table 2).

Similar difficulties were encountered with the translation of the land use terminology. Until inspection on-site, some of the usages remained vague.

Thirty land use classes were originally noted (Table 3). The 30 land use classes were grouped too into associations. The land use maps included also valuable hydrographic information (Table 3).

The data-bases pertaining to the Southern Aral Sea Basin (SASB) and collected during the first study year are given in Tables 1-3 and Figs. 1-5.

The raw cartographic data were obtained from Soviet era maps and literature, and processed by GIS, using the Raster Data Model .

Fig. 1 gives the topography of the Aral Sea area.

Fig. 2 gives the Soil Map of the Aral Sea area.

Fig.3 gives the topography of the representative area.

Fig. 4 gives the Soil Map of the representative area.

TOPOGRPHY OF ARAL SIMULATION AREA

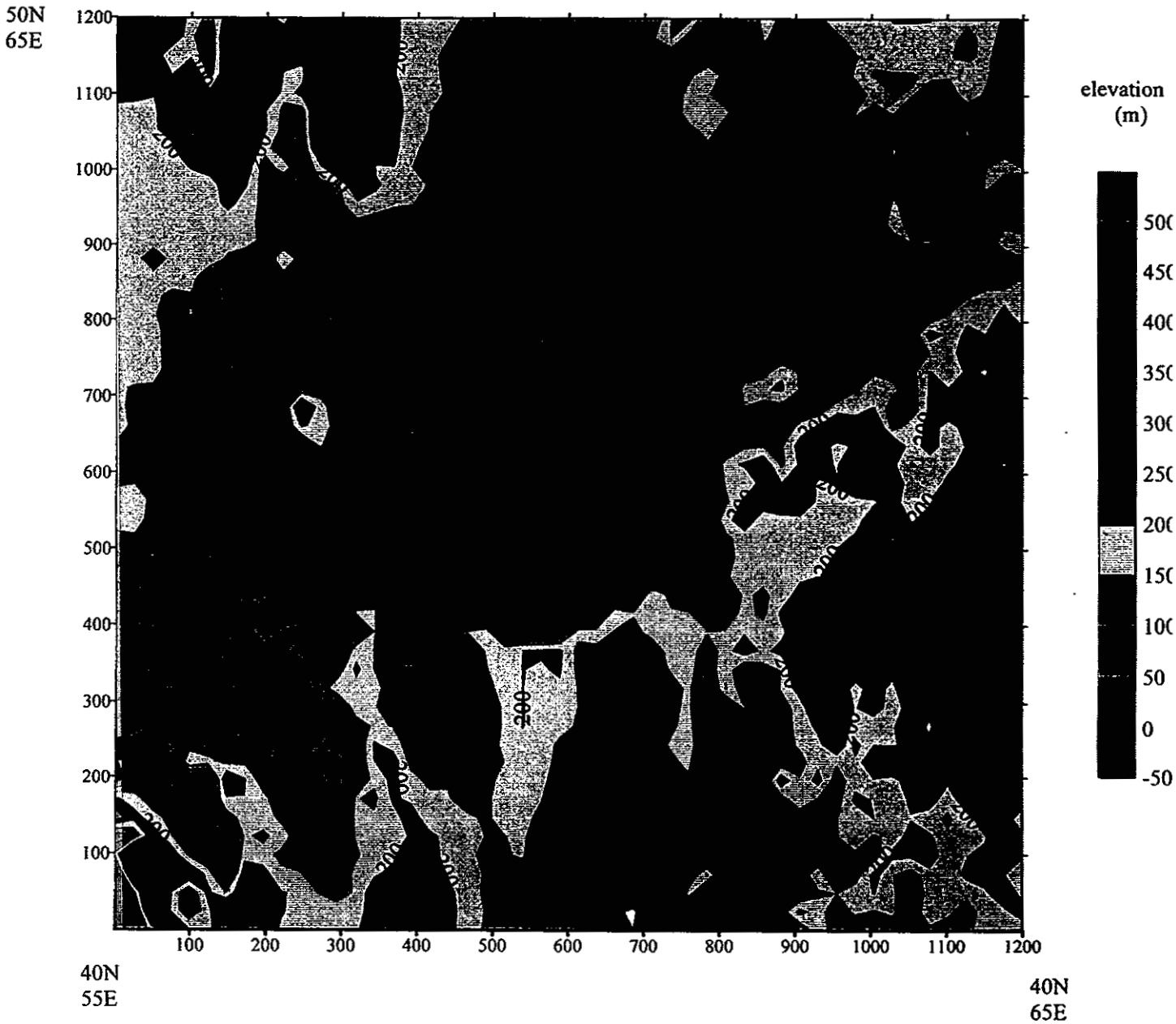

Fig. 1

SOIL MAP OF ARAL SIMULATION AREA
according to Zobler classification

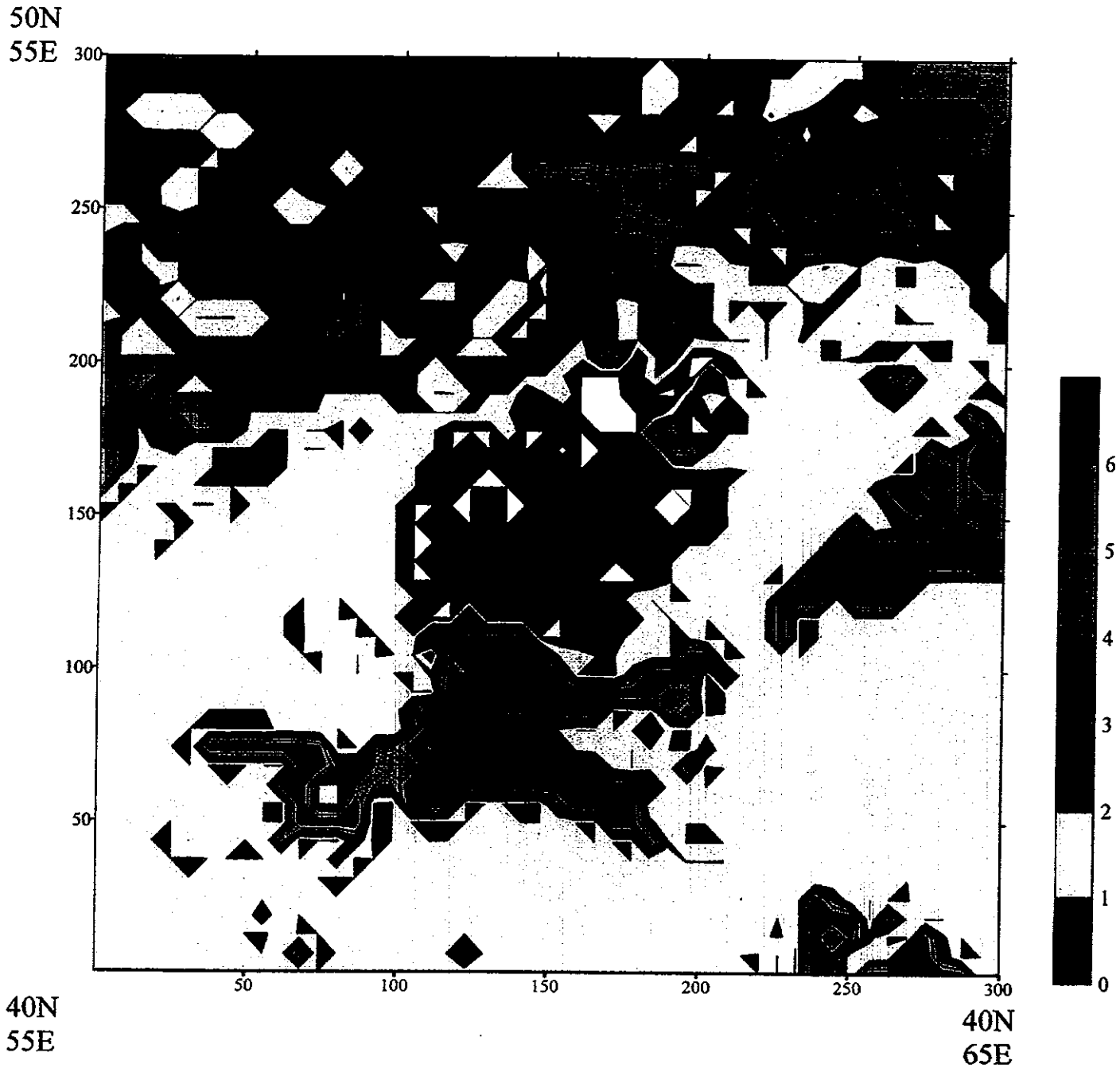

ZOBLER textural classes.

Type	Soil texture
1	Coarse
2	Medium
3	Fine
4	Coarse-medium
5	Coarse-fine
6	Medium-fine
7	Coarse-medium-fine

Fig. 2

Topography of Aral Research Area

Fig. 3

8

Fig. 4

Soil Maps of Aral Research Area

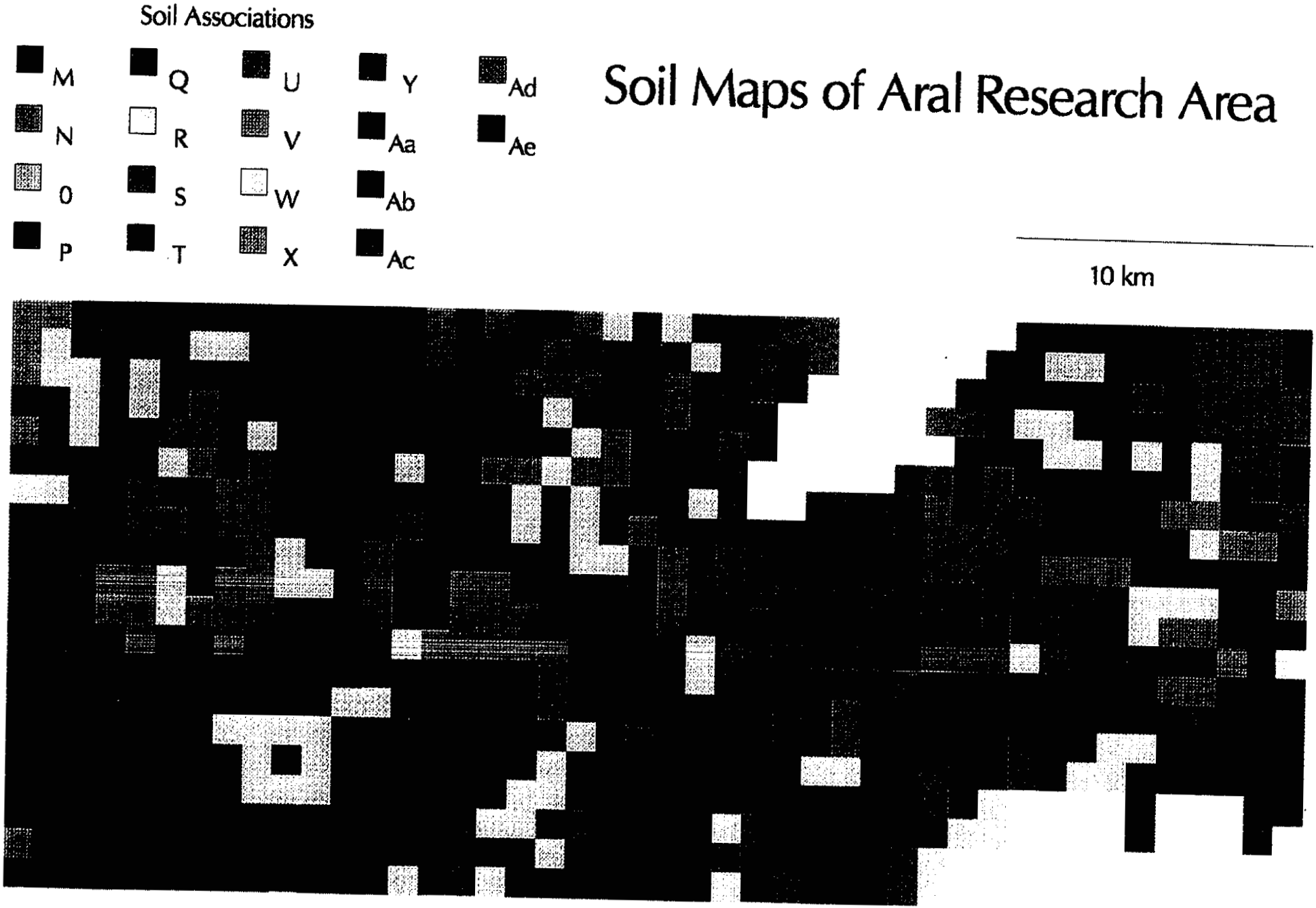

Land Use Map of Aral Research Area

Land Use Units

- *drainage area*
- *forest*
- *gravelly area*
- *grazing*
- *lake*
- *orchard*
- *urban*
- *uncultivated*

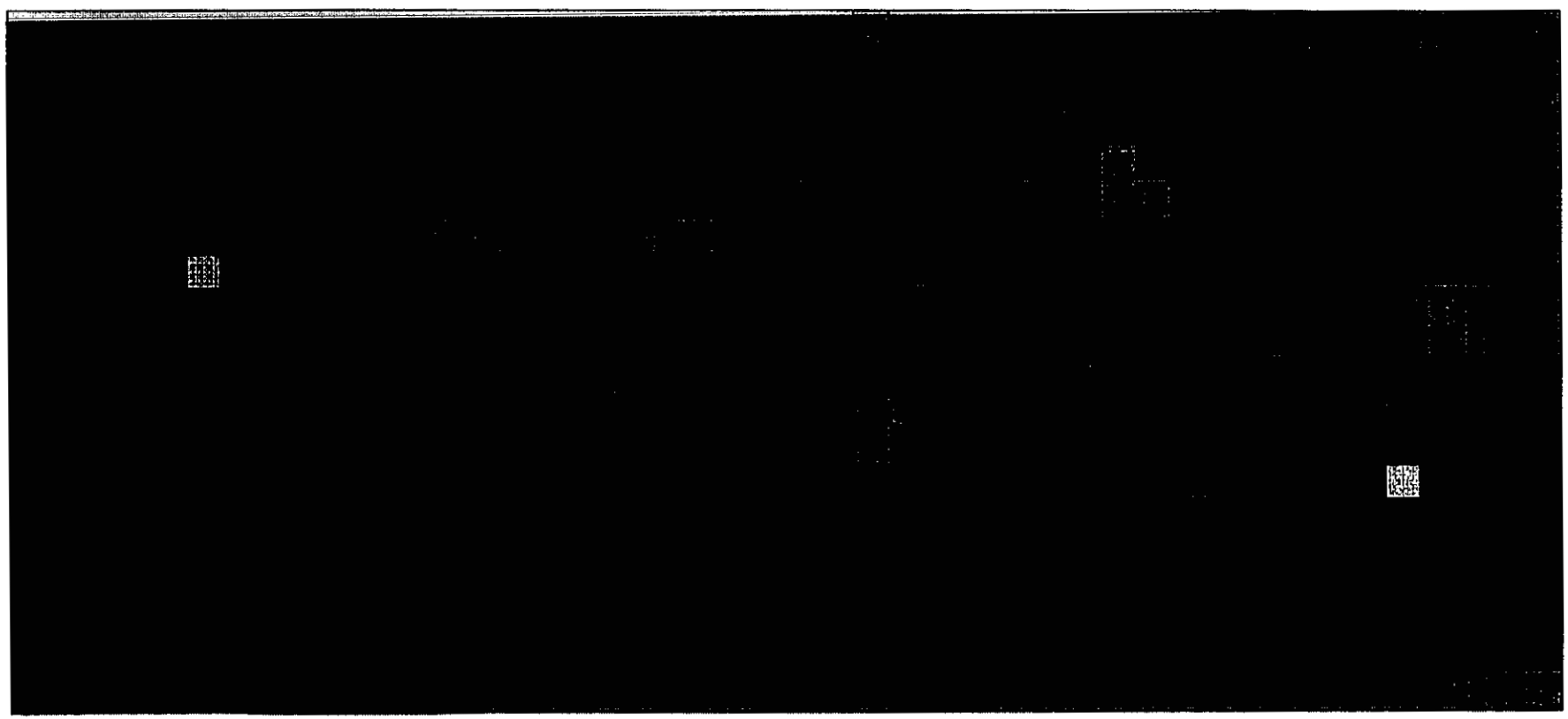

N 42 56
E 59 47

4 km

Fig. 10

Table 1. CONDENSED SOIL MAP LEGEND (soil associations)

1:200,000

(* - more than 5,000 ha; ** - more than 10,000 ha; *** - more than 20,000 ha; **** - more than 40,000 ha).

Ancient Amu Darai delta

A 1,2 - Takyr, hydromorphic, slightly saline, heavy to light clay, newly irrigated.

B 3 - Takyr, hydromorphic, solonchaks, heavy clays.

C 4*,5***,6** - Hydromorphic soils, long time irrigation, slightly saline, heavy to light clays.

D 7,8 - Hydromorphic soils , slightly saline, clay.

E 9,10 - Hydromorphic soils, slightly saline, clay, newly irrigated.

F 11,12 - Hydromorphic soils, moderately saline, heavy clay, newly irrigated.

G 13,14 - Hydromorphic soils, moderately to strongly saline, light clay-sand, non-cultivated.

H 15* - Hydromorphic soils, with moderate to heavy solonchak, clay.

I 16** - Hydromorphic soils, with moderate to heavy solonchak, light clay.

J 17* - Hydromorphic, Tagai soils, light solonchak, heavy clay.

K 18,19 - Boggy hydromorphic soils, moderately saline, heavy clay, non-cultivated.

K_1 20 - Boggy hydromorphic soils, moderate to heavy solonchak, clay and sand.

Modern Amu Darai delta

L 21*,22,23 - Takyr soils, slight to moderately saline, moderately to heavy clay, newly irrigated.

M 24**,25** - Takyr soils, light solonchaks, light to moderate clay.

N 26***, 27**, 28** - Takyr soils, moderate to heavy solonchaks, heavy to light clay.

O 29,30,31 - Takyr soils, with bog remnants, light solonchak, light to moderate clay.

P_1 32,33 - Sandy desert soils with solonchaks, pasture lands.

P_2 34, 35 - Residual solonchaks, moderate to heavy clay.

Q 36* - Desert soils, hydromorphic soils, with some moderate solonchaks, moderate to heavy clay, some cultivated soils.

R 37 - Takyr, hydromorphic soils, slightly saline, moderate clay and sands, newly irrigated, moderately cultivated.

S 38,39 - Takyr, hydromorphic soils, moderate saline, light clay and sand to heavy clay, newly irrigated, slightly cultivated.

T 40*,41**,42,43*,44*,45* - Takyr, hydromorphic soils, moderately to heavy solonchak, moderately clay to sand, newly irrigated.

U 46*,47*,48****,49*** - Takyr, hydromorphic soils, moderate to heavy solonchaks, moderate to heavy clay (with some sand, interlayered?).

V 50,51,52,53 - Hydromorphic soils, lightly saline, moderate clay with sands (interlayered), ancient irrigation, moderately cultivated.

W 54**,55***,56** - Hydromorphic soils, lightly saline, moderately clay with some sand layers, newly irrigated, moderately cultivated.

X 57,58***,59* - Hydromorphic soils, moderately to strongly saline, heavy clay with some sand layers, newly irrigated, slightly cultivated.

Y 60 - Hydromorphic soils, very saline, light clay with sand, newly irrigated, lightly cultivated.

Z 61* - Hydromorphic soils, slightly to moderately saline, light clay, lightly cultivated.

A_a 62**,63** - Hydromorphic soils, with light solonchaks, moderate to heavy clay with some sand layers.

A_b 64****,65**,66***,67 - Hydromorphic soils, strong solonchaks, heavy clay - to light clay with sand (66).

A_c 68 - Typical solonchaks, light clay to sand.

A_d 69*,70****,71****,72* - Hydromorphic soils, solonchak, light clay (with sand) to heavy clay.

A_e 73*** - Sands.

A_f 74* - Not suitable soils.

A_g 75*** - Water surfaces and sands.

Table 2. SOIL TYPES INVENTORY IN THE KARAKALPAKIA AREA

(1:1,000,000)

Amu Darai Delta Plain - alluvial deposits	Area (ha)
1. Clay takyr soils on alluvium	123,625
2. Solonchak clay takyr soils on alluvium	46,700
3. Solonchak clay takyr soils on alluvium and proluvium	385,825
4. Takyr solonchak clay and loam on alluvium	106,525
5. Takyr light solonchak clay and loam on alluvium	62,000
6. Alluvial light solonchak clay soils on deposits	41,775
7. Bog alluvial clay and loam soils, both non-saline and solonchak (leached in springtime by the river) on deposits	671,743
Hilly area on eroded Tertiary rocks	
8. Loamy and sandy gray-brown light solonchak soils on gravelly light clay deposits	139,900
9. Loamy and light clay gray-brown solonetz and light solonchaks together with desert sands	116,250
Tertiary and early Quaternary rocks	
10. Gravelly clay, gray-brown, saline, gypsiferous, on carbonate rocks	130,000
11. Gravelly clay, gray-brown, light solonchaks, gypsiferous, on carbonate rocks	33,000
12. Gravelly clay, gray-brown, light solonchaks, with a solonetz crust, on carbonate rocks	1,852,000
13. Gravelly clay, gray-brown soils with carbonate rocks and marly deposits	573,000
14. Gravelly clay, gray-brown, light solonchaks, on carbonate rocks and marly deposits	825,000
15. Gravelly clay, gray-brown, light solonetz on proluvial and deluvial carbonate rocks	1,941,000

16. Loamy and sandy, gravelly gray-brown light solonetz and light solonchak soils on carbonate and sandy and diverse other rocks	50,000
17. Gravelly clay, gray-brown, light solonetz soils with a solonetz crust on carbonate rocks	210,000
18. Gravelly clay, gray-brown, light solonchaks on carbonate rocks	320,000
19. Clay takyr soils, light solonetz, on alluvial and deluvial deposits	375,000
20. Gravelly loam, gray-brown soils, on carbonate, marl and sandy rocks	684,000
21. Clay soils, lightly solonetz and lightly solonchak, on carbonate marl and sandy rocks	9,000
Hilly area with crystalline (granite) and carbonate rocks	
22. Gray-brown, stony soils, eroded	59,014
Dispersed, in all areas	
23. Typical solonchaks	114,925
24. Solonchaks on eroded material of saline rocks	310,000
25. Orange-colored sand	3,481,959

Glossary

Takyr: Soils of the desert zone, distinguished by their hard, polygonally-cracked surface; with a light gray, highly-porous crusted horizon 2-8 cm; very hard when dry, and compact and sticky when wet; with deep cracks; dried algal coating impart pink color to surface; occasionally peels off and rolls up like paper; 30-40 cm deep; $CaCO_3$ - 4-9%; slightly solonchakic; typical of flat, shallow depressions, devoid of plants.

Hydromorphic soils: "Meadow soils" in the original: soils of the steppe zone formed as a result of sod-forming and gley processes under conditions of increased flooding by surface water linked permanently to subsoil and ground water.

Solonetz: Soils which have in the humus-enriched horizon such quantities of exchangeable Na (in the absence of soluble salts) that specific properties develop: alkaline reaction, formation of Na_2CO_3, solubilization of organic matter, high dispersion (from: Classification and Diagnostics of Soils of the USSR).

Solonchak: Salt soils.

Tagai: Aboreal thicket in river valleys (from Rozanov, 1961).

Table 3. LAND USE AND HYDROGRAPHY LEGENDS

Amu Darai River Delta

(1:500,000)

Cultivated area

Rice field

Fallow after irrigation

Fallow with irrigation installations

Pasture

Pastures on sands, with natural vegetation of grasses

Pastures with vegetation of shrubs and papyrus

Pastures with bogs

Pastures with thorny shrubs

Pastures with woody patches and shrubs

Irrigated and cultivated pastures

Pastures on stony terrains with natural vegetation of grasses

Soil with basic drainage installations

Afforested areas

Fruit trees

Vineyards

Mulberry trees

Shrubs

Accessible solonchaks

Non-accessible solonchaks

Bogs with papyrus

Papyrus

Pasture for silage

Thorny shrubs

Sands

Sands with natural grass vegetation

Terrains with clay and gravel

Cemetries

Takyrs

Uncultivated soil

Hydrography

Rivers, dry creeks

Lakes

Seasonal (ephemeral) lakes

Irrigation installation

Drainage and sewage installation

Wells, including artesian wells

Water

Springs

Water storage

Water pumping stations

Water holes

Underground water pipes

Fig. 5 gives the Land Use Map of the Aral Sea area.

Table 1. Condensed soil map legend (soil associations) 1:200,000.

Table 2. Soil types inventory in the Karalkapakia area 1:1,000,000.

Table 3. Land use and hydrography legends 1:500,000.

GIS map representation

The Raster Data Model was used for a representative section of the Amu Darya delta basin. This section extends over an area of 44 x 20 km, with a spatial resolution of 1 km (Fig. 1). The lower left corner of this area is at 42°56'N and 59°47'E. It straddles a portion of the right-hand side of the delta, from west to east. It was selected because of its relative proximity to the southern, dried-out portions of the Aral Sea, and because it represents a cross-section of land surfaces from very close to the present river channel, to the more remote areas in the east.

The physiography is that of a river flood area. Relief is very low, and elevations are in the range of 28-67m (Fig. 1). Data for the topographic map were taken from Global 30 arc Second Elevation Data Set of the U.S. Geological Survey's EROS Data Center. For the soil types representation, the legend appearing in Table 1 was used. Out of the associations that appear in this legend, 18 are represented in this section (Fig. 2). From this representation, it can be seen that hydromorphic soils, of various types, dominate the section. The land use exhibits much less variety (Fig. 3, Table 3). Pastures of various kinds dominate the section. A sizable portion is also taken up by uncultivated areas. The hydrography of this section, that was processed by the Vector Model (the Raster Model could not be applied in this case), demonstrates the dense irrigation network (Fig. 4).

Based on the GIS cartographic data including soil types, salinities, textures, hydromorphism, land management and land use, super-positions of the respective layers were created, yielding important results, presented below in tables 1-9.

Table 4 gives the areas of 5 soil type groups, as obtained from the Amu Darya delta soil map. The 25 soil types were condensed into 5 principal groups: hydromorphic soils, takyrs, solonchaks, sands, and gray soils. There is a certain overlap between hydromorphic soils and solonchaks.

Table 4. Areas of the principal soil type groups in the Amu Darya river delta.

Soil type group	Area (polygons)	Units (m^2)
Hydromorphic soils	1206	5.18×10^9
Takyrs	477	2.61×10^9
Sands	149	5.47×10^8
Solonchaks	50	1.85×10^8
Gray soils	23	0.85×10^8
Other areas	262	1.13×10^8

This table indicates that about 2/3 of the soils are affected by hydromorphism, i.e. Are not drained; most of these soils are also saline: another large group are the takyrs, that exhibit surface crusting, but are only mildly saline. Solonchak soils, as well as some of the hydromorphic soils, exhibit salt crusting.

Table 5 grades the major soil type groups according to their salinity status. Five salinity grades were defined: 0 – very low salinity; 1 – lightly saline (<0.2%); 2 – moderately saline (0.2-0.5%); 3 – strongly saline (0.5-2%); 4 – very strongly saline (>2%); data for soil salinity were taken from existing Uzbek literature.

Table 5. Soil types of the Amu Darya river delta and their average salinities. GIS super-position of soil salinity over soil type.

Soil type	Extent (polygons)	Ave. Salinity	Min. Salinity	Max. Salinity
Takyrs	10	2.1	1	3
Solonchaks	3	3	3	3
Hydromorphic Soils	17	2.3	1	4
Gray soils	2	2.5	2	3
Sands	1	0	0	0
Unmapped	2	0	0	0

This table indicates that only sands are not afflicted by salinity. The highest salinity is exhibited by some hydromorphic soils. These would probably qualify for the definition of

solonchaks. Other hydromorphic soils are only slightly saline. The most consistently saline soils are the solonchaks. Takyrs and gray soils are only mildly saline.

Table 6 examines the relation between the texture of soils and their salinity status. Soil texture was defined in grades between sandy and heavy clay. No equivalent of loamy texture (in the usda) was found in the russian classification. Mixed textures are soils where sandy material is interlayered in clay-rich soils.

Table 6. Soil texture of the Amu Darya river delta soils and their salinity state. GIS super-position of salinity state over soil texture.

Soil texture	Extent (polygons)	Ave. Salinity	Min. Salinity	Max. Salinity
No defined Texture	2	0	0	0
Sandy	2	1	0	2
Light clay	10	2	1	4
Moderate clay	8	2	1	3
Heavy clay	8	2.9	1	4
Mixed clay	5	2.6	2	3

Table 6 indicates that light clay soils (probably equivalent to loam or silty loam in the usda) dominate. The extent of sandy soils is very limited. Only sandy soils are not saline or slightly saline. The heavy soils are the most saline. The soils with mixed texture are quite saline too.

In table 7, the hydromorphism of the soils in the Amu Darya river delta is superposed on their texture. The hydromorphism is expressed in three grades: 0 – no hydromorphism; 1 – mild hydromorphism; 2 – strong hydromorphism. In grade 2, the soils are water-saturated most of the year, in grade 1, only part of the year.

Table 7. Soil texture of the Amu Darya river delta and their hydromorphic state. GIS superposition of hydromorphic state over soil texture.

Soil texture	Extent (polygons)	Ave. Hydromorphism	Min. Hydromorphism	Max. Hydromorphism
No	2	0.5	0	1
Sandy	2	0	0	0
Light clay	10	1.3	0	2
Moderate clay	8	1	0	2
Heavy clay	8	1.7	1	2
Mixed clay	5	1.6	0	2

Table 7 shows that in sandy soils, hydromorphism does not occur. Hydromorphism is strongest in the heavy clay soils. Also, soils with "mixed" texture are strongly affected by hydromorphism. These relationships are as expected.

In table 8, the relationship between salinity of soils and their hydromorphic state are represented. Non-saline soils are only slightly hydromorphic. The most saline soils are those with the strongest hydromorphism. This suggests that salinity is strongly associated with water, either rising groundwater or irrigation water. It is also noteworthy that some mildly or even strongly saline soils are not hydromorphous.

Table 8. Saline soils of the Amu Darya river delta and their hydromorphism. GIS superposition of hydromorphic state over soil salinity.

Soil salinity	Extent (polygons)	Ave. Hydromorphism	Min. Hydromorphism	Max. Hydromorphism
0	3	0.3	0	1
1	7	1.4	0	2
2	10	1.1	0	2
3	13	1.4	0	2
4	2	2	2	2

In table 9, the major land-use types in the Amu Darya river delta are shown, with the salinities of the associated soils. The area covered by these types is much larger than the area of the

soil types, since the land use maps were more extensive. Only principal land-use types are indicated.

Table 9. Land use types in the Amu Darya river delta and the salinities of the respective soils. GIS superposition of soil salinity over land use.

Land use	Extent (polygons)	Ave. Salinity	Min. Salinity	Max. Salinity
Cultivated land	9	2.62	2	3
Pasture (natural)	3285	2.30	0	4
Horticulture	224	2.22	0	4
Sands	2387	2.16	0	4
Irrigated fields	148	2.64	0	4
Fields with drainage	34	2.09	0	4
Planted forest trees	58	2.03	0	4
Semi-dry solonchaks	24	1.70	0	3
Rice fields	43	2.14	1	4
Cobbly terrain	29	2.10	0	3
Uncultivated land	363	1.82	0	4

Pasture (natural) takes up the largest area. While some of this pasture land is strongly saline, other lands are salt-free. Sands are also widespread, and are partly hydromorphic. It is remarkable that the land use defined as "cultivated" is, on the average, the most saline. The land use defined as "irrigated fields" probably is drained and is also quite saline. This suggests that cultivation in these environments inevitably leads to salinization.

Table 10 shows land management of Amu Darya river delta lands and the salinities of the respective lands. Land management refers to irrigation, history of irrigation and pasture. This table shows that all irrigated lands and all pasture lands are saline to some degree, while some non-irrigated lands are not saline. The pasture lands are moderately saline, while in the other land all salinity grades are represented.

Table 10. Land management of the Amu Darya river delta and the salinities of the respective lands. GIS superposition of soil salinity over land management.

Land management	Extent (polygons)	Average salinity	Minimum salinity	Maximum salinity
Non-irrigated	18/35	2.2	0	4
Recently irrigated	12/35	2	1	4
Longtime irrigated	4/35	2	1	3
Pasture	1/35	2	2	2

In Table 11, land management is shown as related to texture. This table indicates that while pasture land as a rule is sandy, the irrigated lands are clay textured. It can be deduced that sandy lands were deemed unsuitable for irrigated cultivation.

Table 11. Land management of the Amu Darya river delta and the textures of the respective lands. GIS superposition of land textures over land management.

Land management	Extent (polygons)	Common land texture	Range of land textures
No irrigation	18/35	Light clay	Sandy-heavy clay
Recent irrigation	12/35	Light clay	Light clay-heavy clay
Old irrigation	4/35	Moderate clay	Light clay-heavy clay
Pasture	1/35	Sandy	Sandy

Table 12 shows land management in the Amu Darya river delta related to hydromorphic state. Pasture land can be seen to be non-hydromorphic, as contrasted with irrigated land, part of which is affected by hydromorphism. Old irrigated land is invariably strongly hydromorphic, while newly-irrigated land is only partly hydromorphic.

Table 12. Land management of the Amu Darya river delta and its hydromorphic state. GIS superposition of hydromorphism over land use.

Land management	Extent (polygons)	Ave. Hydromorphism	Min. Hydromorphism	Max. Hydromorphism
No irrigation	18/35	1.05	0	2
Recently irrigated	12/35	1.42	0	2
Old irrigation	4/35	2	2	2
Pasture	1/35	0	0	0

Fig. 6 shows the desiccation sequence of the Aral Sea between 1957 and 1998.

For GIS representation, two key regions were selected, based on their importance as centers of urban and rural development, and also on the availability of data. The key areas are:

Fig. 7 (1) the area surrounding the town of Chimbay, in the east of the delta (a in fig. 2) and (2) the area surrounding the town of Kungrad, in the west of the delta (b in fig. 2). For the area surrounding the town of Muynak (e in fig. 2), not enough data was available.

Fig. 8(a) shows the salinity distribution in the Chimbay area.

Fig. 8(b) shows the salinity distribution in the Kungrad area.

Fig. 9(a) shows the soil texture distribution in the Chimbay area.

Fig. 9(b) shows the soil texture distribution in the Kungrad area.

Fig. 10(a) shows the soil type distribution in the Chimbay area.

Fig. 10(b) shows the soil type distribution in the Kungrad area.

Fig. 11(a) shows the hydromorphism distribution in the Chimbay area.

Fig. 11(b) shows the hydromorphism distribution in the Kungrad area.

Fig. 12(a) shows the land management type distribution in the Chimbay area.

Fig. 12(b) shows the land management type distribution in the Kungrad area.

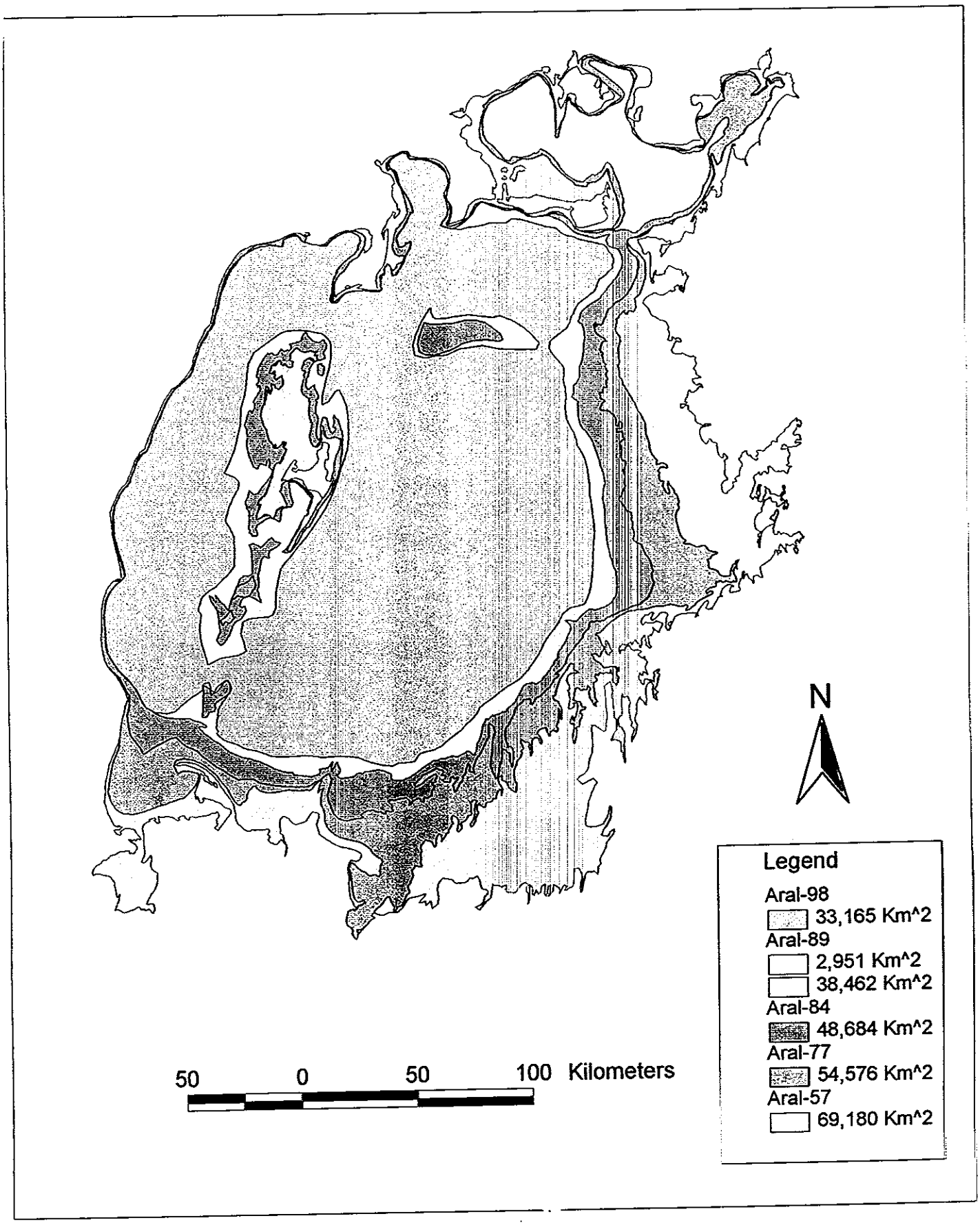
N
Legend
Aral-98
33,165 Km^2
Aral-89
2,951 Km^2
38,462 Km^2
Aral-84
48,684 Km^2
Aral-77
54,576 Km^2
Aral-57
69,180 Km^2
50 0 50 100 Kilometers

Fig. 6 -23-

Fig. 7

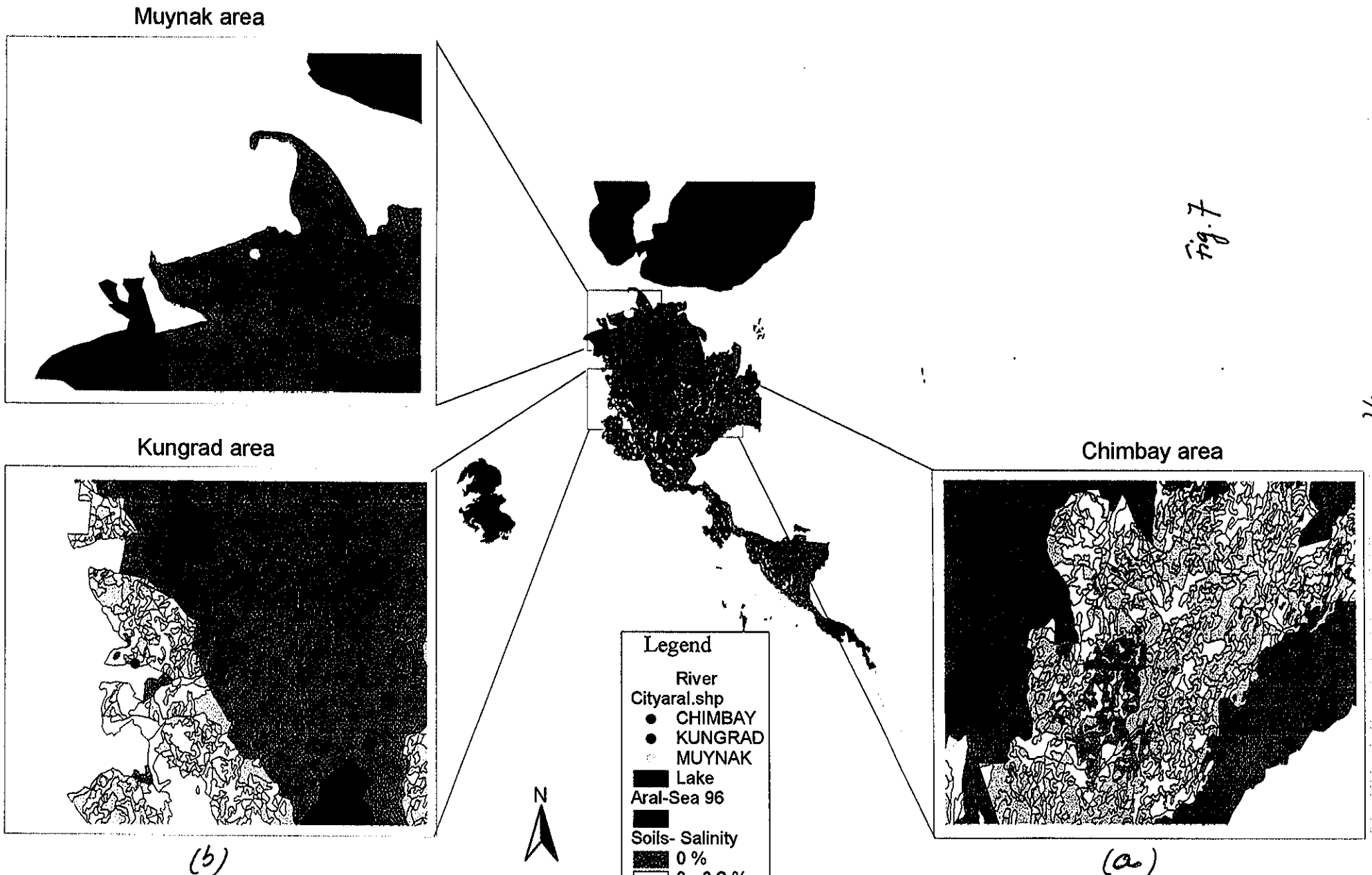
Muynak area
Kungrad area
Chimbay area
(b)
(a)
N
Legend
River
Cityaral.shp
CHIMBAY
KUNGRAD
MUYNAK
Lake
Aral-Sea 96
Soils- Salinity
0 %
0 - 0.2 %
0.2 - 0.5 %
0.5 - 2 %
> 2 %
Landuse2

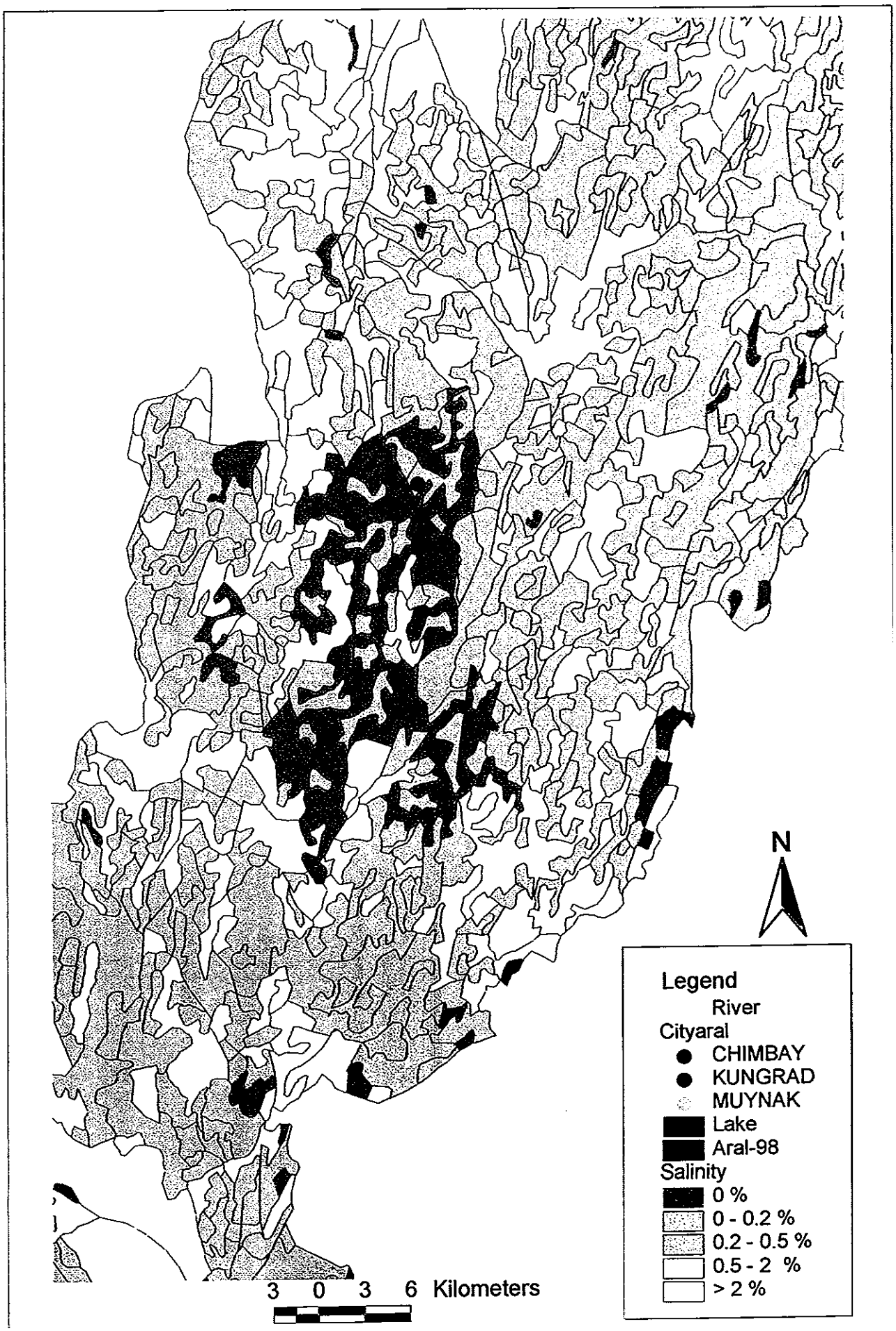
N
Legend
River
Cityaral
CHIMBAY
KUNGRAD
MUYNAK
Lake
Aral-98
Salinity
0 %
0 - 0.2 %
0.2 - 0.5 %
0.5 - 2 %
> 2 %
3 0 3 6 Kilometers

Fig. 8 (a) -25-

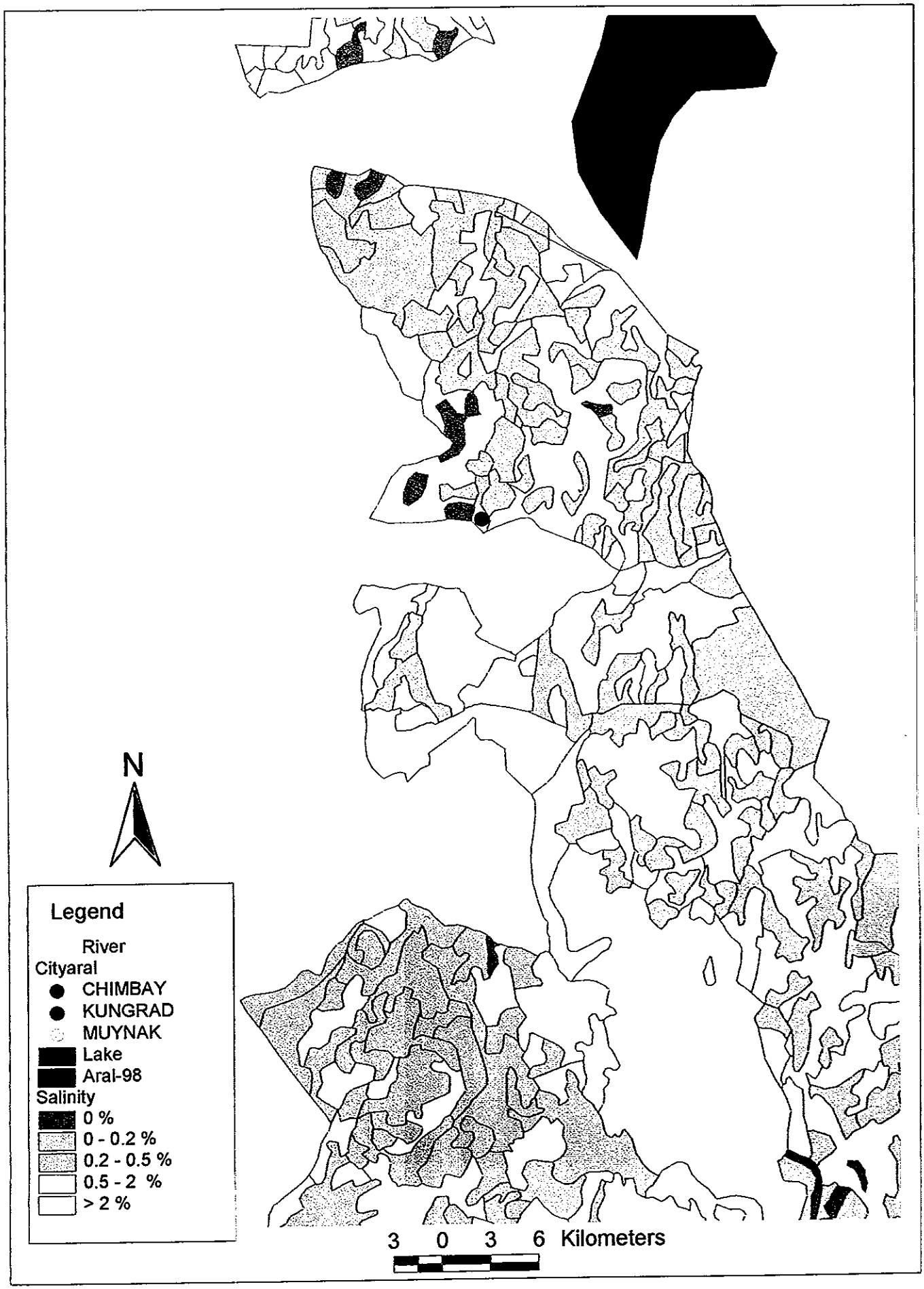
N
Legend
River
Cityaral
CHIMBAY
KUNGRAD
MUYNAK
Lake
Aral-98
Salinity
0 %
0 - 0.2 %
0.2 - 0.5 %
0.5 - 2 %
> 2 %
3 0 3 6 Kilometers

Fig. 8(b) -26-

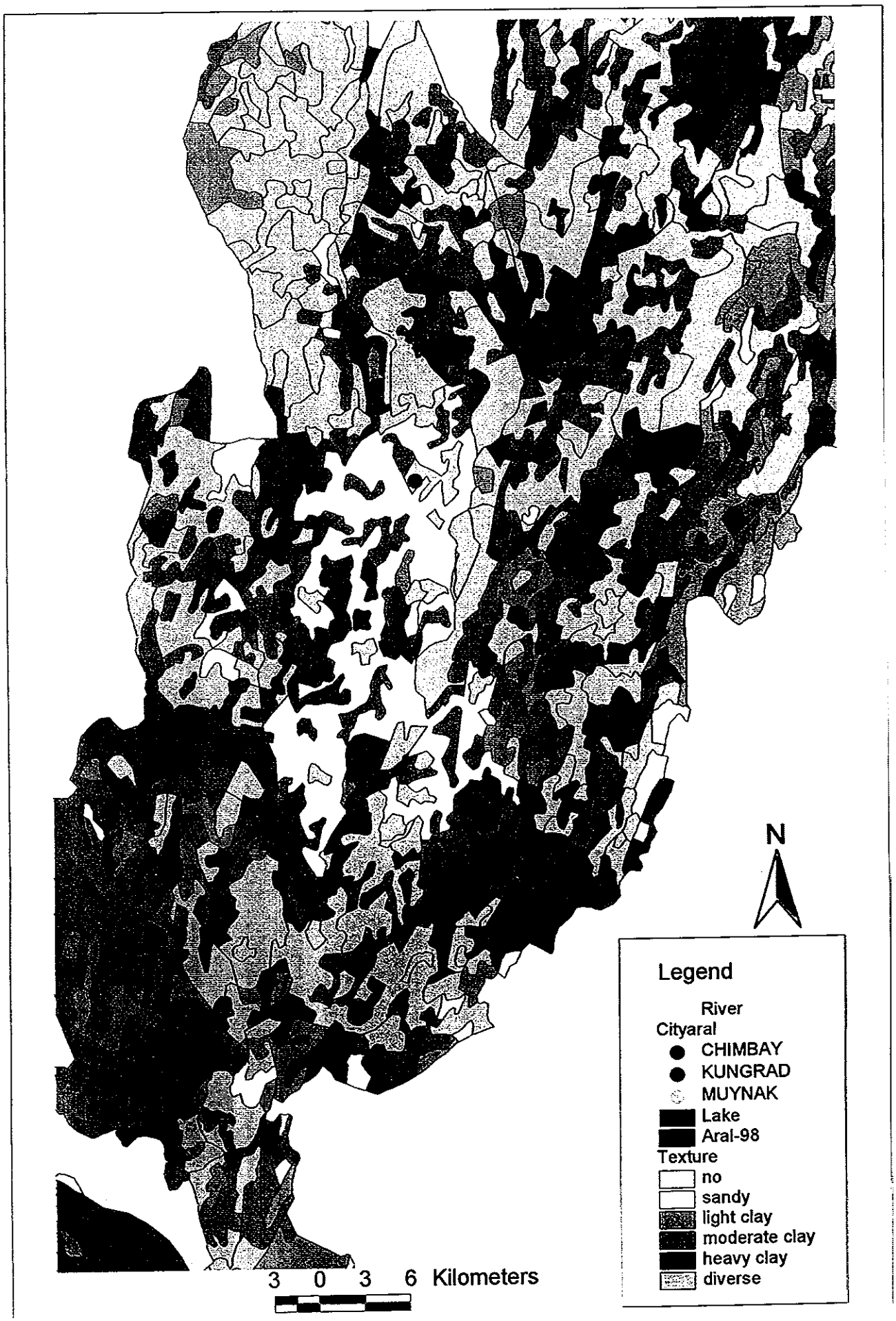
N
Legend
River
Cityaral
CHIMBAY
KUNGRAD
MUYNAK
Lake
Aral-98
Texture
no
sandy
light clay
moderate clay
heavy clay
diverse
3 0 3 6 Kilometers

fig. 9(a) -27-

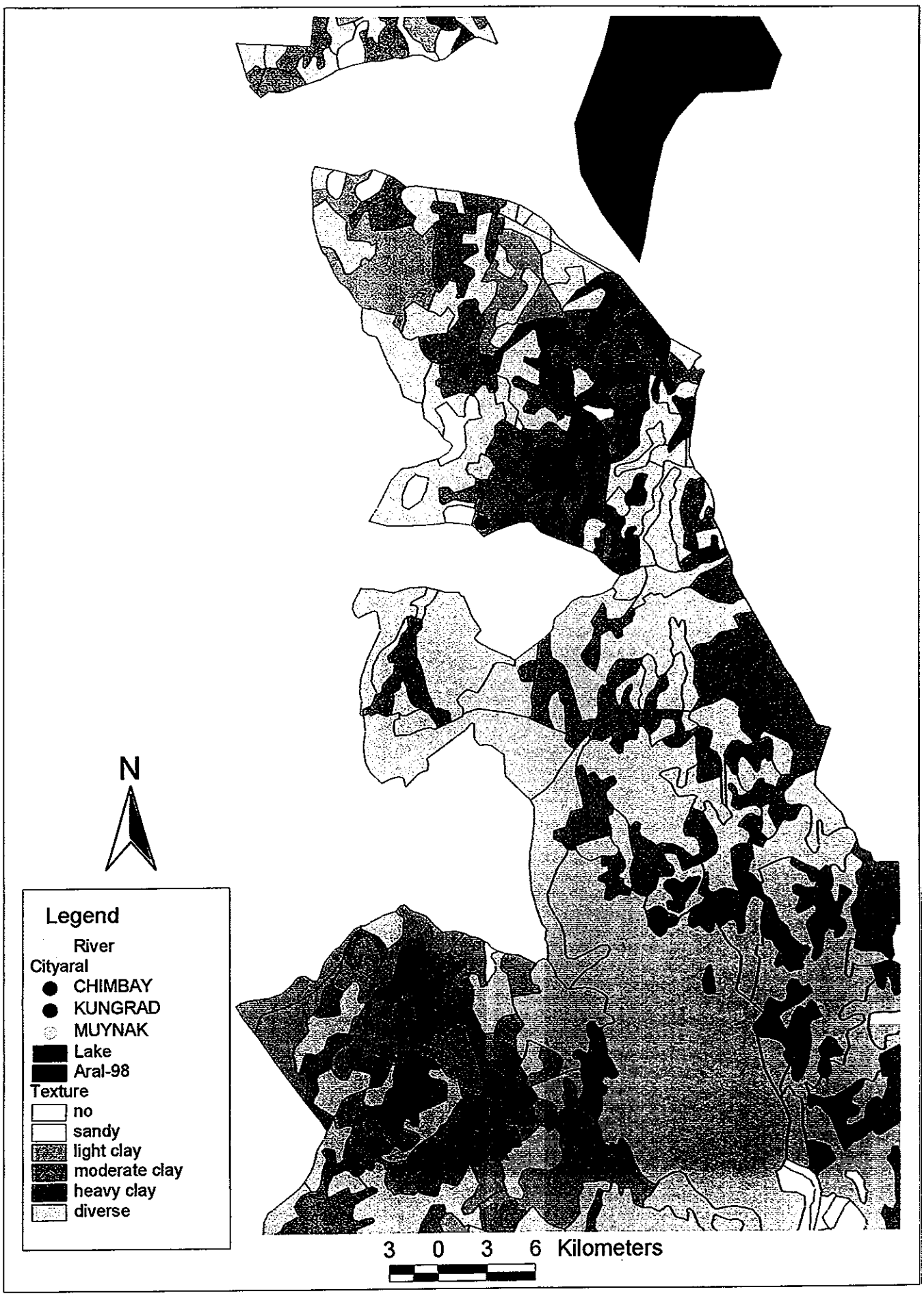
N
Legend
River
Cityaral
CHIMBAY
KUNGRAD
MUYNAK
Lake
Aral-98
Texture
no
sandy
light clay
moderate clay
heavy clay
diverse
3 0 3 6 Kilometers

Fig. 9(b) -26-

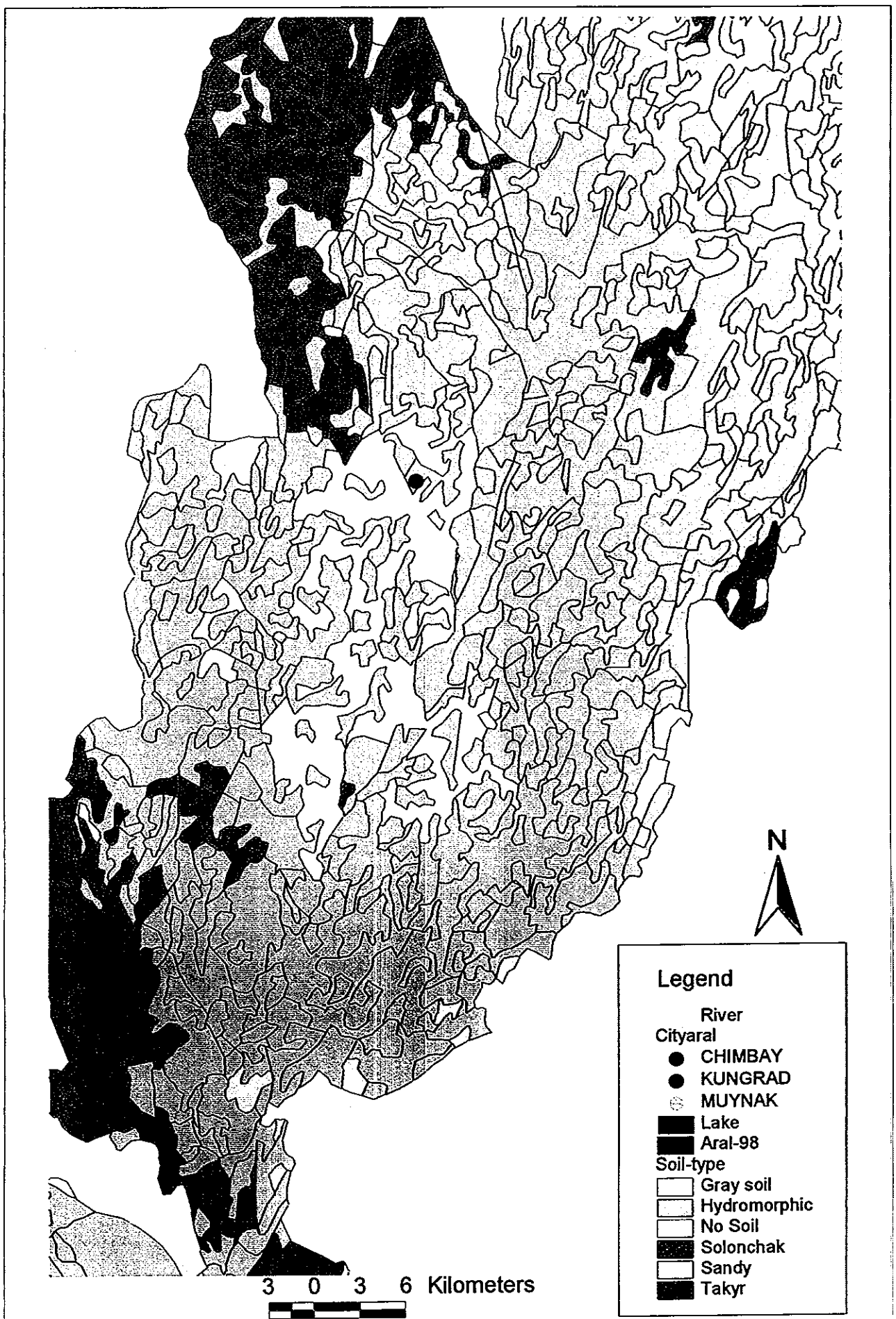
N
Legend
River
Cityaral
CHIMBAY
KUNGRAD
MUYNAK
Lake
Aral-98
Soil-type
Gray soil
Hydromorphic
No Soil
Solonchak
Sandy
Takyr
3 0 3 6 Kilometers

Fig. 10 (a)

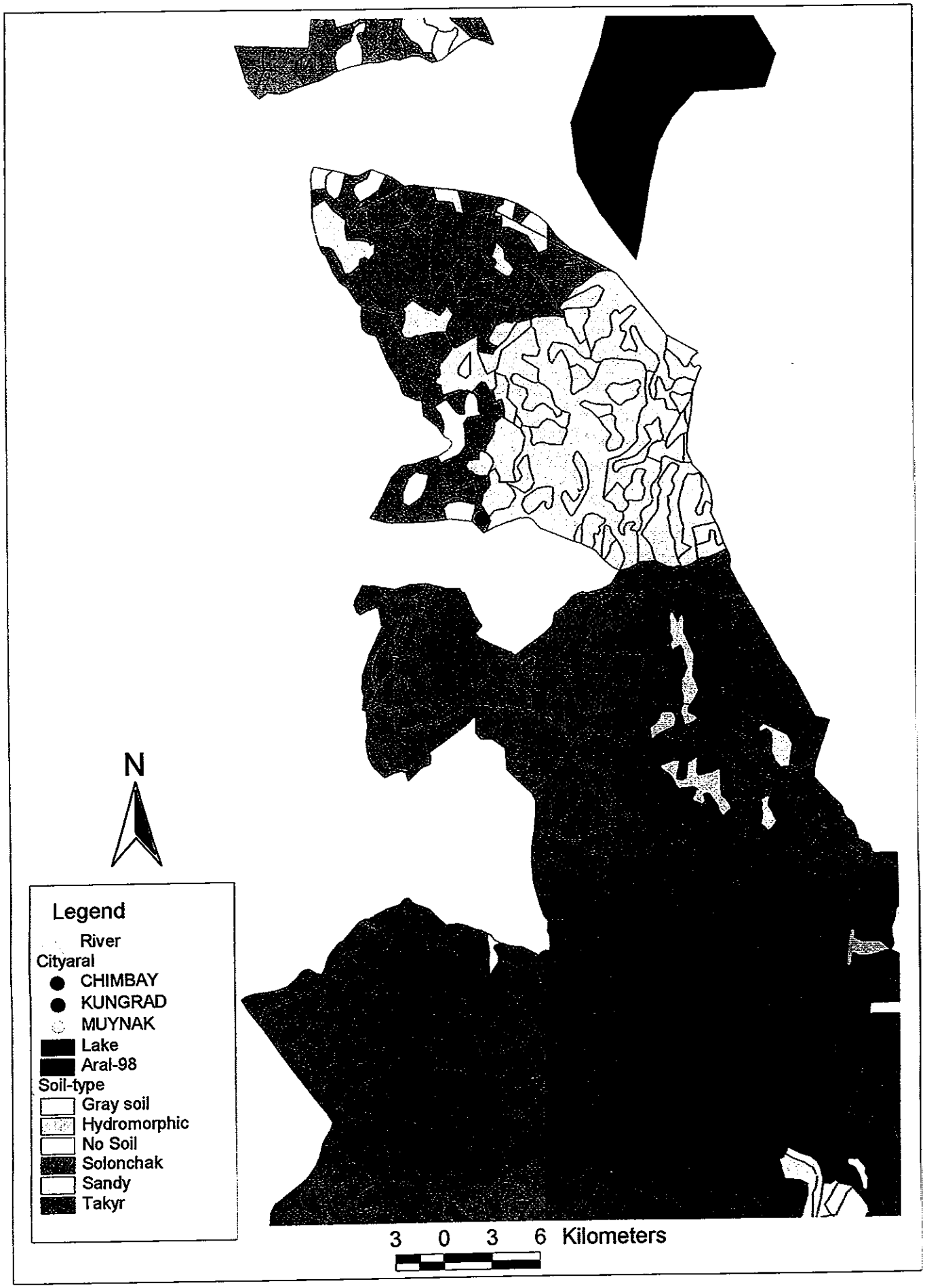
N
Legend
River
Cityaral
CHIMBAY
KUNGRAD
MUYNAK
Lake
Aral-98
Soil-type
Gray soil
Hydromorphic
No Soil
Solonchak
Sandy
Takyr
3 0 3 6 Kilometers

Fig. 10(b) - 30-

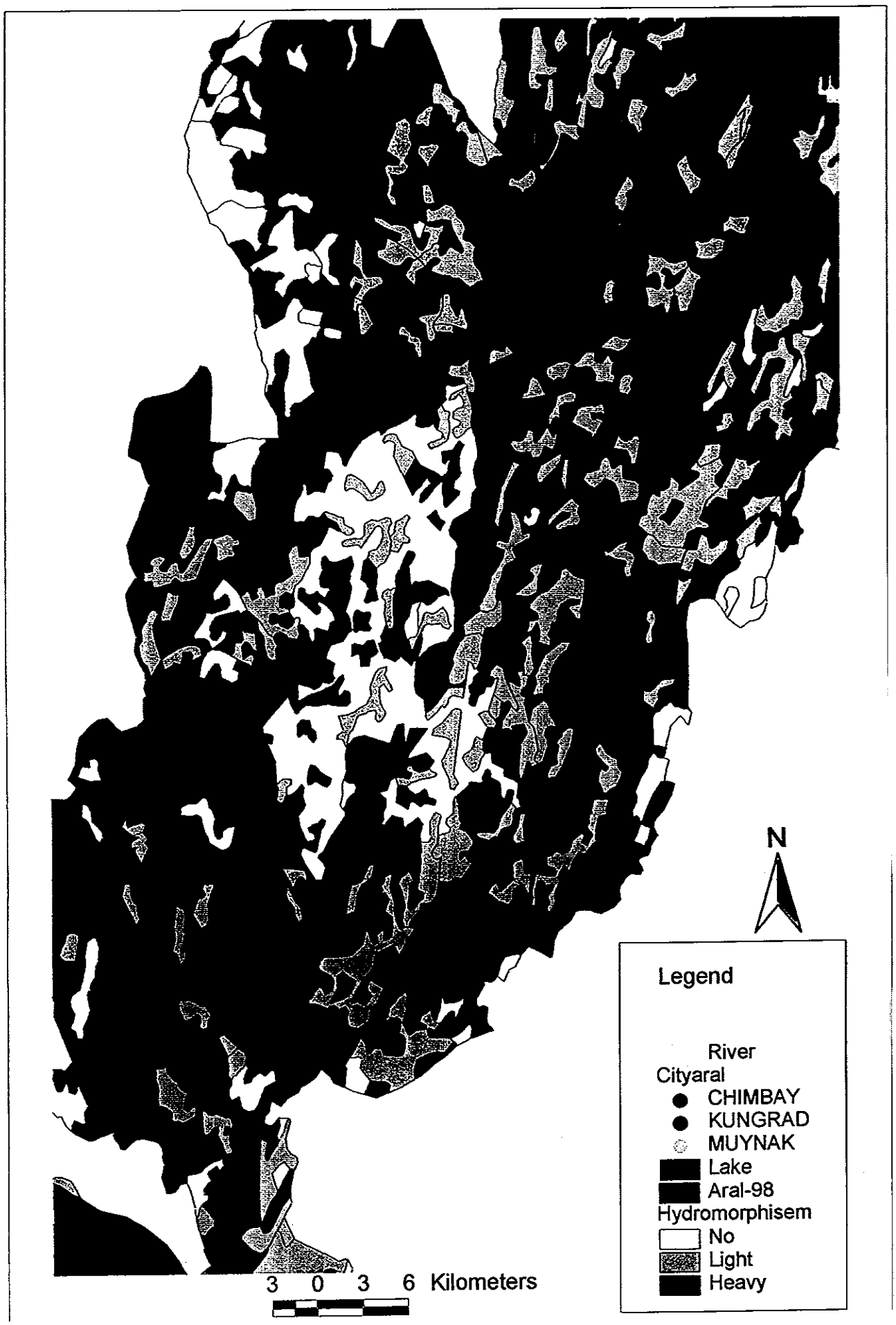
N
Legend
River
Cityaral
CHIMBAY
KUNGRAD
MUYNAK
Lake
Aral-98
Hydromorphisem
No
Light
Heavy
3 0 3 6 Kilometers

Fig. 11(a) - 31-

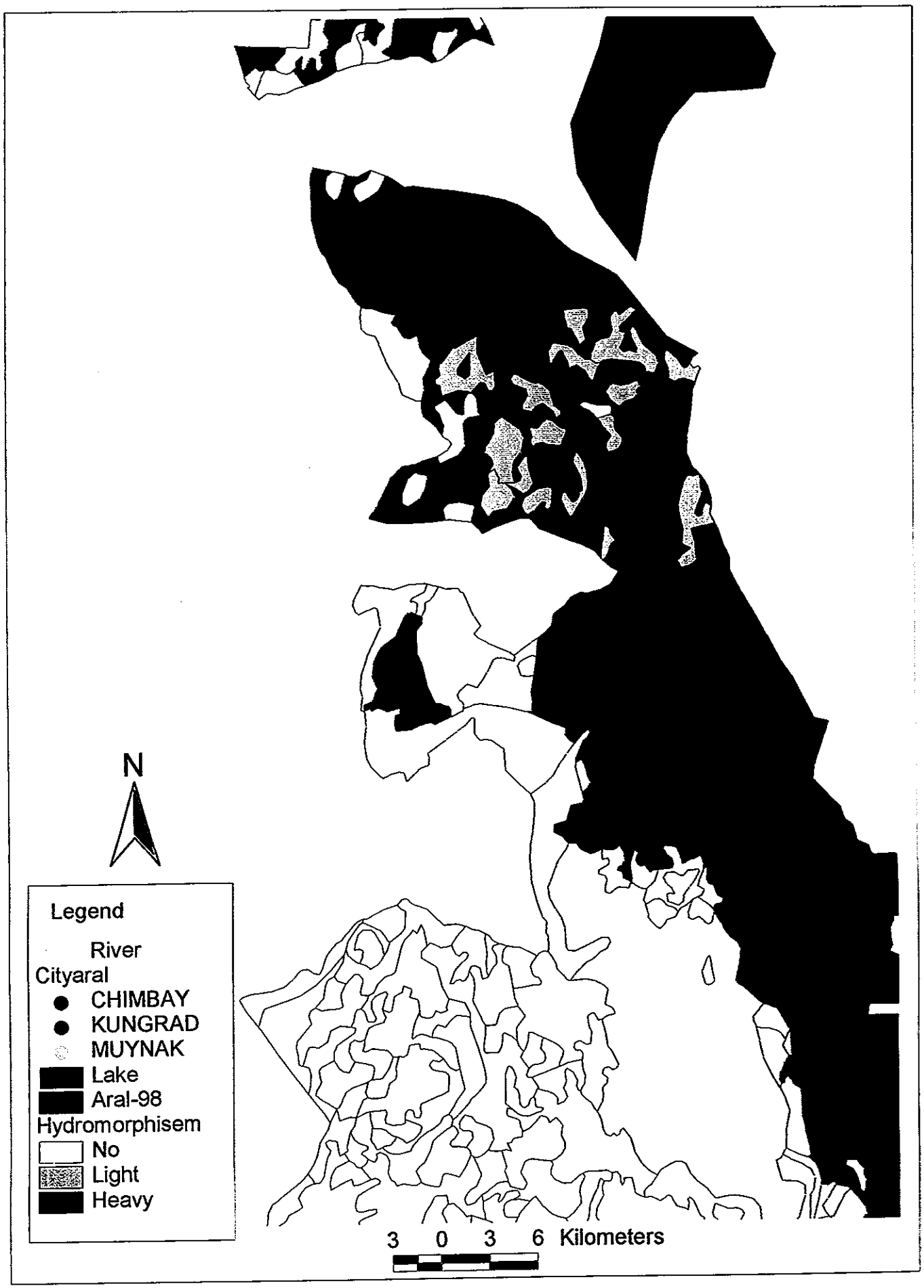
N
Legend
River
Cityaral
CHIMBAY
KUNGRAD
MUYNAK
Lake
Aral-98
Hydromorphisem
No
Light
Heavy
3 0 3 6 Kilometers

Fig. 11(b) 32-

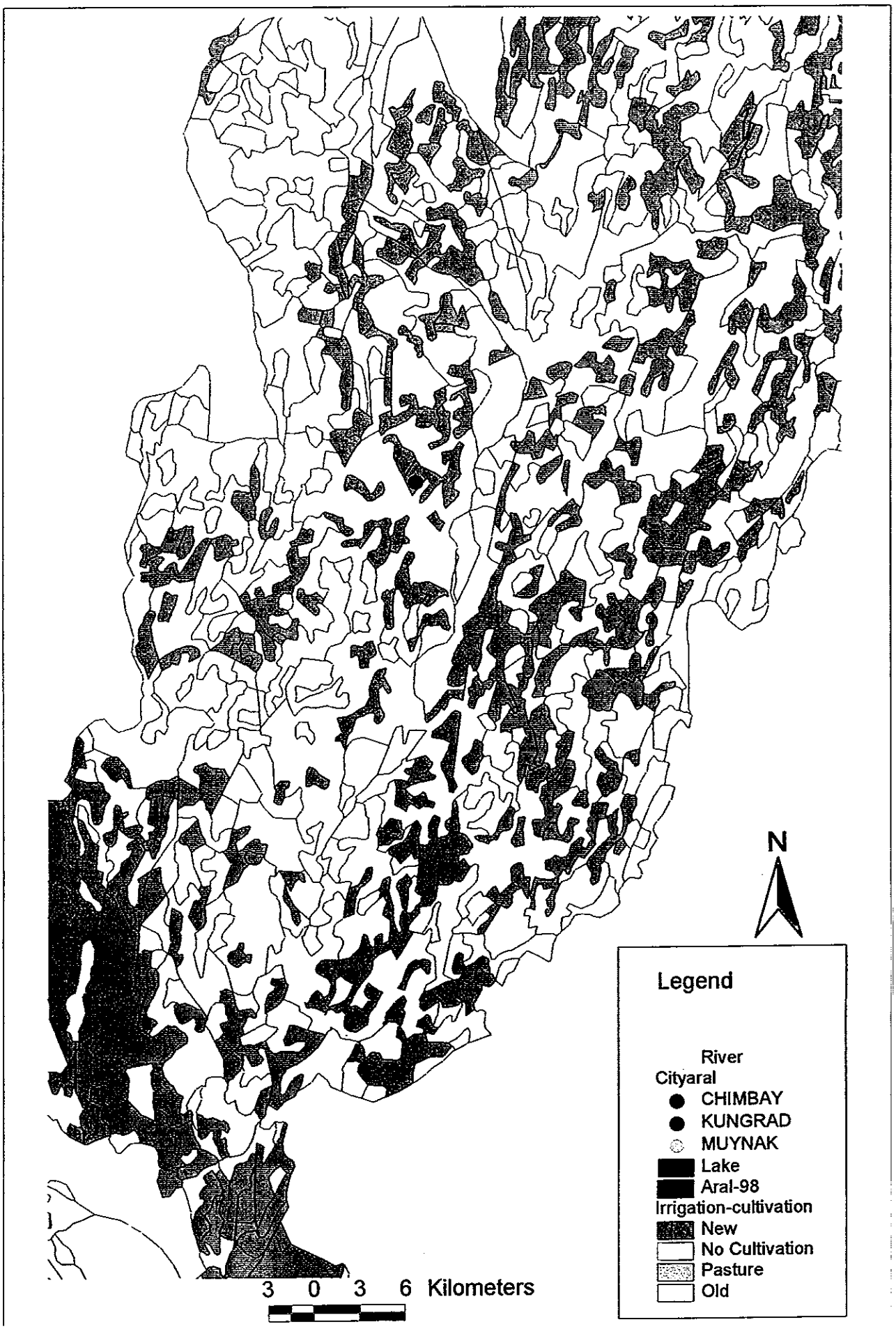
N
Legend
River
Cityaral
CHIMBAY
KUNGRAD
MUYNAK
Lake
Aral-98
Irrigation-cultivation
New
No Cultivation
Pasture
Old
3 0 3 6 Kilometers

Fig. 12 (a)

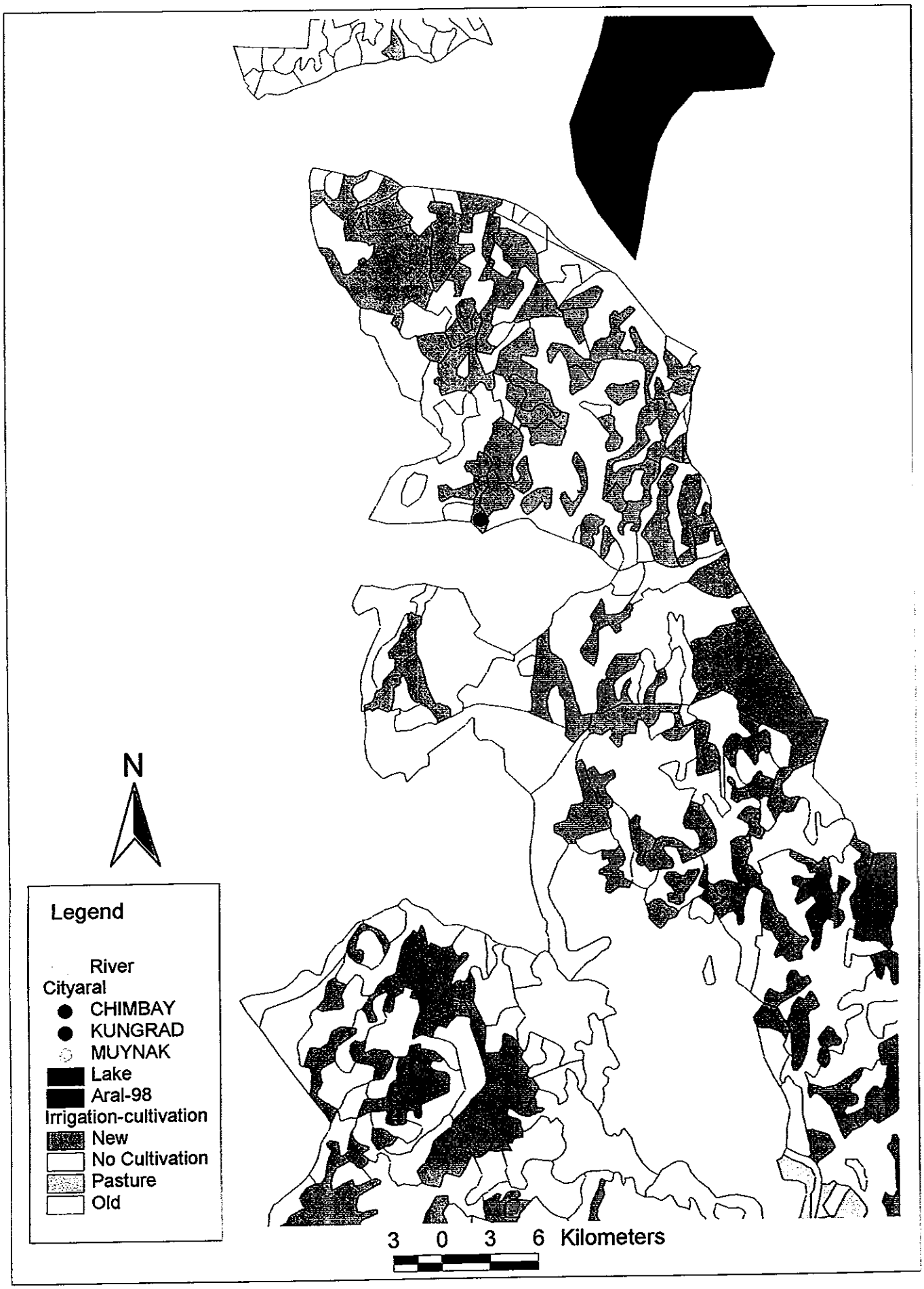
N
Legend
River
Cityaral
CHIMBAY
KUNGRAD
MUYNAK
Lake
Aral-98
Irrigation-cultivation
New
No Cultivation
Pasture
Old
3 0 3 6 Kilometers

Fig. 12(b)

Meteorological model for dust transfer and deposition

Background material for the modeling

The background material for the modeling included two sources:

1. Meteorological data collected by meteorological (radiosonde) stations on site in the Amu Darya delta area.
2. Data retrieved from ECMWF (European Center Meteorological Weather Forecast).

Simulation set-up

For the simulation, the ECMWF analysis data were used. Specifically, the 0.5x0.5 degree latitude-longitude analysis fields at standard pressure levels were used for initialization and nudging the boundaries of the model domain every 6 hours. The initial topography, land-use and soil textural class data sets used have a resolution of 30 arc sec, 10 arc min and 2 arc min, respectively (Figs. 1-5). The grid has a mesh of 140x140 points and a 0.1 degree (6 arc min) horizontal grid increment. The top of the domain is at 17 km and the number of vertical layers is 32. The time step increment was 30 sec. The grid increment used is sufficient to resolve the important regional scale flow. The model domain includes the area from latitude 37N to 52N and from longitude 53E to 67E (the Aral Sea is at about the center of the domain; Fig. 1). Soil textural classes for part of this domain are illustrated in Fig. 2 and are according to the ZOBLER classification (Papadopoulos et al., in preparation).

Numerical aspects

For the purpose of this study, we chose a horizontal grid interval of 0.125 degree (8 arc min). In the vertical, the atmosphere was divided into 32 layers up to the height of 17 km. The time step of the integration was 30 sec. The model domain includes the area from latitude 37N to 52N and from 53E to 67E (the Aral Sea is about the center of the domain). The large-scale atmospheric condition at the initial time added every six hours during the simulation periods were obtained from the European Center Meteorological Weather Forecast (ECMWF) data. We used the 0.5x0.5 degree latitude-longitude analysis fields at standard pressure levels. In order to check the effect of introducing artificial water bodies in the south of Aral Sea area, the numerical simulations were performed for three scenarios:

1. No artificial water bodies added.
2. Big artificial water bodies (BWB) included – "The big option" (Fig. 13).
3. Small artificial water bodies (SWB) added – "The small option" (Fig. 14).

The shapes of the proposed water bodies for each scenario digitized into the model data. Figs. 6 and 7 show the refined shape of Aral Sea as had been obtained by observers on site. The major dust sources with which we were concerned were from the dried parts of the Aral Sea.

Results

Twelve model simulations were performed for the Aral Sea area, for two storms: on the 8-10/07/91; and on the 7-8/05/93.

We simulated three scenarios for each storm, one with dust particles the size of 2.5μm and the second with 15 μm size particles.

The effect of the two storms on 2.5 μm particle sizes, and the difference between the BWB and SWB scenarios, are given in Figs.15-21.

The first simulation was performed on the storm of July 8-10, 1991, with the big artificial water bodies (BWB). The second and third simulations were performed on the same storm but with small artificial water bodies (SWB), and with no artificial water bodies (a placebo scenario). At the beginning of the storm, there were north to northwesterly winds up to 10 m/s strong prevailing in the Aral Sea area.

Fig. 15 (a,b) illustrates the calculated accumulated dust concentration near the surface during the first 18 hr (18:00-8/7/91) of the simulation. The strong wind speed (indicated by the small arrows) caused an uptake of large amounts of dust from the surface. Values of 500 to 1000 kg/km^2 can be seen in the south part of the Sea and farther south.

In the second simulation with the small artificial water bodies, the winds that were prevailing were almost the same as in the first simulation. As can be seen in Fig. 15 in the south end of the dust cloud, the ISO-dust lines in this scenario show a higher concentration of over 1500 kg/km^2 in some places (marked by an arrow).

Twelve hours later, at 06:00-9/7/91, we can see in those two simulations (Fig. 16 (a,b)) that the wind speed had decreased below 7 m/s. In the simulation with the big artificial water bodies (Fig. 16a), the area of the dust cloud is smaller than that of the simulation with small artificial water bodies (Fig. 16b). The main cloud is situated in the southeast part of the Aral Sea. The added area is to the west of the main cloud (marked by an arrow).

The difference between the BWB and SWB scenarios continued throughout the simulation.

Fig. 17 (a,b) shows the calculated accumulated dust concentration near the surface in the first 36 hr (12:00-9/7/91) of the simulation. It can be seen that there was no difference in the results between the second scenario with the small artificial water bodies (SWB), to that with the placebo one. This result continued throughout all the simulations.

In the second storm, on the 7-8/5/93, it can be seen that the difference between the scenarios was not as marked as in the storm of July 1991. Fig. 18(a,b) shows a very big uptake of dust made by northeasterly winds of a velocity of up to 15 m/s. The dust cloud is situated above the Aral Sea and farther southwest to the Caspian Sea. Values of 1000 to 6000 kg/km^2 can be seen in that cloud.

The arrows in Figs. 18a and 18b show the areas where there is a difference between the BWB and SWB scenarios. The area of the dust cloud marked by the arrow is bigger in SWB than in BWB.

The seventh up to the twelfth simulations were performed for the same scenarious on particles the size of 15 μm.

Fig. 19 (a,b) illustrates the calculated accumulated dust concentration near the surface in the first 18 hr on the 8/7/91, for the seventh simulation. Northwesterly to north winds up to 10 m/s strong were prevailing in the area. The strong wind speed (indicated by the arrows) caused an uptake of large amounts of dust from the surface. Values of 100 to 600 kg/km^2 can be seen in the southeast part of the Sea.

The difference between the SWB and the BWB scenarios can be seen in the size and the accumulated concentrations of the dust cloud at the southeast corner of the Aral Sea. The cloud is bigger and ISO-dust concentration lines are denser in the SWB scenario.

In Fig. 20 (a,b) 12 hr later 06:00-9/7/91, the winds that prevail in the area are now up to 7 m/s. One can see that the size of the dust cloud is much bigger in the SWB scenario than in that of the BWB scenario (marked by an arrow).

Six hours later, at 12:00-9/7/91, the north to northwesterly winds that prevail in the area are still up to7 m/s. As marked in Fig. 21 (a,b) by the arrow, one can see that the cloud of dust in the southeast corner of the Aral Sea is bigger in the SWB scenario (Fig. 21b).

Conclusions

The effect of the scenario with big artificial water bodies on the dispersion of the dust clouds that pass above and near them is significant.

As seen in the results, there was no difference between the placebo and SWB (small artificial water bodies) scenario. Possibly because the mash of the grid was too big to be affected by the size of the small artificial water bodies, it is impossible to ascertain whether the small artificial water bodies had an effect at all. Therefore we can not decide what size of artificial water bodies is more effective. On the other hand, it is evident that the big artificial water bodies were effective in reducing the dust load by 2-20%.

Our opinion is that further simulations have to be done in order to improve results of the small water body scenario by using a better resolution of the model, and to examine the effect of bigger artificial water bodies.

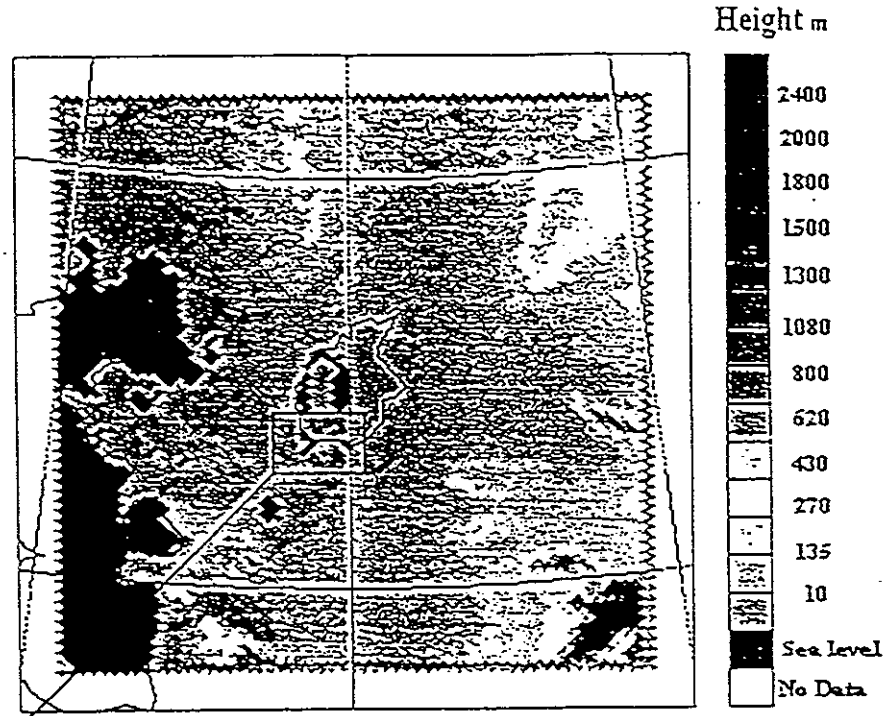

Fig/3 The big artificial water bodies scenario (BWB).

rtificial water
odies

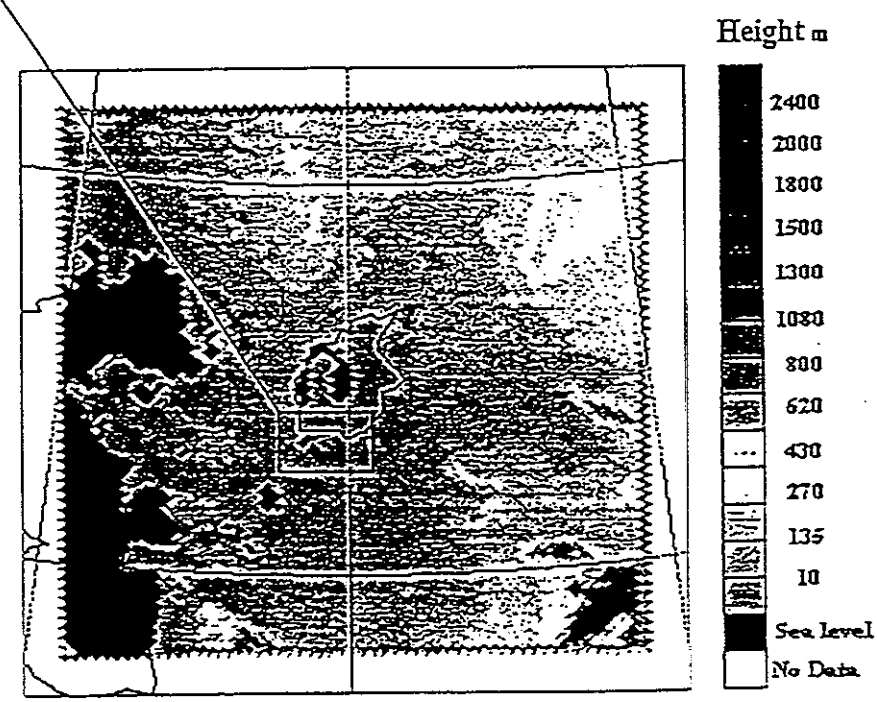

Fig/4 The small artificial water bodies scenario (SWB).

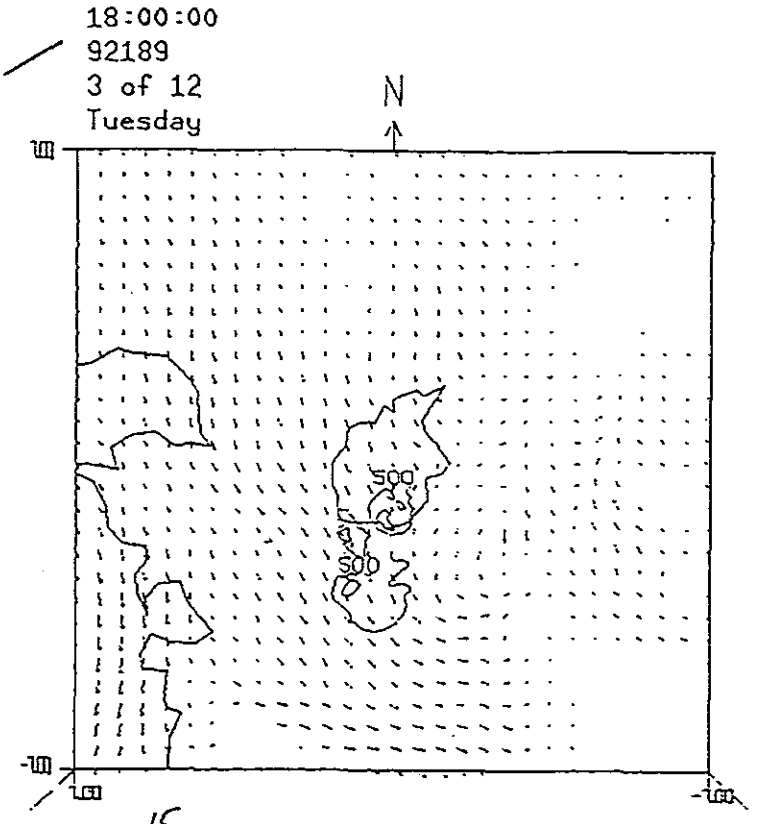

Fig 15a. The big water bodies scenario (BWB).

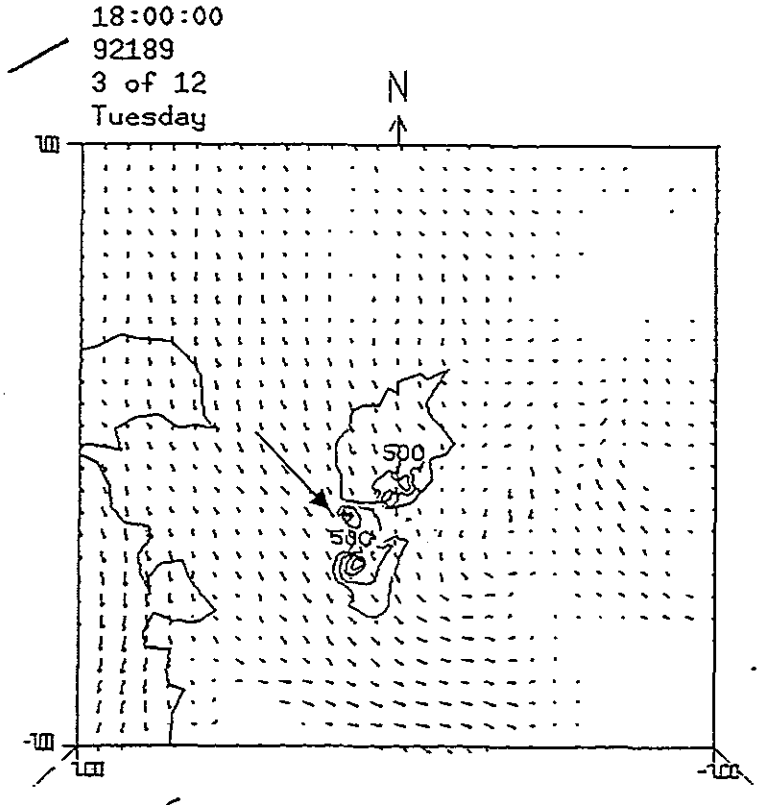

Fig 15b. The small water bodies scenario (SWB).

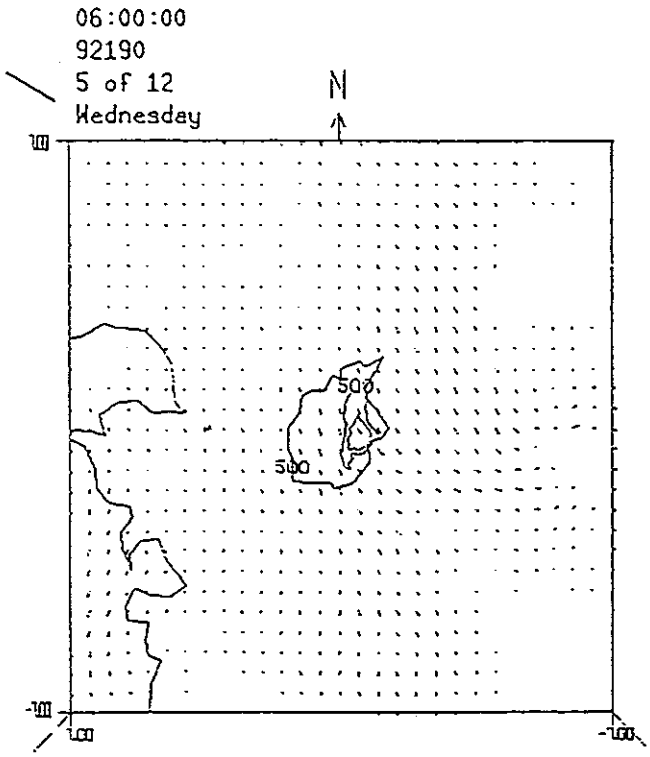

Fig/6a. The big water bodies scenario (BWB).

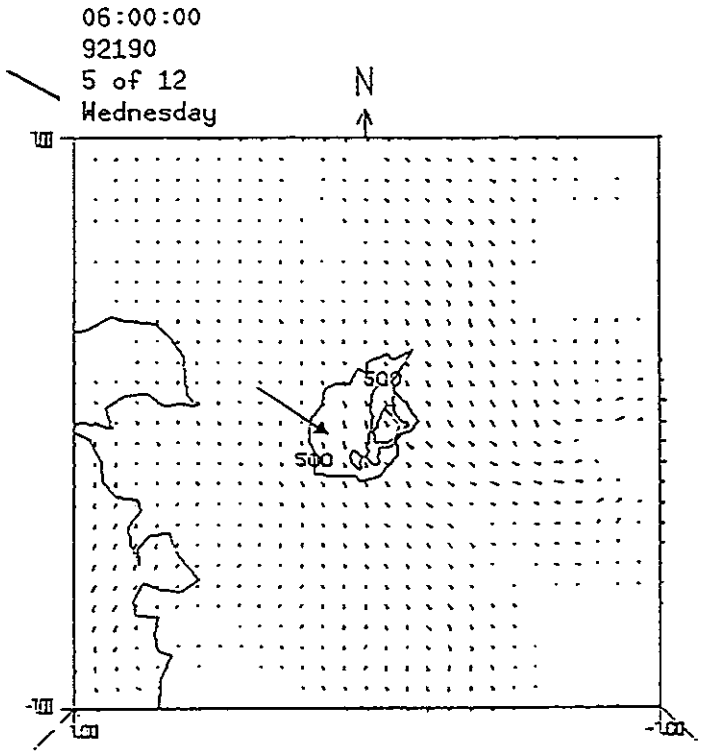

Fig/6b. The small water bodies scenario (SWB).

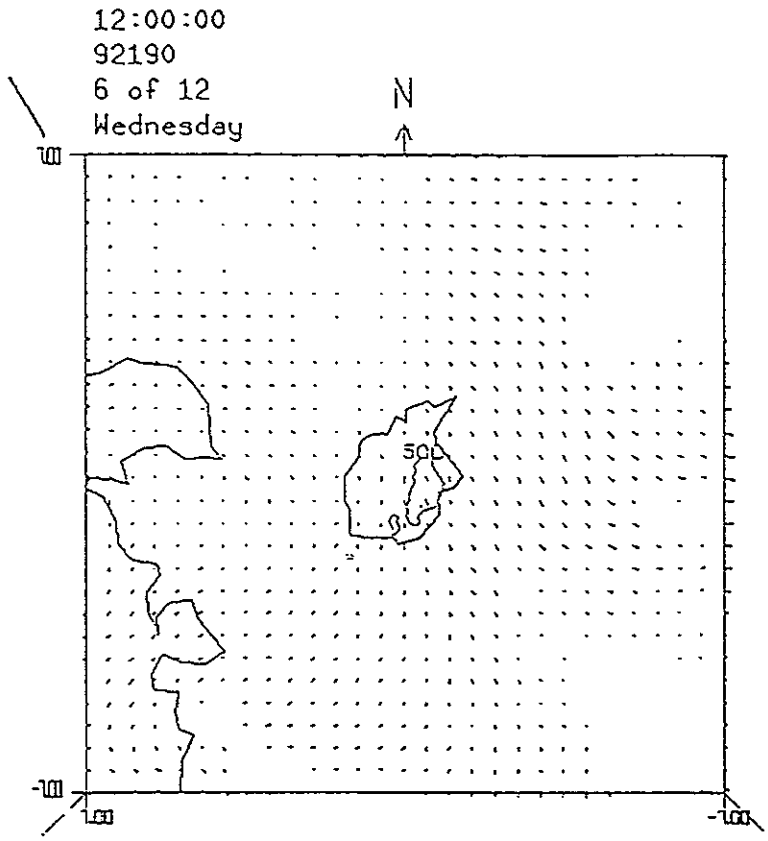

Fig/7a. The placebo scenario.

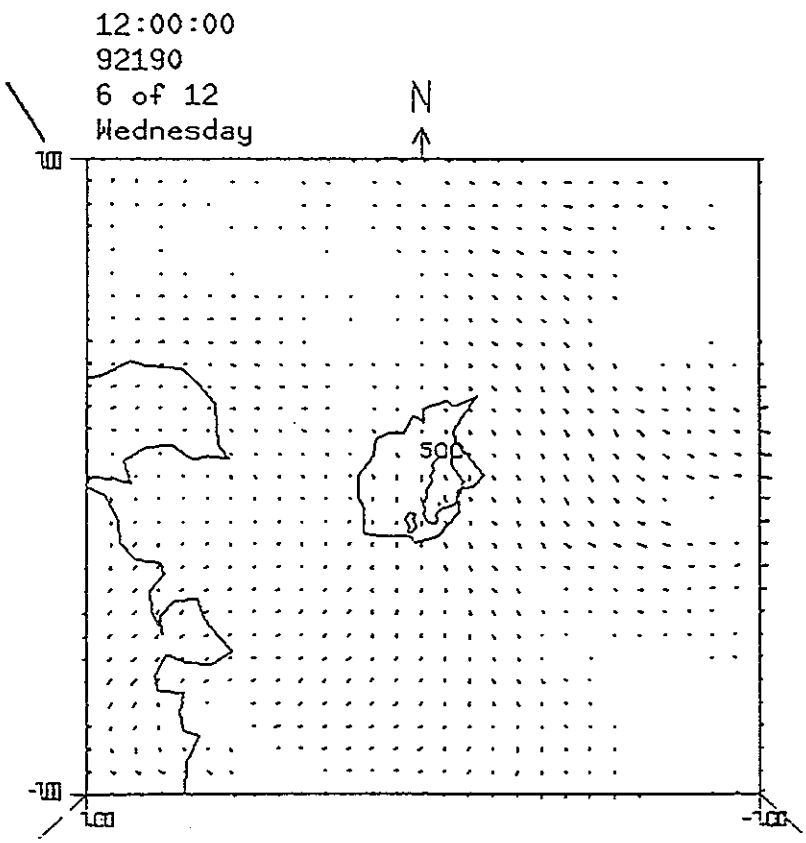

Fig/7b. The small water bodies scenario (SWB).

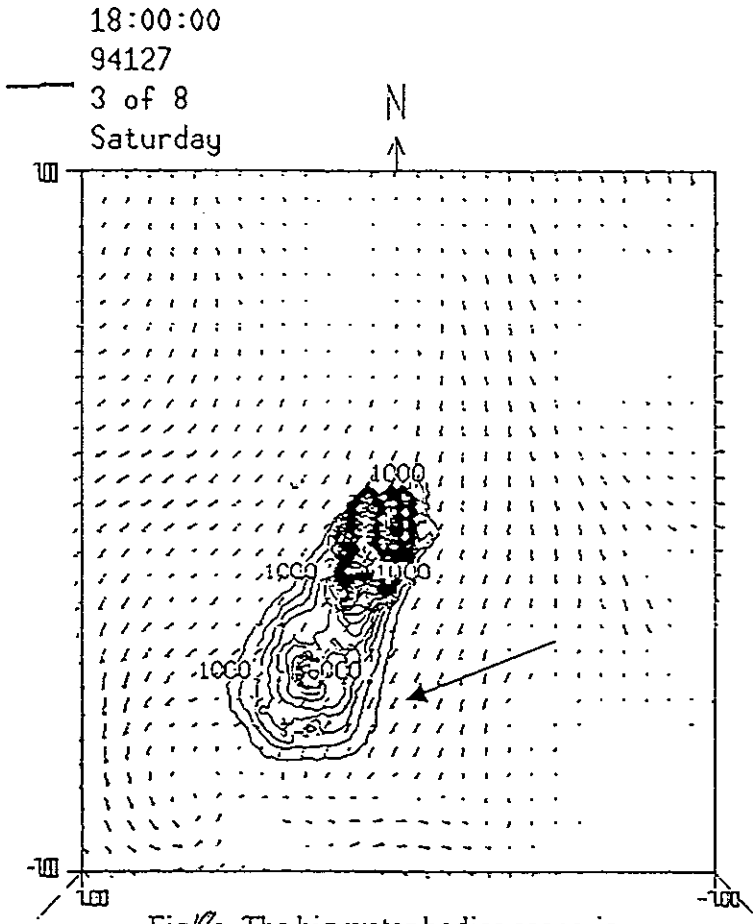

Fig/8a. The big water bodies scenario (BWB).

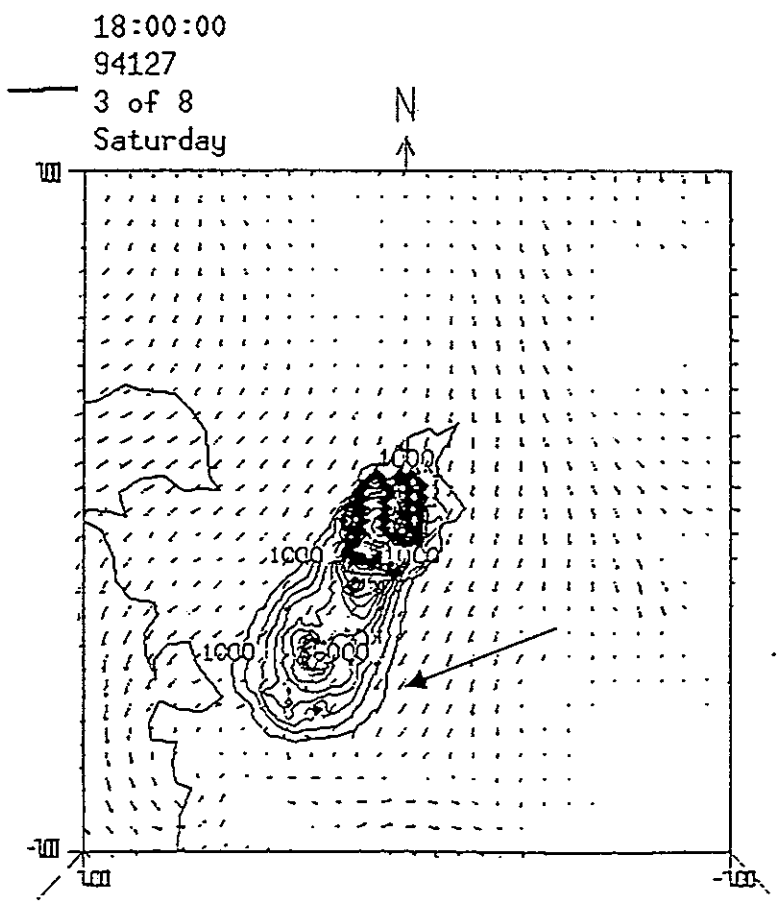

Fig/8b. The small water bodies scenario (SWB).

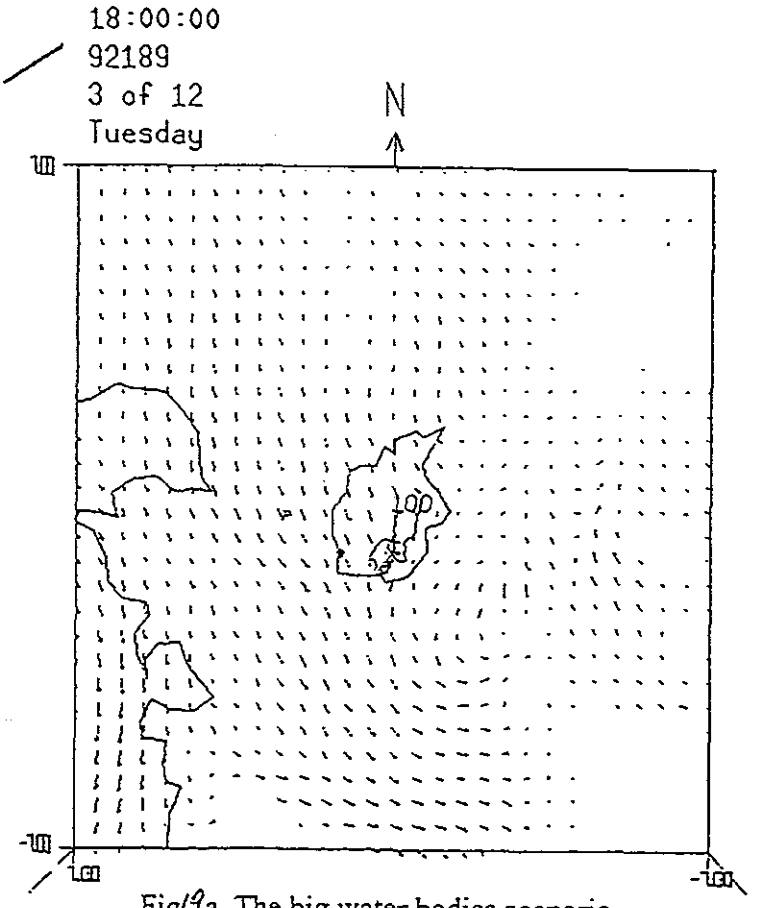

Fig/9a. The big water bodies scenario (BWB).

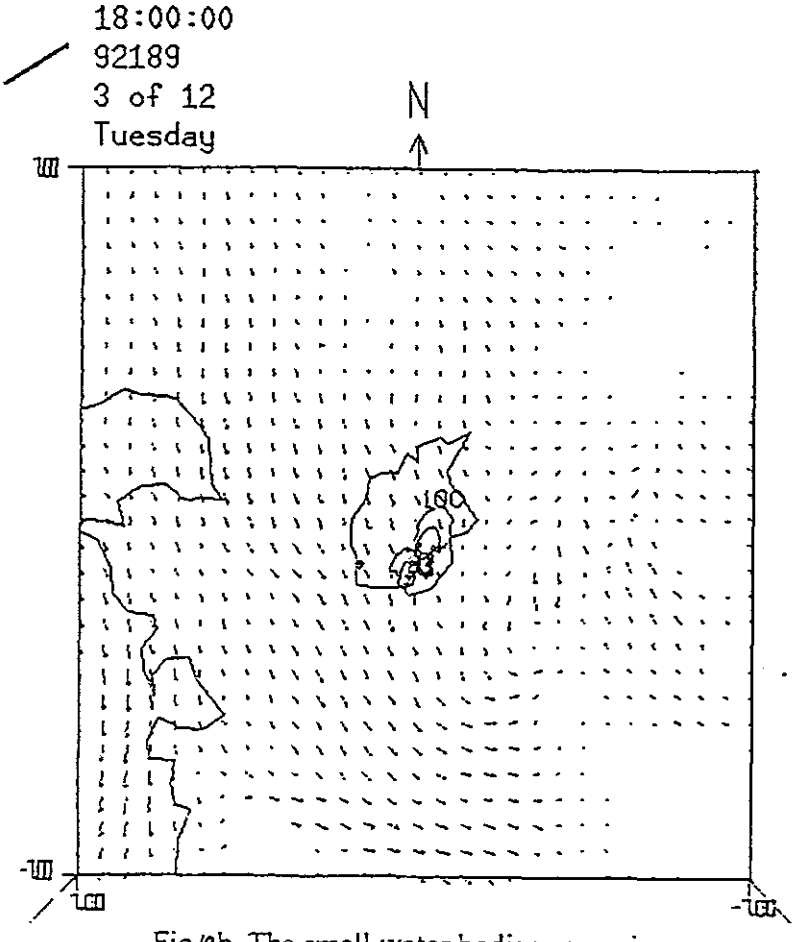

Fig/9b. The small water bodies scenario (SWB).

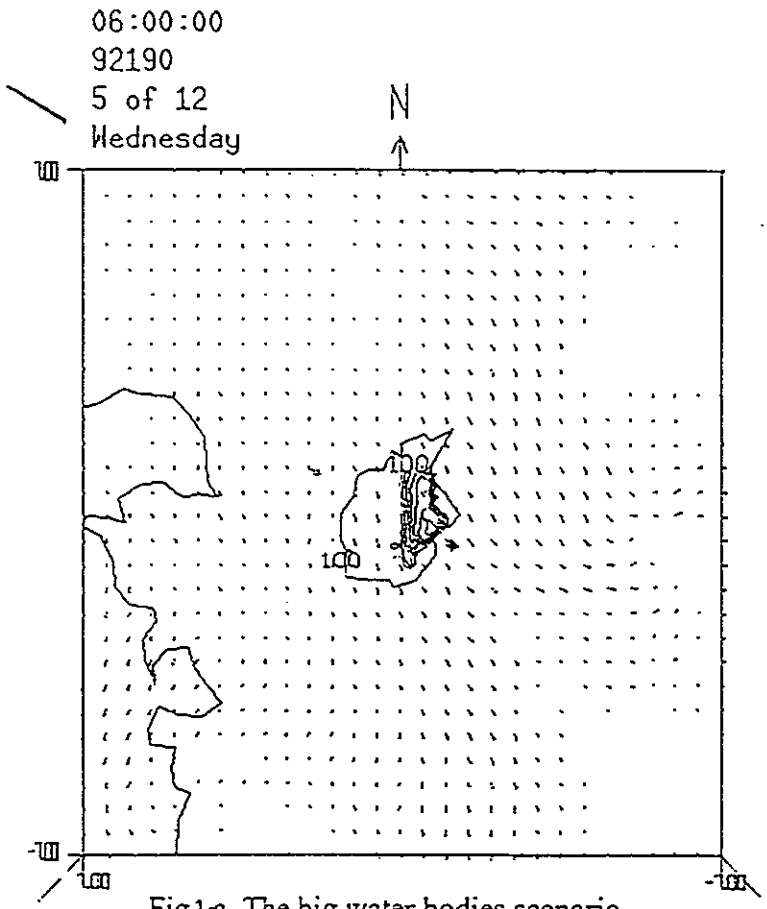

Fig 1a. The big water bodies scenario (BWB).

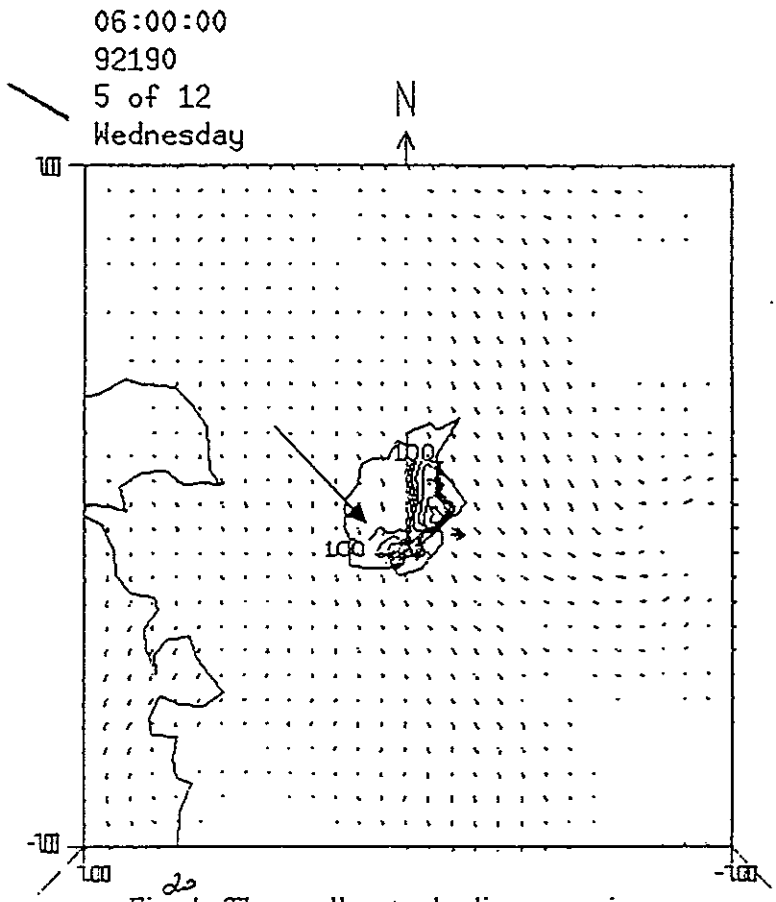

Fig 2b. The small water bodies scenario (SWB).

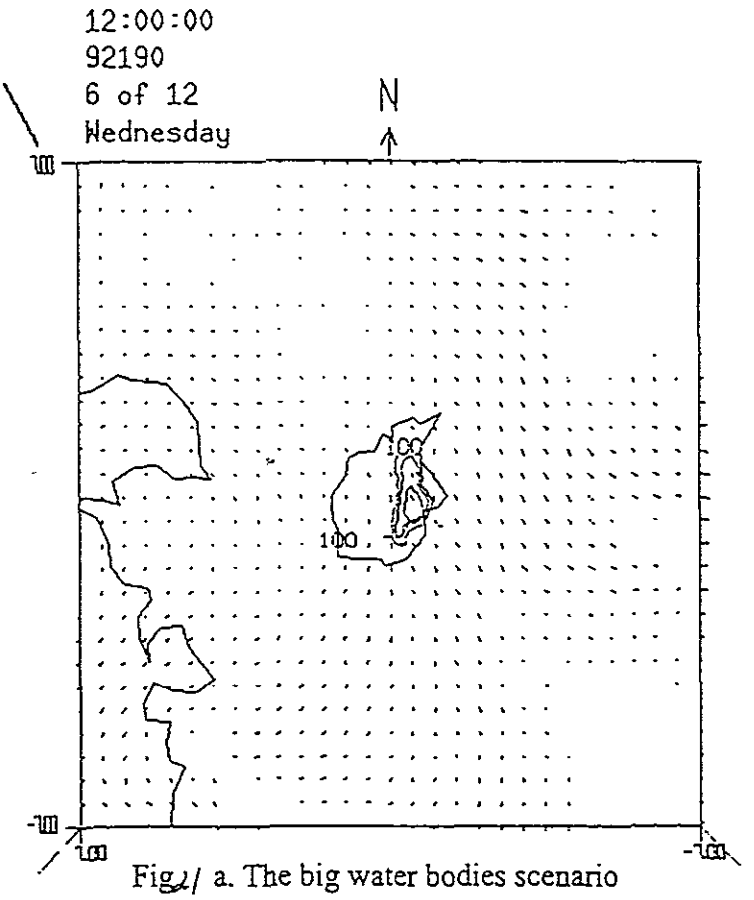

Fig. 21 a. The big water bodies scenario (BWB).

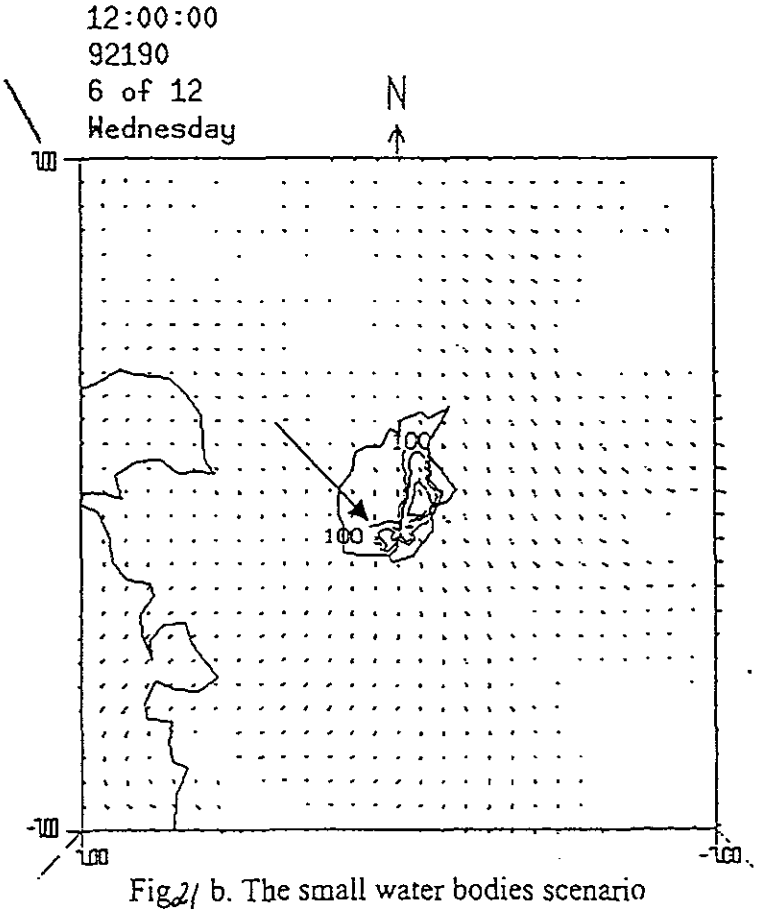

Fig. 21 b. The small water bodies scenario (SWB).

Prof. Y. Mahrer participated in the international workshop on "Mineral Dust" held in Boulder, Colorado, during June 1999, and presented a paper on the application of a three-dimensional numerical meteorological model to dust generation and transport in the Aral Sea region. The paper was co-authored by E. Weinroth from Israel and M. Gilenko from Tashkent, Uzbekistan. Below is the wording of the paper.

Dust Propagation Following Desiccation of the Aral Sea

Y. Mahrer*, E. Weinroth* and M. Gilenko**

*The Hebrew University of Jerusalem, Department of Soil and Water Sciences, Rehovot 76100 Israel. **"Vodproject" Victor Malaysov Str. 3, Tashkent 7000, Uzbekistan.

A three-dimensional numerical meteorological model was used to study the process of salt transfer, propagation and deposition in the Amu Darai river delta, southern Aral Sea. Most of the dust appears to be generated by wind deflating the desiccated sea bottom, as well as adjacent areas covered with salt crusts. The dust contains up to 70% salts. These salts are distributed by the dust plume over wide distances affecting human health and contaminating soils.

The model simulates all major phases of atmospheric dust life cycles:

source and sink processes, vertical turbulent mixing, lateral diffusion and horizontal and vertical advection. One of the tasks of the model simulations was to provide recommendations related to the plans to construct artificial water bodies/reservoirs in order to reduce dust transport. In order to examine the ameliorative effect of artificial water bodies on the propagation of dust we performed three model scenarios: 1. No artificial water bodies; 2. Big artificial water bodies placed to the south of Aral Sea; 3. Small artificial water bodies to the

south of Aral Sea. The simulations were performed for two storms, one from 1991 and the other from 1993. Two dust particle sizes were considered, 2.5 m and 15 m. Results have indicated that artificial water bodies reduce the size of the dust plume.

1. Introduction

"The mighty inland Sea lies stricken now... as its waters dry to salt and blow away as noxious dust to strike the people with illness and death... " (W.S. Ellis 1990)

The atmospheric mineral dust cycle –generation, transportation, deposition and the related climatic and environmental impacts are attracting the attention of the scientific community. Long range transport of dust causes numerous environmental effects: scattering of incoming solar radiation (Carlson and Prospero, 1972; Ackerman and Chung, 1992; Chen et al, 1995; Li et al, 1996) and blooming of algae in the sea (Donaghay et al, 1992).

The local and regional transport and deposition of dust significantly influence the quality of life. In regions with high desert dust productivity, such regional dust storms can cause loss of life and serious property damages, as occurred in Egypt in May 1997 (Nickovic et al.1997).

In addition, since salts are major components of the dust, dust storms will distribute the salt over vast areas, salinizing their soils and water bodies.

Many studies used the Eulerian type transport models to gain a detailed picture of temporal and spatial distribution of dust concentration in the atmosphere and represent all major phases of dust life cycle, from deflation to deposition.

(Westphal et al, 1987, 1988; Joussaume, 1990; Nickovic and Dobricic, 1996 and Nickovic et al 1997).

This study focuses on the dust cycle in the desiccated parts of the Aral Sea. The Aral Sea, once a 26,000 square mile body of water, has now shrunk to around 40% of its former size due to the diversion of the rivers flowing into it for agricultural purposes. The receding waters have left vast areas of sea bed exposed, covered with dust composed of 70% salt. The dust has caused various health problems in the local population (Goren, 1997). This study discusses the eventual effects of constructing artificial water bodies/reservoirs on the process of dust plume transfer/deposition, and the possibility of reduction of the dust plume.

2. The model

The ETA model (Mesinger 1977,1984; Mesinger et al 1988; Nickovic et al, 1997; Janjic 1984, 1990, 1994) is used in order to calculate the dust concentration continuity equation considering the atmospheric conditions.

The model simulates all major phases of an atmospheric dust life cycle: source and sink processes, vertical turbulent mixing, lateral diffusion and horizontal and vertical advection. In the model, dust is considered as a chemically and thermodynamically passive substance of uniform particle size.

An Euler - type dust concentration equation is introduced as an additional component into the ETA coordinate model. The ETA model is a limited-area grid point model that uses the ETA vertical coordinate and includes sophisticated dynamical and physical schemes (Mesinger et al., 1988; Janjic, 1990, 1994). The ETA coordinate is a generalized sigma (mass-type) coordinate that creates step-like model mountains (Mesinger et al., 1988).

The meteorological fields are governed by aerosol-induced meteorological effects. We use a single concentration equation, assuming that the dust material contains particles of uniform size.

The dust concentration C satisfies a continuity equation of the form:

$$\frac{\partial C}{\partial t} = -u\frac{\partial C}{\partial x} - v\frac{\partial C}{\partial y} - \dot{\eta}\frac{\partial C}{\partial \eta} - \nabla K_L \nabla C - \frac{\partial}{\partial \eta}(K_H \frac{\partial C}{\partial \eta}) + S$$

Where u, v, and η are the wind components, K_H is the turbulent exchange coefficient for dust, K_L is the lateral diffusion coefficient, ∇ is the horizontal nabla operator, S is the net dust source/sink (S includes kinematic deflation of dust from the ground, wet removal by the model precipitation, and turbulent and gravitational dry deposition), and subscripts t, x, y and η denote time and space local derivatives.

Dust source areas are introduced in the Jarmoi area that was dried out. It is assumed that the process of aerosol input into the atmosphere occurs in two phases (Dobricic 1996):

1. Dust is mobilized at the ground when the lowest model level wind overcomes a threshold value.
2. The mobilized dust at the ground is vertically mixed by turbulence, as done for the other model variables.

3. Dust storm simulation

Numerical Aspects.

For the purpose of this study we chose horizontal grid interval of 0.0625 degree (16 arc min) resolution. In the vertical dimension, the atmosphere was divided into 32 layers up to the height of 17 km. The time step of the integration was 15 seconds. The model domain includes the area from latitude 37N to 52N and from 53E to 67E (the Aral Sea is at the approximate center of the domain). The large scale atmospheric conditions are inserted at the initial time and updated every six hours henceforth. The atmospheric conditions for the simulation periods were obtained from European Center Meteorological Weather Forecast (ECMWF) data. We used the 0.5x0.5 degree latitude-longitude analysis fields at standard pressure levels.

In order to check the effect of introducing artificial water bodies in the south of Aral Sea area, the numerical simulations were performed for:

1. No artificial water bodies added (PLA) (fig 1a).
2. Big artificial water bodies (BWB) added – "The big option"(fig 1b).
3. Small artificial water bodies (SWB) added - "The small option"(fig 1c).

The shapes of the proposed water bodies for each scenario were digitized into the model data. Fig 1(a, b, c) shows the refined shape of Aral Sea as obtained by observers on site. As can be seen in fig 2 the major dust sources with which we were concerned were from the dried parts of the Aral Sea.

Results

Twelve model simulations were performed for the Aral Sea area, for two storms: one on the 8-10/07/91 and the other on the 7-8/05/93.

We simulated the three above described scenarios for each storm, and for each scenario we performed one simulation with 2.5μm dust particles and another with 15 μm particles.

The difference between the BWB and SWB and PLA scenarios, is shown in figs 1(a, b, c).

The effect of the two storms on 2.5μm particle size:

The first three simulations (BWB, SWB, PLA) were performed on the storm of July 8-10, 1991. At the beginning of the storm there were north to northwesterly winds up to 10 m/s strong prevailing in the Aral Sea area.

Fig. 3(a, b, c) illustrates the calculated accumulated dust concentration near the surface during the first 30 hours (06:00- 9/7/91) of the simulation. The strong wind speed (indicated by the small arrows) caused an uptake of large amounts of dust from the surface. Values of 500 to1500 kg/km^2 can be seen in the south eastern part of the Sea. Six hundred kilometers farther to the south there is a large area of the dust cloud with a concentration of 500 kg/km^2.

In the second simulation with the small artificial water bodies (SWB) the winds that were prevailing were almost the same as in the first simulation. As can be seen in Fig. 3b, the area of dust cloud is bigger at the west and south parts of the dust clouds, than it is in the simulation of the BWB in 2% - 5% (marked by arrows). In the PLA simulation of that storm (fig 3c), we can see that there are larger areas of dust clouds than compared with the SWB simulation, as can be seen in the western part of the northern dust cloud (marked by blue arrows) and in the southern dust cloud. There is also an increase of the dust load in the middle of the southern cloud, up to 1000 kg/km^2. The difference between SWB and PLA simulations in the areas of the dust clouds is about 10%.

Six hours later, at 12:00-9/7/91, we can see in these three simulations (Fig 4.(a, b, c)) that the wind speed has decreased below 7 m/s. The main cloud is situated in the southeast part of the Aral Sea. Concentrations of 1000 kg/km^2 can be seen in the dust cloud. In the BWB simulation (Fig. 4a) the area of the dust plume is 10% smaller than that of the SWB simulation (Fig. 4b). There is an added area to the west of the main cloud (marked by a black arrow). The difference between the PLA and SWB simulation is mostly in area of the dust plume, and not in the concentration of the dust particles. This trend of differences between the BWB, SWB and PLA scenarios continued throughout the simulations of both storms with the 2.5μm particle size.

The next simulations were performed, for the same scenarios, on 15μm particles.

Fig 5(a, b, c) illustrates the calculated accumulated dust concentration near the surface after the first 36 hours (at 12:00 9/7/91). The north to northwesterly winds that prevail in the area are still up to 7 m/s. Fig 5(a, b, c) has been magnified so as to enable the viewer to discern the details in the different scenarios. As marked in fig 5(a, b) by the arrows, one can see that the area of the dust cloud in the southwest corner of Aral Sea is 5% bigger in the PLA scenario than in the SWB scenario. Comparing figures 5(b) and 5(c), we can see that the area of the

dust cloud in the BWB scenario is about 10% smaller than that of the SWB dust cloud, and the ISO-dust concentration lines are not as dense. We can see that there is also a reduction in the concentration of the dust load inside the dust cloud located 90-100 km east of the Southwest corner of the old Aral Sea.

4. Conclusions

The effect of the simulated big artificial water bodies on the dispersion of the dust clouds that pass in their vicinity is significant.

As seen in the results, there is an approximate 5% reduction of the dust load between the PLA (placebo) and SWB (small artificial water bodies) scenarios. There is 15% reduction of dust load between PLA and BWB. This reduction was consistent throughout the simulations.

Several improvements may be made with similar studies in the future. The first is a detailed examination of the effects different scenarios for the further shrinkage of lake Aral will have on dust generation and distribution. The second would be the examination of the effects of vegetation cover on dust generation. Another improvement would be comparison of the results of the simulations against true measurements.

Acknowledgments

This research was supported under Grant No. CA16-013 U.S.-Israel Cooperation Development Research Program, Economic Growth, U.S. Agency of International Development.

References

- Ackerman S.A., and Chung H., 1992: Radiative effects of airborne dust on regional energy budgets at the top of the atmosphere. *J. Appl. Meteor.*, 31, 223-233.
- Carlson T.N., and Prospero J.N., 1972: The large-scale movement of Saharan air outbreaks over the equatorial north Atlantic. *J. Appl. Meteor.*, 11, 289-297.
- Chen S.J., Kuo Y.H., Ming W., and Ying H., 1995: The effect of dust radiative heating on low-level frontogenesis. *J. Atmos. Sci.*, 52, 1414-1420.

- Dobricic S., 1996: Atmospheric transphort of desert dust toward European seas: Model parameterization and a simulated case. *Sensitivity of North Sea, Baltic Sea and Black Sea to Antropogenic and Climatic Changes.* Ozsoy E and Mikaelyan A., Eds., Kluwer Academic.
- Donaghay P.L., Liss P.S., Duce R.A., Kester D.R., Hanson A.K., Villareal T.,
- Tindale N.W., and Gifford D.J., 1992: The role of episodic atmospheric nutrient inputs in the chemical and biological dynamics of oceanic ecosystems. *Oceanography*, 4, 62-70.
- Ellis W.S., 1990: Lies Dying. *National Geographic* February 1990, 73-92.
- Ellis W.G., and Merrill J.T., 1995: Trajectories for Saharan dust transported to Barbados using Strokes's law to describe gravitational settling. *J. Appl. Meteor.*, 34, 1716-1726.
- Goren A., et al., 1997: Respiratory conditions among children associated with community exposure to airborne particles. *Environ. Res. Forum*, 8, 483-489.
- Janjic Z.I., 1984: Non-linear advection schemes and energy cacade on semi-staggered grids. *Monthly Weather Review, 112, 1234-1245.*
- Janjic Z.I, 1990: The step-mountain coordinate: physical package. *Monthly Weather Review*, 118, 1429-1443.
- Janjic Z.I., 1994: The step-mountain ETA coordinate model: Further developments of the convection, viscous sublayer and turbulence closure schemes. *Monthly Weather Review*, 122, 927-945.
- Joussaume S., 1990: Three-dimensional simulations of the atmospheric cycle of desert dust particles using a general circulation model. *J. Geophys. Res.*, 95, 1909-1941.
- Li X., Maring H., Savoie D., Voss K., and Prospero M., 1996: Dominance of mineral dust in aerosol light-scattering in the North Atlantic trade winds. *Nature* 380, 416-419.
- Mesinger F., Janjie Z.I, Nickovic S., Gavrilov D., and Deaven D.G., 1988: The step-mountain coordinate: Model description and performance for cases of Alpine lee cyclogenesis and for a case of Appalachian redevelopment. *Mon. Wea. Rev.*, 116, 1493-1518.
- Mesinger F., 1997: Forward-backward scheme, and its use in a limited area model. *Contributions to Atmospheric Physics*, 50, 200-210.

- Mesinger F., 1984: A blocking technique for representation of mountains in atmospheric models. *Rivista di Meteorologia Aeronautica,* 44, 195-202.
- Nickovic S., and Dobricic S., 1996: A model for long-range transport of desert dust. *American Meteorological Society Monthly Weather Review*, 124, 2537-2544.
- Nickovic S., 1996: Modeling of dust process for the Saharan and Mediterranean area. *The Impact of Desert Dust Across the Mediterranean*, 15-23, Guerzoni S and Chester R., Eds., Kluwer Academic Publishers.
- Nickovic S., Kakaliagou O., Kallos G., and Jovic D., 1997: ETA dust model: Sensitivity to model resolution and desert source specification.
- Westphal D.L., Toon O.B., and Carlson T.N., 1987: A two-dimensional numerical investigation of the dynamics and micro-physics of Saharan dust storms. *J. Geophys. Res.*, 92, 3027-3049.
- Westphal D.L., 1988: A case study of mobilization and transport of Saharan dust. *J. Atmos. Sci.*, 45, 2145-2175.

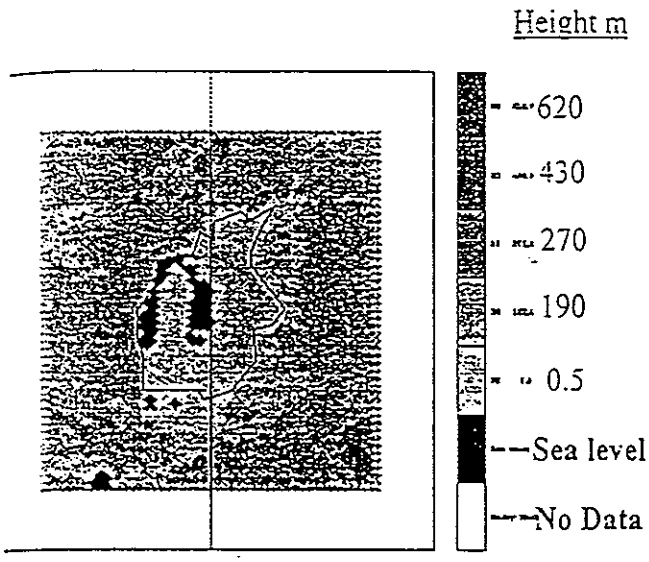

FIG 1a. The Aral Sea with no artificial water bodies

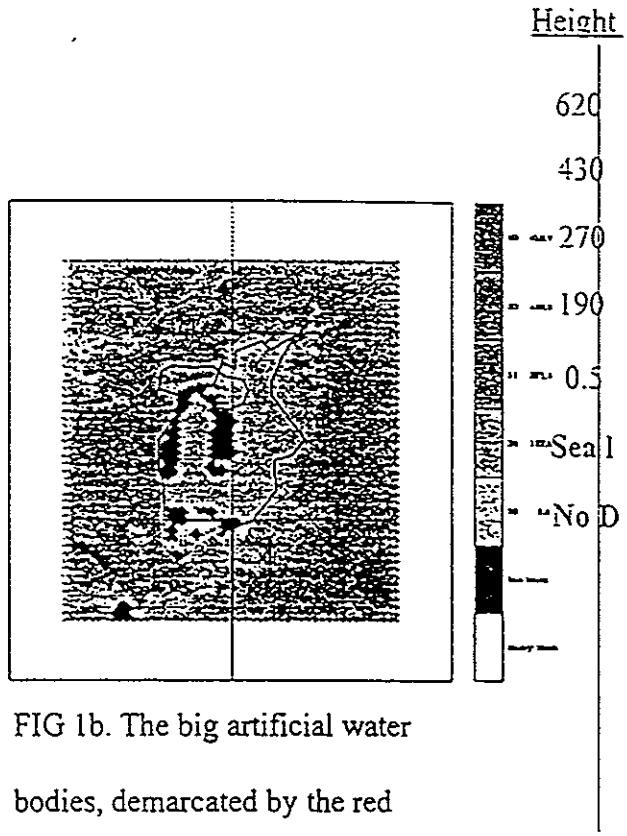

FIG 1b. The big artificial water bodies, demarcated by the red

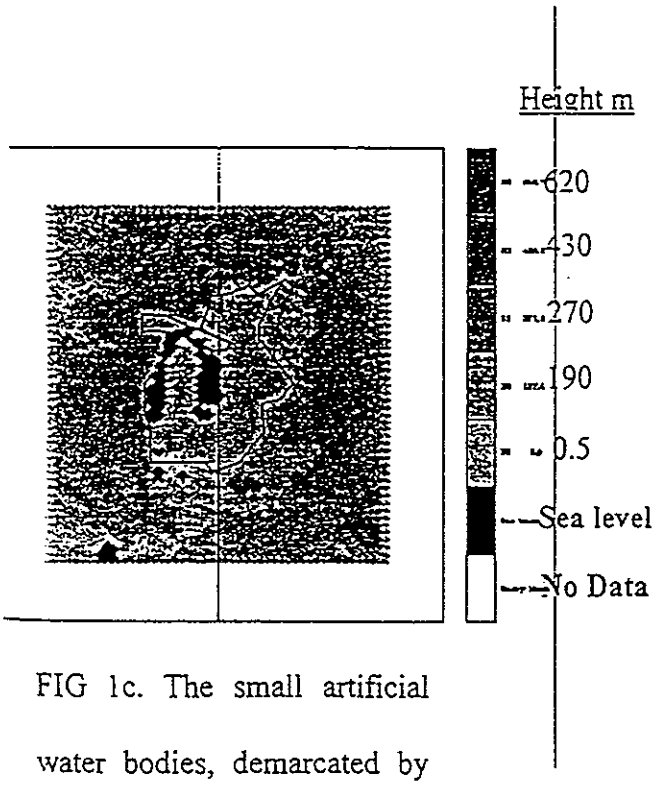

FIG 1c. The small artificial water bodies, demarcated by the yellow and black line

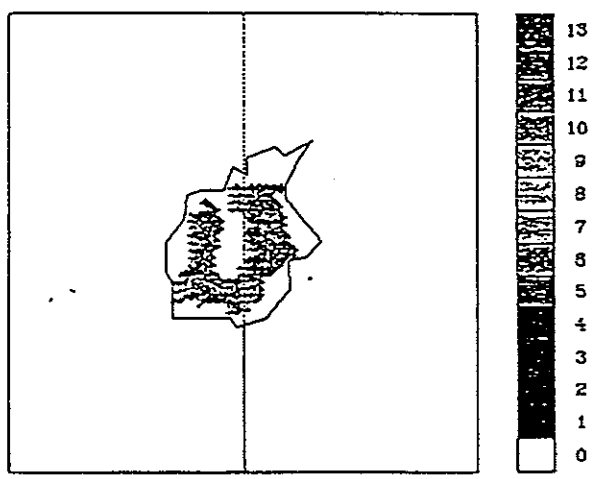

FIG 2. Dust sources from the dried areas of the Aral Sea

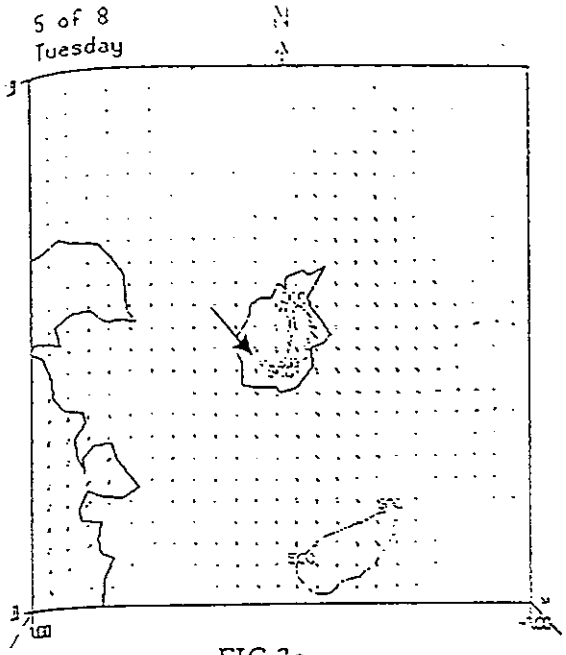

FIG 3a.

Vis5D

FIG 3a. Result of the BWB simulation. Surface Horizontal wind field and dust concentration 30 hours (06:00- 9/7/91) after beginning of the simulation. The red lines are ISO-Dust contours of dust concentration of 500 kg/km^2. Size of particles is 2.5μm.

FIG 3b. Result of the SWB simulation. Surface Horizontal wind field and dust concentration 30 hours (06:00- 9/7/91) after beginning of the simulation. Dust concentration gets to 1500 kg/km^2 in some places. The arrows mark the area with difference between the simulations.

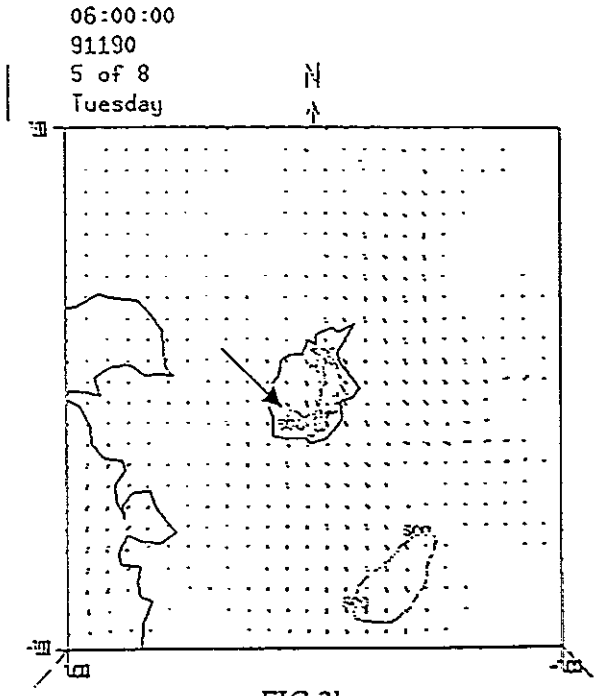

FIG 3b

Vis5D

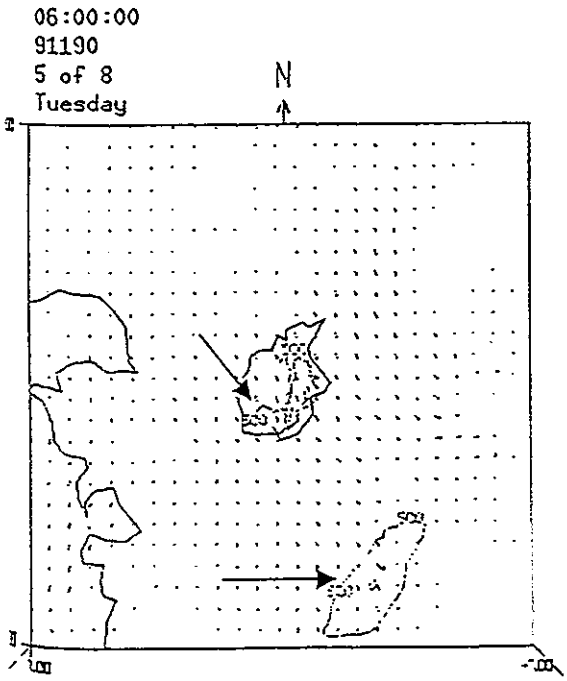

FIG 3c

Vis5D

FIG 3c. Result of the PLA simulation. Surface Horizontal wind field and dust concentration 30 hours (06:00- 9/7/91) after beginning of the simulation. Dust concentrations are about 1500 kg/km^2 in various places.

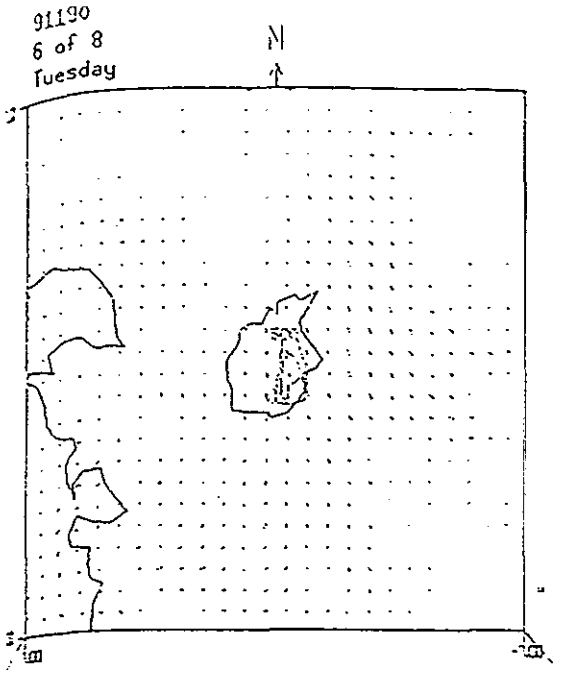

FIG 4a

Vis5D

FIG 4a. Result of the BWB simulation. Surface Horizontal wind field and dust concentration 36 hours (12:00- 9/7/91) after beginning of the simulation. The red lines are ISO-Dust contours of dust concentration of 500 kg/km^2. Size of particles is 2.5μm.

FIG 4b. Result of the SWB simulation. Surface Horizontal wind field and dust concentration 36 hours (12:00- 9/7/91) after beginning of the simulation. Dust concentrations are up to 1000 kg/km^2. The arrow marks the area of difference between the simulations.

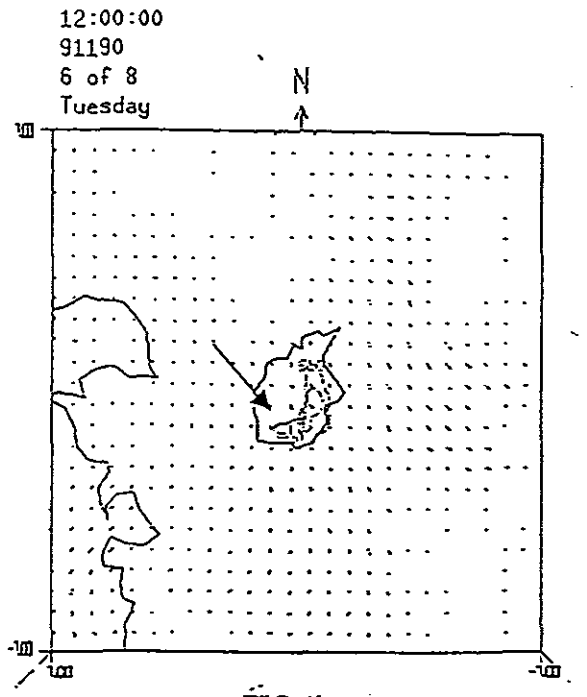

FIG 4b

Vis5

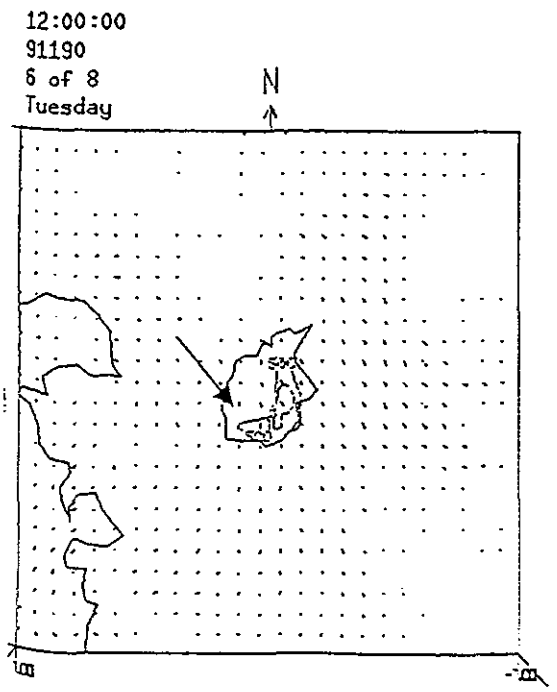

FIG 4c

Vis5D

FIG 4c. Result of the PLA simulation. Surface Horizontal wind field and dust concentration 36 hours (12:00- 9/7/91) after beginning of the simulation. The arrow marks the area of difference between the simulations.

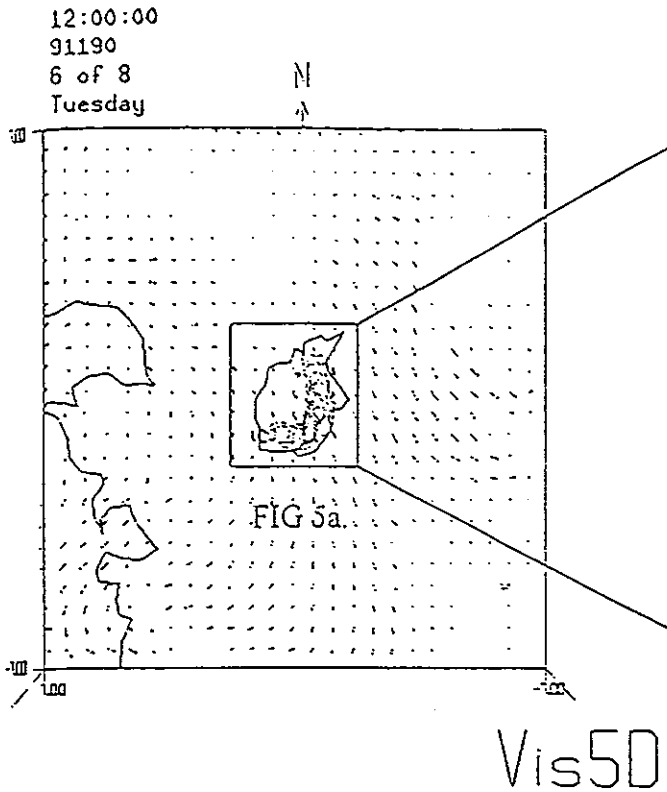

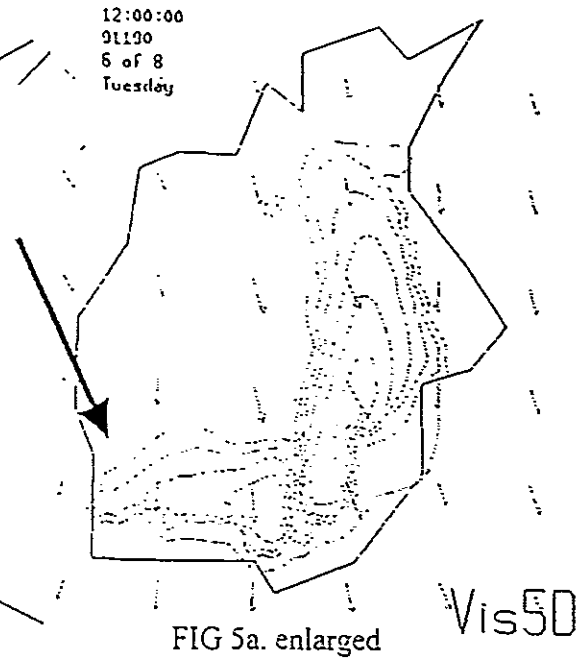

FIG 5a. enlarged

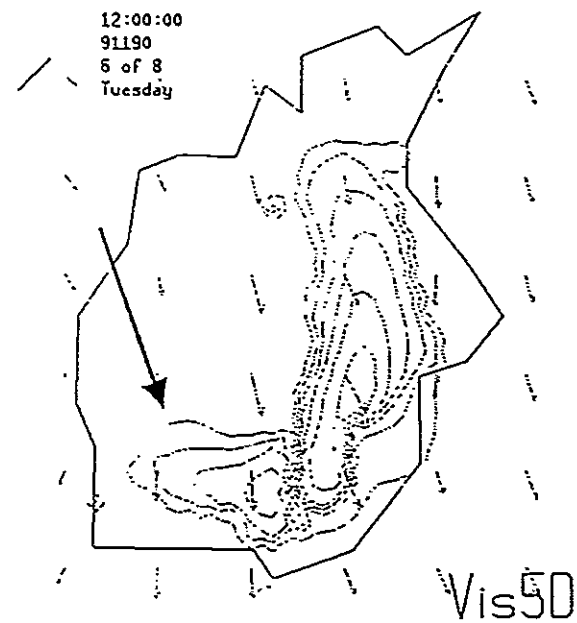

FIG 5b.

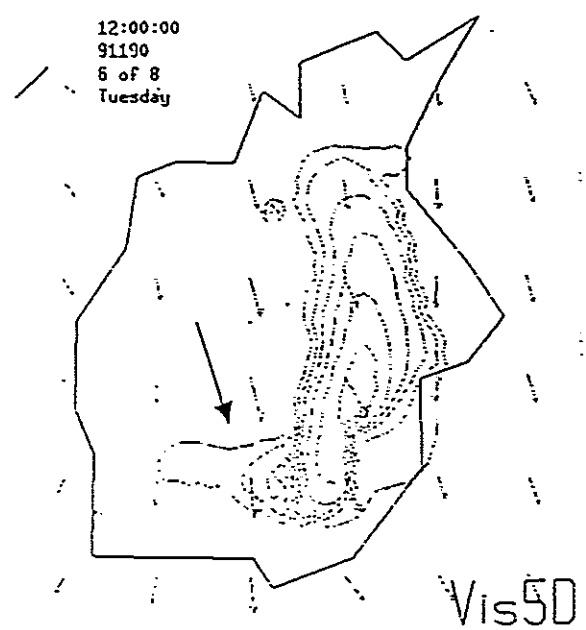

FIG 5c.

FIG 5. Surface Horizontal wind field and dust concentration 36 hr (12:00- 9/7/91) after beginning of the simulation. The red lines are ISO-Dust contours of dust concentration of 100 kg/km^2. Size of particles is 15μm.
FIG 5a. Result of the PLA simulation. FIG 5b. Result of the SWB simulation. FIG 5c. Result of the BWB simulation.The black arrows mark the area with difference between the simulations.

Wind erosion potential of the Southern Aral Sea Basin (SASB) soils and sediments

General

As a result of the accelerated desiccation of the Aral Sea, deflation (wind erosion) of some of the soils in the Aral Sea Basin and of the dry Aral Sea bottom, has created an ecological disaster of gigantic proportion. The dust, generated on various land surfaces, is being moved in enormous quantities and deposited in far away areas. Containing a host of noxious compounds, including salts and pesticide/herbicide residues, the dust, where deposited, pollutes the soils and water bodies. Where inhaled by living beings, it causes chronic maladies and even early death. Studies leading to an elimination, or at least reduction in the dust generating process, are therefore of utmost importance.

Estimate of wind erosion potential of the soils

The soil size fraction of <850 μm eq. diameter (PM 850) was considered as a measure of the potential for wind erosion of the soils. Fig. 4 gives the data for the 8 Amu Darya soils, obtained by dry-sieving of uncrushed soils. From this figure, it can be seen that all soils have a very high proportion of particles <850 μm, and thus a very high wind erosion potential. The least endangered is the salt crust in soils 1, that has the relatively highest proportion of >850 μm particles.

Wind erosion parameters

During wind erosion, soil is transported in various modes, and the transport mode for a particular size particle is controlled by windspeed. In the wind erosion process, eroded particles move in creep, saltation, or suspension. Creep particles roll along the ground and have a diameter of 1 to 2 mm. Saltating particles have a diameter of 0.1 to 1.0 mm, and depending on surface roughness, particle size, distribution, and wind speed, move in a series of short hops at heights generally below 1 m. The suspended particles range from <0.001 to 0.1 mm in diameter and are subject to long-range transport.

In the following, friction velocity, threshold wind velocity and the effects of treatments on threshold wind velocity were determined. The treatments were moisture content and crust formation.

Equipment

Friction velocity and threshold wind velocity determinations were carried out in an open circuit wind tunnel of the suction type (Fig. 16). The wind tunnel had a working length of 9956 cm, and a height of 1200 cm.

Friction velocity

Under normal atmospheric conditions on flat, unvegetated surfaces and in the absence of intense solar heating, the turbulent velocity profile plots as a straight line on a semi-logarithmic chart. The gradient of the semi-logarithmic profile is a result of the surface roughness producing a

drag on the overlying airflow. If the gradient of the velocity profile is known, the shear stress at the surface can be determined. A common method for describing the gradient of the velocity profile is in terms of the friction velocity (u_*). The friction velocity is proportional to the velocity profile gradient and can be calculated from two velocities at known heights. Very close to the surface, the wind velocity is zero. The height of this zero-velocity region is termed the aerodynamic roughness length (z_0) and it is an important parameter for it is a function of the surface roughness and it partly controls the gradient of the velocity profile, and hence u_*. If friction velocities (u_*) increase, sediment transport would be likely to rise too.

The relationship between aerodynamic roughness (z_0), friction velocity (u_*) and wind velocity (u) at a height (z) are described by the Karman-Prandtl velocity distribution.

$$\frac{u}{u_*} = \frac{1}{\kappa} \ln \frac{(z-d)}{z_0}$$

where: κ = von Karman's constant ($\approx$0.4) and d=zero-plane displacement. Friction velocity (u_*) is commonly determined from regression analysis of time-averaged velocity measurements at several known heights.

Determination of friction velocity

The friction velocities results were obtained at the Ben-Gurion University wind tunnel (suction type). Soil moisture was measured for each soil sample on air-dry samples. The friction velocity was determined by the Karman-Prandtl equation:

$$u(z) = {u_*}/{k} \ln {z}/{z_0}$$

The wind velocities above soil surface were measured at 5-10 mm intervals, in order to receive a proper curve. For each wind velocity, three repetitions were made at each height above soil surface, for a minimum of 8 data points.

The conditions under which all the experiments were carried out were as follows:

- The soil surface was leveled by hand with a plastic roller, so that roughness varied only slightly, depending only on the size of the soil aggregates.
- The soil was uniformly mixed and free from visible organic residues.
- The soils, that had been passed through a 2.5 mm sieve, were air dried at the same conditions (humidity, temperature).
- The soil samples were placed on a plastic tray having the following dimensions: 1200Lx650Wx10H (cm). The tray was positioned inside the test section of the wind tunnel.
- The wind tunnel test section is: 1900Lx700Wx700H (cm), with a Plexiglas roof and door.
- The relative air humidity during the tests was constant (Beer-Sheva in summer).

- The relative air humidity during the tests was constant (Beer-Sheva in summer).
- The air flow within the tunnel was free from suspended particles, by working with a barred lab and air-conditioned system working during the tests.
- Pitot tubes measuring the wind velocity, were connected to a manometer (mm H_2O), and data logger.
- For each height above soil surface, the time for collecting data was at least three minutes, the first minute to stabilize wind velocity and the others to collect the data. The data were collected after the data logger, that was attached to the system, was showing a linear/parallel line on the computer screen (Figs. 4-7).

Three wind velocities were measured for each soil sample, below the saltation layer (at the range of 0-4.5 m/sec). The results for every soil sample are as follows:

With soil no.1 (crust) and soil no.2 it was clear that Z_0 was different at wind velocities greater than 4 m/sec. During the experiment, a creep motion of the soil surface was observed. This motion was not observed at smaller wind velocities or with the other soil samples at the wind velocities range that was measured.

The uncertainty of height measurement is +\- 1 mm.

Friction velocities (u*) and roughness height (z) of some Amu Darya soils.

Soil type	Friction velocity (m/sec) U*	Roughness height (mm) z
1 (crust)	0.225	1.313
	0.252	1.661
	0.234	0.541
1 (1-15)	0.163	0.415
	0.161	0.243
	0.191	0.282
2 (crust)	0.217	0.979
	0.189	0.939
	0.213	0.366
3	0.200	0.452
	0.187	0.313
	0.171	0.238

Threshold wind velocity

Sediment is entrained into the airflow when forces acting to move a stationary particle overcome the forces resisting sediment movement. Particles are subjected to three forces of movement: lift, surface drag and form drag. Lift is a result of the air flowing directly over the particle forming a region of low pressure. Surface drag is the shear stress on the particle provided by the velocity profile, and the form drag is also related to pressure differences around the particle. When these forces overcome the forces of particle cohesion, packing and weight, the particle tends to shake in place and then lift-off spinning into the airstream.

Aerodynamic entrainment is primarily a function of the mean grain size of the particles involved and the shear velocity of the wind. Bagnold (1941) studied these relationships and derived values of critical threshold friction velocity (u_{*ct}) for a wide range of particle sizes, with the principal determinant as the square root of grain diameter:

$$u_{*ct} = A\sqrt{\left[\frac{(\sigma-\rho)}{\rho}\right]gd}$$

where σ=particle density, g=acceleration due to gravity, d=grain diameter and A=constant dependent upon the grain Reynolds number ($\approx$0.1).

In general, larger particles have a higher threshold of entrainment. However, smaller particles (with diameters less than about 0.06 mm) also require higher shear velocities to entrain them. This is because particles in this size range and smaller tend to have additional molecular and electrostatic forces of cohesion. The most susceptible grain size for entrainment is seen to be between about 0.04 and 0.40 mm, i.e. sand-sized particles. The critical thresholds of motion on natural sediment beds are influenced by variations in factors such as sediment mixtures, surface crusting, surface slope, moisture and vegetation.

Moisture content

Although the potential influence of moisture content on the threshold of friction velocity has long been recognized, the exact physical nature of the relationship is still unknown. The theoretical basis for the available models are that the critical shear velocity increases as a function of the increased surface tension associated with pore moisture.

The Sensit

For the determination of the threshold wind velocity, a SENSIT instrument was used.

The Sensit Wind Eroding Mass Sensor gives researchers the ability to examine high-resolution erosion activity. The Sensit responds linearly to the impacting kinetic energy of wind blown particles. The Sensit output is representative of electrical charges produced by the

deformation of the piezoelectric sensor. This charge is proportional to the energy of impacting particles.

The relationship of total charge (q), voltage (V) and capacitance (C) is expressed as q=CV. The voltage developed across the integrating capacitor represents the charge in the capacitor as V=q/C. The voltage waveform of the charging integrator capacitor resembles an irregular stair step where each step represents a contribution of charge produced by the kinetic energy of individual impacting particles. When the voltage across the integrating capacitors exceeds an internal voltage reference, the capacitors are discharged allowing the process to repeat. The fast discharge pulse is stretched to become the kinetic energy output pulse representing a data value of one fixed unit of accumulated kinetic energy. A field calibration constant is obtained when the sum of output pulses from the sensor is referenced to the total collected mass from a sand catcher for an erosion event.

A minimum detectable particle diameter is difficult to estimate because of combined effects of mass, velocity and coefficient of drag. The sensor response drops off at roughly a 5th order function to particle diameter. This sharp cut-off function defeats response at approximately 50 to 75 microns for low velocity particles. The sensor does respond to high velocity particles from 10 to 50 micron in diameter. Particle diameters less than 10 microns tend to flow around the sensor due to the coefficients of drag.

The instrument has two data outputs. Kinetic energy and number of particle impacts. For reasons yet to be fully understood, the **kinetic energy** output has better than 0.997 r2 correlation to impacting mass and is used to measure saltating mass. The **particle impacts** output responds to individual impacting particles. All outputs are CMOS-TTL compatible (Q) pulses of 0→5 volts having a pulse width of greater than 650 uS producing a maximum data rate of 1538 pulses per second. Data acquisition is accomplished by a data logger counting the number pulses of both outputs for a user selected sampling period.

The kinetic energy output is the primary output. Each time the capacitor is discharged, an output pulse is produced. One pulse represents a fixed amount of accumulated energy. When the mass collected by a catcher is divided by the total number of KE output pulses for an erosion event, a rudimentary mass calibration constant is obtained. Multiplying the KE count for each sampling period by this constant reconstructs an informative high-resolution picture of the mass movement.

The kinetic energy signal is a continual background count for whatever data system sampling period is used. The background is the combination of a weak artificial current intentionally introduced into the integrator and natural electronic noise from the crystal sensor. All integrator current sources including electronic noise generated within electrical components contribute to the integration. This technique insure positive integration at all times and no threshold associated with the energy measurement.

The minimum detectable energy level is a function of the stability of background count. Detectivity and increased resolution is obtained by increasing the sampling time.

The second output is the number of particle impacts. Plotting this data as a function of shear stress (often synonymous with Friction Velocity (U^*) shows the threshold level of friction velocity where movement begins. Determining threshold is a valuable application of the Sensit since threshold changes as conditions change throughout an erosion event. Threshold depicts the minimum wind energy required to cause moment. Internally, this output does have an electrical trigger level. One pulse is produced for every particle impact of sufficient energy to trigger the particle count output circuitry.

Working method of threshold wind velocity

The wind velocity at the wind tunnel was determined by a resistor, and was measured at the center of the wind tunnel, out of the boundary layer, in order to obtain real velocity values without influence of the tunnel boundaries. The pitot tubes were calibrated by a differential pressure manometer (mmH_2O) in the range of 0-10 m/sec.

The values of the initial velocity were determined by pre-experiments that were carried out on local soils (Gilat, Nirim, Rehovot) with a soil texture similar to that of the Amu-Darya soils (with the exception of Rehovot soil). These soils gave us the ranges for the expected threshold wind velocities.

With the help of the computerized system it was possible to determine the velocity at which particle movement started.

The frequency of the measurement was 16 Hz (16 readings per second). The wind velocity and the particles impact are averages of 960 data points that were measured during the experiments (60 sec for each wind velocity level). That, in order to reduce the variance between the repetitions and to increase the resolution of the data points. The 16 Hz frequencies were determined by early experiments that were carried out. Since the experiments were controlled at lab conditions, we were able to measure with a high resolution compared to experiments carried out in the field.

The soil sample was placed 18 cm ahead of the "SENSIT" system. At any other distances, we noticed disturbances that the system caused, expressed by the large variance between the repetitions at the same wind velocity (Figs. 8a, b, c, d).

Results

Soil characteristics

(1) Particle size distribution (by Laser), salt-free (Fig. 2).

(2) Particle size distribution (by sedimentation), salt-free (Fig. 3 and Table 1).

(3) Soil characteristics – Table 2.

Soil characteristics relevant to wind erodibility evaluation (Table 2)

(1) PM_{850} particles in soils, by dry sieving (including salts) Fig. 4.

(2) 70-140 μm particles in soils, by dry sieving (including salts) Fig.5.

(3) Aggregate size distribution in soils, by dry sieving (including salts) Fig. 6.

Evaluation of soil erodibility in the wind tunnel

Wind speeds during some recent dust storms in the Southern Aral Sea Basin (Table 3).

(1) Determination of roughness length and friction velocity. Roughness length and friction velocity were determined for 3 wind velocities (Table 4).

(2) Determination of threshold wind velocity (TWV) for the soil samples at air moisture (Table 5).

(3) Determination of threshold friction velocity (TFV) for the soil samples, both measured and calculated (Table 6). TWV is given for the first grain "incipient" detachment, and also for the continuous detachment. Threshold friction velocity profiles for threshold wind velocity for the soil samples are shown in Fig. 7.

Evaluation of the effects of treatments on soil erodibility

(1) Effects of moisture on threshold wind velocity. Tables 7, 8, 9 show the effects of three levels of moisture on TWV in the 8 soil samples. Determinations were made for the first particle detachment and for the continuous detachments. Also shown is air humidity, temperature and barometric pressure, that all have an effect on the calculation of the threshold friction velocity (TFV). Repetitions of each moisture level are not the same, as it was impossible to obtain them. At all moisture levels examined, a significant increase in TWV with moisture was observed. This increase was due to the formation of a fine crust as a result of the desiccation.

(2) Effects of chemical soil stabilizer on threshold wind velocity.

Table 10 shows the effects of treatments including a low level (50 GPA) of stabilizer application, and a high level (65 GPA), on 5 soil samples. The salt crust from site 1, and the

desiccated sea bottom samples (sites 6 and 7) were not submitted to this test, since the application of chemical soil stabilizers to salt crusts was not deemed relevant. Evaluation of effects was by comparison to the TWV of the first detachment and of the continuous detachment for treated and untreated soils. Fig. 8 shows particle movements as registered by the SENSIT during the determination of TWV for the soil/crust samples, treated and untreated.

(3) The effects of soil crusts on their erodibility.

As a first step in the determination of wind erodibility on the soil crusts, these crusts had to be re-established from the loose material sampled on site. The salt crusts were recreated by the slow (up to 45 days) evaporation of water from water-saturated material placed on a specially built tray. Figs. 9-14 show the natural and the reconstructed crusts. Table 7 gives the TWV of the crusts, compared to the TWV of the loose material from which these crusts were reconstructed. For all the crusts, a dramatic increase in the TWV, both for the first (incipient) detachments, and for the continuous detachments, was registered. Fig. 15 shows the TWV on the crusts, as registered by the SENSIT The results of the erodibility trials on soil crusts indicate that no significant saltation movement of particles takes place as long as the crusts are intact. This is indicated by the very strong increase in the TWV. The wind energy created in the wind tunnel did not attain the level at which the friction pressure on the crust surfaces surpassed the threshold value necessary for the detachment of the particles. It is, however, known (see Table 3), that the peak wind velocity of many storms that occur yearly in the southern Aral Sea Basin surpasses the TWV for saltation movement of particles from crusts. This indicates that even surfaces covered by crusts in the area are not protected from wind erosion.

Sites from which samples were taken (Fig. 1):

Site 1: Taken from location 43°30'/59°56'.

Salt crust on a solonchak-like soil. The surface is covered by a bare, white, crust, 3-5 mm thick. The soil underneath is moist, of a grayish color (YR 6/1, Munsell). The texture is silty near the surface, and turns fine sandy with soil depth. Groundwater was encountered at 90 cm depth. A sample was taken from the salt crust and another from the soil underneath, 1-15 cm depth.

Site 2: Taken from location 43°25'/59°35' (Kazakhdarya).

Takyr crust on a takyr-like soil. The sampling surface is bare, but nearby the soil is cultivated. The dry, 5-10 mm thick crust is cracked into 10-15 cm wide polygons. The sample was taken from the crust.

Site 3: Taken from location 43°50'/59°05' (near Muynak)

Takyr-like soil. The surface is planted to acacia-like trees and plowed. The soil sample, taken from 0-25 cm depth, had a silty-loam texture. Because of the broken-up surface, no crust could be observed.

Site 4: Taken from location 43°28'/58°22'. Kungrad area.

The soil is a hydromorphic solonchak, covered with a soil crust. Sparse cover of shrubs. The soil crust was sampled.

Site 5: Taken from location 43°50'/58°35', Kungrad area.

Solonchak soil with salt cover. Very sparse cover of grasses. The salt crust was sampled.

Site 6: Taken from location 44°15'/58°23'. For about 10° years desiccated Aral Sea bottom, near the southern shore. Solonchak in development, with thick (2-3 cm) salt crust, bare, no vegetation.

Site 7: Taken from location 43°58'/59°02'. For about 15 years desiccated Aral Sea bottom, near to Muynak. Developing solonchak, with thick salt crust. No vegetation. The salt crust (2-3 cm thick) was sampled.

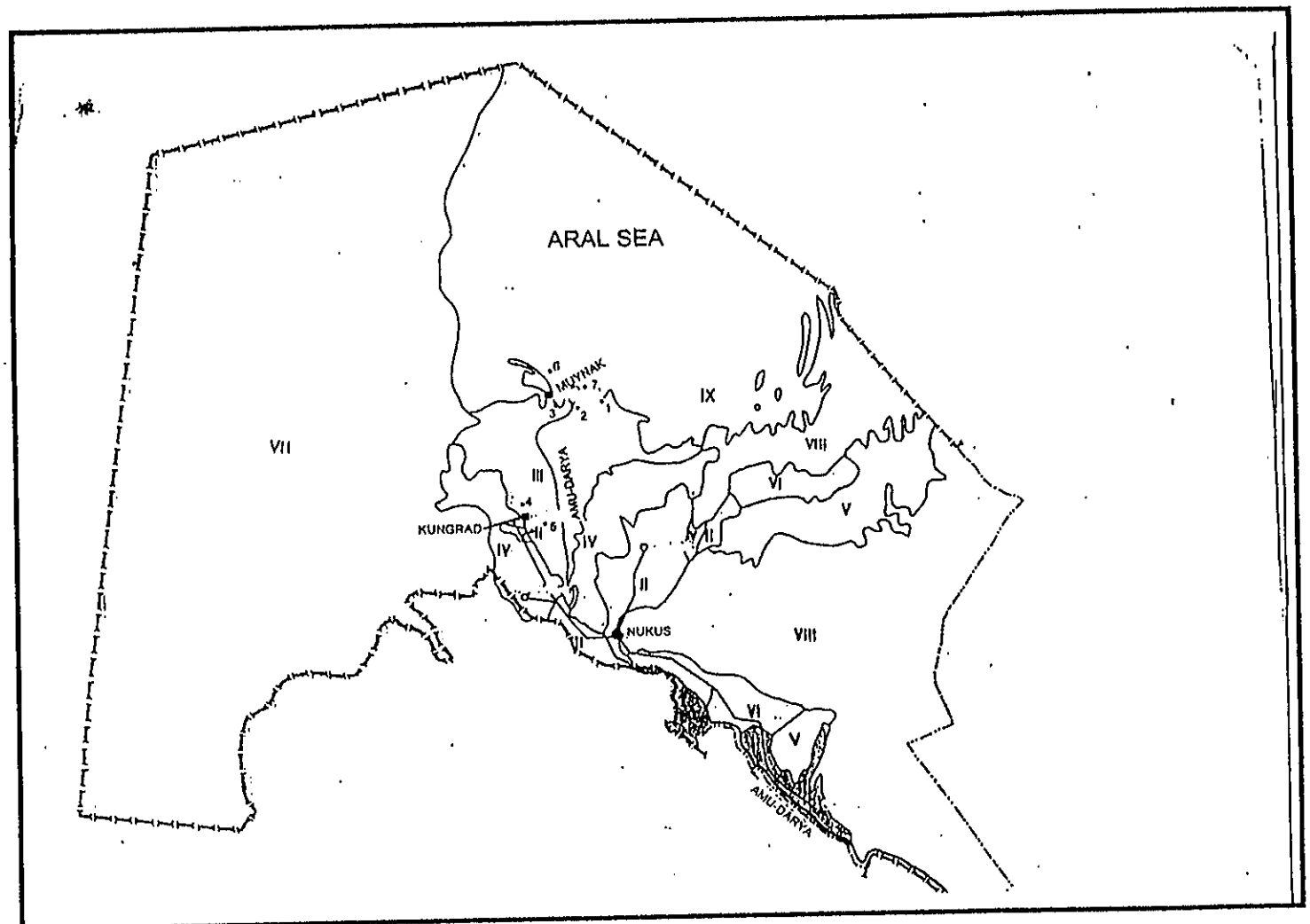

Figure 1: Schematic soil map of the Amu-darya river delta with sampling sites: 1 – site 1 with salt crust; 2 – Takyr crust; 3 – Takyr like soil's; 4 – Hydromorphic Solonchak; 5 – Solonchak; 6 – Desiccated sea bottom; 7 – Desiccated sea bottom.

Siegmar-W. Breckle · Maik Veste · Walter Wucherer (Eds.)

Sustainable Land Use in Deserts

With 122 Figures, 16 in Colour

Springer

Soil Crusts in the Amudarya River Delta: Properties and Formation

Arieh Singer, Amos Banin, Lev Poberejzsky and Moshe Gilenko

Keywords. Salt crusts, solonchaks, takyr soils, crust micromorphology, soil development

Abstract. Particle size distribution, salt content and composition, mineralogy and micromorphology of a solonchak salt crust and a takyr crust from the Amudarya River Delta (ADRD) were determined. In the (salt-free) salt crust, 100-μm particles dominate, while silt and fine sand are present in minor quantities only and clay is absent. The soil below the crust has a similar particle size distribution. In the takyr crust, fine particles dominate. In both crusts, quartz dominates, and is accompanied by calcite and mica. Clay minerals (chlorite and kaolinite) appear in minor amounts only. Cl is the major anion among the soluble salts, followed closely by sulfate. The salt crust contains four times more salt than the takyr crust. The salt in the salt crust appears in the form of crystallites of halite and Na, Mg sulfates such as thenardite and epsomite, in addition to gypsum. The size of the interlocking crystallites is 5–10 μm. The takyr crust is highly porous, with fine pores on the upper surface, and coarse pores in the bottom part of the crust. It is proposed that particle size distribution of the sediment and groundwater are among the important factors in determining the development pattern of Amudarya River delta soils. A fine particle size composition and absence of groundwater (including drainage water) close to the surface will lead to takyr formation. A relatively coarser particle size distribution and the presence of groundwater close to the surface will lead to solonchak (+salt crust) formation.

Introduction

The soils of the Amudarya River Delta (ADRD) can roughly be divided into soils associated with and affected by the floodplain (former and present) of the river. These include wetlands consisting of hydromorphic meadow and bog soils with a relatively high clay content, that are slightly to moderately saline; these soils, that were closest to the river, were subjected to annual spring flooding and were therefore only in limited agricultural use; their extent is approximately 800 000 ha. Other soils are hydromorphic meadow and bog soil formed on alluvium, that are

non-saline or only slightly saline; their extent is about 148 000 ha; finally, to this group of soils also belong hydromorphic meadow soils that are mildly to strongly saline and can consequently be termed solonchaks; their extent is over 460 000 ha. A second group of soils, more removed from the river bed, are the takyr soils; these soils are mildly to moderately saline, and partly also sodic; their extent is over 1 million ha; associated with them are gray-brown, sandy to loamy soils that are slightly saline; their extent is 306 000 ha. Finally, more removed from the river bed and on more elevated terrain to the west, are shallow, stony soils that are saline to varying degrees, from slightly saline when they are sandy, to more developed gypsic soils; their extent is 740 000 ha (Soil Survey Staff 1969).

This distribution of the ADRD suggests that with time and development, the river sediments develop either into strongly saline solonchak types of soils, or into less saline takyr types of soils. The most salient features of most solonchaks and takyrs are their crusts. In the following, some features of one solonchak crust and one takyr crust are given.

Sites and Methods of Examination

Sites

Sampling site I. Salt crust. Location: 43°30'/59°56'. The surface is covered by a nearly continuous whitish, 2–3-mm-thick salt crust (Fig. 1a). Small patches of reeds intervene between the salt covered surfaces. A core was taken down to 1 m depth. The profile is uniform, fairly wet, of a gray (10 YR 6/1, Munsell) color. Groundwater was encountered at 90 cm depth. The texture was silty at the surface, becoming more sandy (fine sand) with soil depth.

Sampling site II: takyr crust. Kasakhdaria. Location: 43°25'/59°35'. Cultivated fields are mainly on the northern side of the village. A sample was taken from an uncultivated area to the south of the village. Part of the surfaces was wet after some light rains. The dry surface portions were cracked into polygons, of roughly 5–10-cm diameter (Fig. 1b). The surface, partly occupied by bushes, was covered with a not very firm, undeveloped crust about 0.5 cm thick. Only the crust was sampled. The texture of the soil was silty clay.

Sampling site III. Muynak. Location: coord. 43°50'/59°05'. Stabilized surfaces, with a fairly dense cover of planted tamarisk-jangill. The sample was taken from an uncultivated field about 25 m east of a 10–12-m-wide ditch filled with water, that emptied a (storage?) lake near to Muynak into the Aral Sea. The sample of surface soil (up to 25 cm depth) was wet and had a sandy silt structure. No crusting could be observed. The wetness of the soil was due to rains that fell during the preceding night.

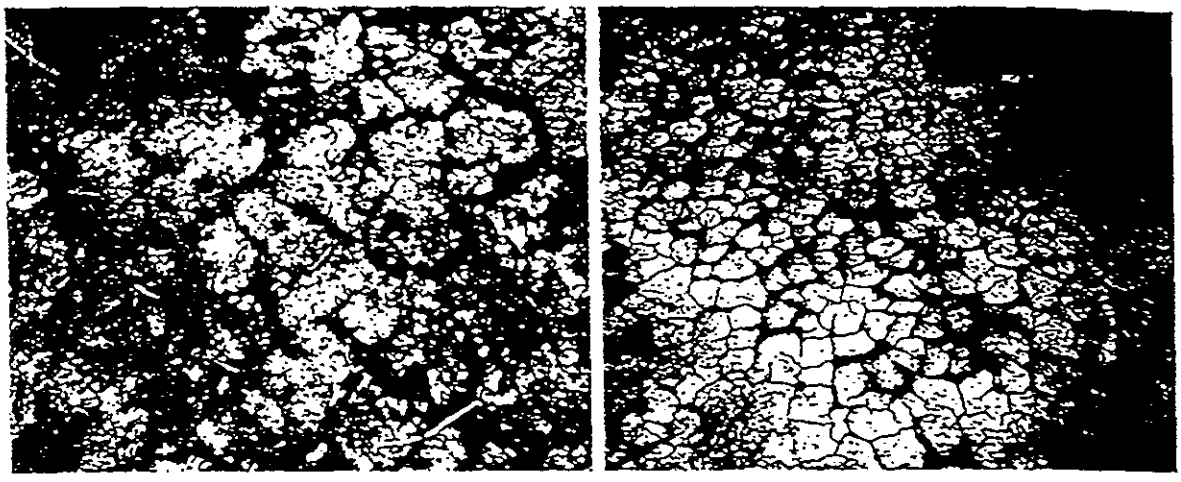

a b

Fig. 1.a.,b. Soil crusts in the Amudarya River Delta. a Salt crust at site I; b Takyr crust at site II

Soluble salts were extracted and analyzed by ICP and ion chromatography. Particle size distribution was determined by the sedimentation method and also by laser. Mineralogy of both natural and salt-free material was determined by XRD. The micromorphology and chemical composition of the crusts was examined by scanning electron microscopy, to which an EDSA was attached.

Results and Discussion

Particle-Size Distribution

The salt-free particle-size distribution of the salt crust is given in Fig. 2a as determined by laser and in Fig. 2b as determined by sedimentation. Particles of 100 μm equivalent diameter absolutely dominate. Coarse sand and clay are negligible; silt and fine sand are present in minor quantities only. The soil below the crust has a very similar composition. In the takyr crust from site II, on the other hand, the maxima had shifted to lower sizes, with a major peak at about 65 μm, and a smaller peak at 8 μm. This corresponds to finer sand and a sizable silt fraction. The soil at site III resembles the takyr crust. That suggests that takyr formation is favored when the particle–size distribution of the material is relatively finer.

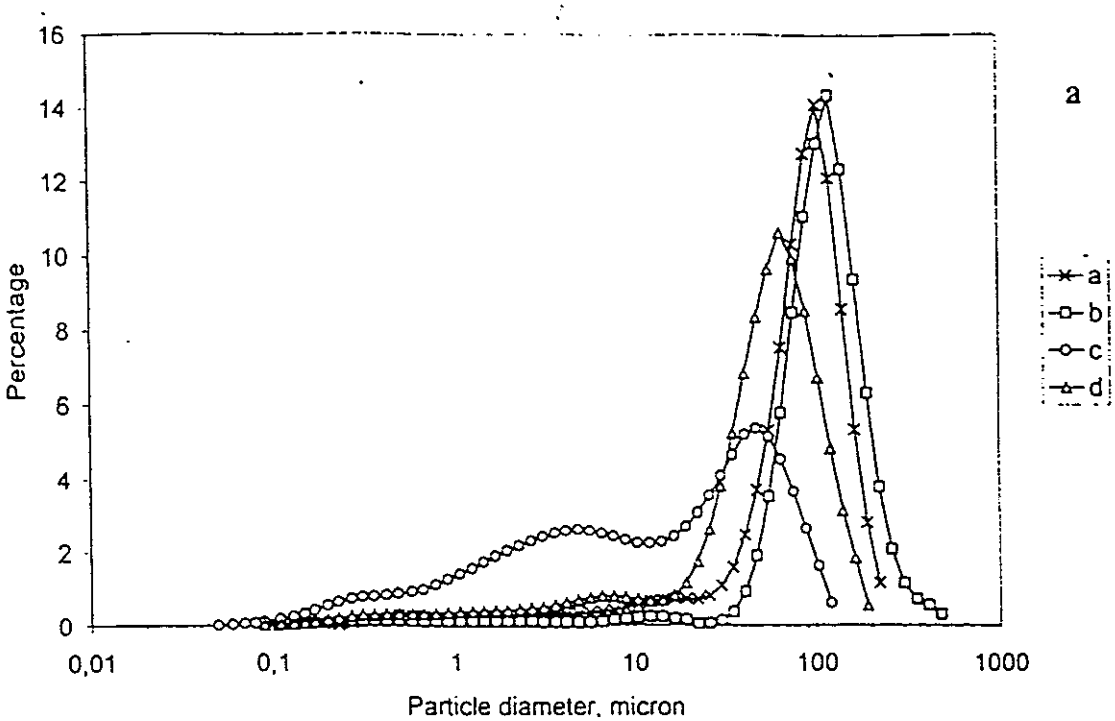

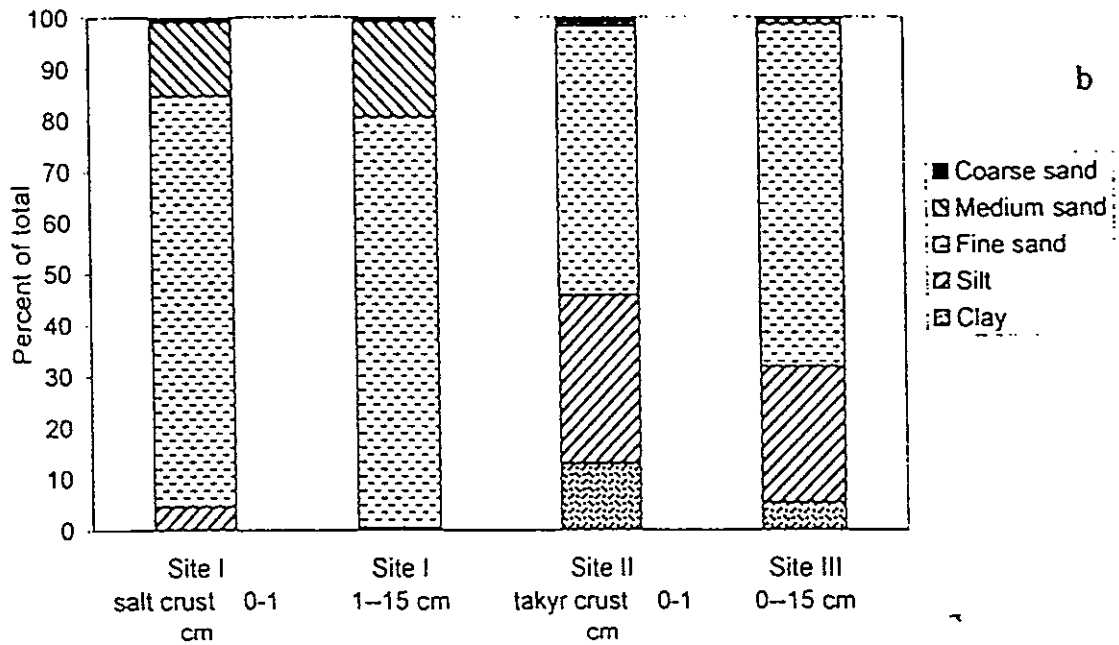

Fig. 2.a.,b. Salt-free particle size distribution of the crusts and soils. a as determined by Laser, *a* salt crust, site I; *b* soil below crust, site I; *c* Takyr crust, site II; *d* soil-plough layer, site III; b as determined by the sedimentation method

Mineral Composition

In the (salt-free) coarse sand of the solonchak crust (site I), quartz dominates, being accompanied by sizeable amounts of calcite and mica. Chlorite and kaolinite appear in minor amounts (Fig. 3.a). Only quartz is present in the medium and fine sand. In the silt, quartz is accompanied by kaolinite, mica, chlorite and feldspar. Below the crust, only quartz and calcite were identified in the coarse sand. In the finer fractions, calcite disappears, and feldspar, kaolinite, mica and chlorite appear in minor quantities. In the coarse sand of the takyr crust, quartz is accompanied by minor calcite. The fine sand has a similar composition, but in the medium sand, mica, chlorite and kaolinite are sizeable (Fig. 3.c). The silt has a similar composition. In the clay fraction also, quartz dominates, with minor kaolinite and mica. As in the crust of site I, calcite decreases with decreasing particle size.

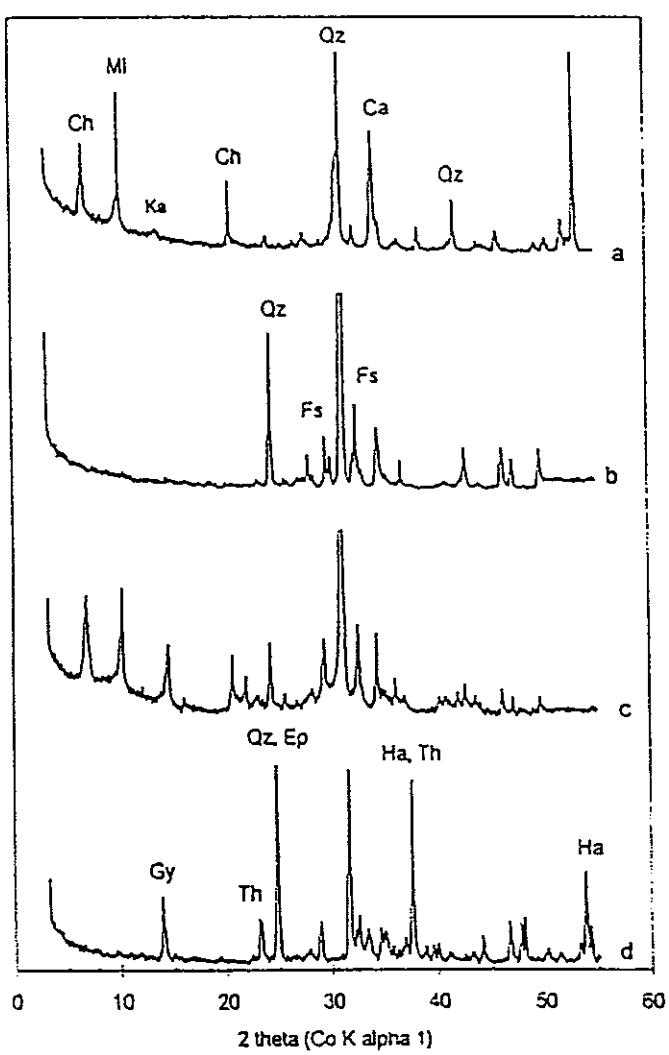

Fig. 3.a.-d. Mineral composition of crusts and soils as determined by XRD. a salt-free coarse sand of the salt crust at site I; b salt-free medium sand of the salt crust at site I; c medium sand of the takyr crust at site II; d bulk material including salts from the salt crust at site I; *Ch* chlorite; *Mi* mica; *Ka* kaolinite; *Qz* quartz; *Ca* calcite; *Fs* feldspar; *Gy* gypsum; *Ha* halite; *Th* thenardite; *Ep* epsomite

The mineral composition of the plough layer of site III is similar to that of the crust in site II, but calcite is preserved even in the fine-particle size fractions. The data indicate that there are no marked differences in the mineral (salt-free) composition of the solonchak and takyr crusts, and also that of the muynak soil.

Soluble Salts

Soluble salts were extracted from the soils (or crusts) by shaking in distilled water at a 1:10 ratio. Soluble cations were determined by ICP and soluble anions by ion gas chromatography. Soluble salt composition is given in Tables 1, 2 and 3. X-ray diffractometry was carried out using a Philips Model 1720 diffractometer.

Salts in the Crusts

From Table 1, it can be seen that the crust sampled from site I consisted of about 19% salt. Evidently, when the crust was sampled in the field much silicate material from below the salt crust proper, that adhered to it, was included in the sample. The salt content in the soil below the crust decreased to 3.1%. The crust on site II contained only 5.7% salt. Only 0.3% salt were determined in the crust-free soil from site III. The electrical conductivity (EC) measured in the extracts reflected these salt contents.

Table 1. Weight concentrations of salts in the crust/soils.

Site	Depth (cm)	Cations (%)	Anions (%)	Salt
I	Crust	5.11	14.05	19.15
I	1–15	1.02	2.07	3.09
II	Crust	1.71	3.98	5.68
III	0–15	0.11	0.19	0.30

Chloride was the major anion, followed closely by sulfate in the salt crusts of sites I and II (Table 2, and Fig. 4a,b). In the soil below the crust of site I and in the soil of site III, the concentration of sulfates was higher than that of chlorides. Nitrates were not present, except for traces in the crust of site II. The dominant cation in the salt crust of site I is sodium. Concentrations of Ca, Mg and K are relatively low (Table 2, Fig. 4b). In the soil below this crust, however, calcium dominates over sodium. Such is the case also in the soil of site III. In the crust of site II, concentrations of sodium and calcium are balanced. Potassium concentrations are also relatively high in the soil below the crust at site I.

The equivalent concentrations of Ca^{2+} and SO_4^{2-} are roughly equal in the soil of site I and the crust of site II, both being in the range of 20–30 $mEql^{-1}$. In the crust of site I, Ca concentration is also within this range. This suggests saturation with respect to solid phase $CaSO_4$ during the extraction and may have caused

underestimation of total salt content in these soil samples due to incomplete extraction of $CaSO_4$.

Table 2. Ionic composition of soluble salts in 1:10 soil:water extracts of some Amudarya River Delta soils. Table 2.a. Anions; Table 2.b. Cations

2.a. Anions (in $mEql^{-1}$)

Site	I	I	II	III
Depth (cm)	Crust	1–15	Crust	0–15
Cl^- Conc	159.3	17.7	54.1	0.2
(%)	54.9	43.9	62.9	6.7
SO_4^{2-} Conc.	131.1	22.6	31.7	2.7
(%)	45	56.1	36.8	90.0
NO_3^- Conc.	0	0	0.4	0.1
(%)	0	0	0.4	3.3
ΣA	290.4	40.3	86.2	3.0

2.b. Cations (in $mEql^{-1}$)

Site	I	I	II	III
Depth (cm)	Crust	1–15	Crust	0–15
Na^+ Conc.	189.0	11.4	38.3	0.8
(%)	81.8	24.3	47.5	15.4
K^+ Conc.	1.0	4.4	0.8	0.3
(%)	0.4	9.4	0.9	5.8
Mg^{2+} Conc.	13.5	4.4	4.8	0.5
(%)	4.3	9.4	5.9	9.6
Ca^{2+} Conc.	28.0	26.5	36.7	3.6
(%)	1.2	56.5	45.5	69.2
ΣC	231.4	40.3	80.6	5.2
RE	11.3	0	3.3	0

$$RE = \frac{\sum A - \sum C}{\sum A + \sum C}$$

It appears, even on the basis of these preliminary analyses, that Na and Cl are not the dominant cation and anion in this environment, and that it is dominated by Ca and SO_4.

The RE(%) is negative in three out of the four samples. This is probably due to the lack of data for carbonate/bicarbonate concentration in the extracts.

The soil from site III has low salinity and is practically well-leached. It is sandy-silty in texture and represents the eventual salinity state to which dried lake -bottom topsoils may evolve, following decades of downward leaching (by rain) and in the absence of capillary rise. Soils in sites I and II, on the other hand, represent conditions of active capillary-rise from shallow groundwater.

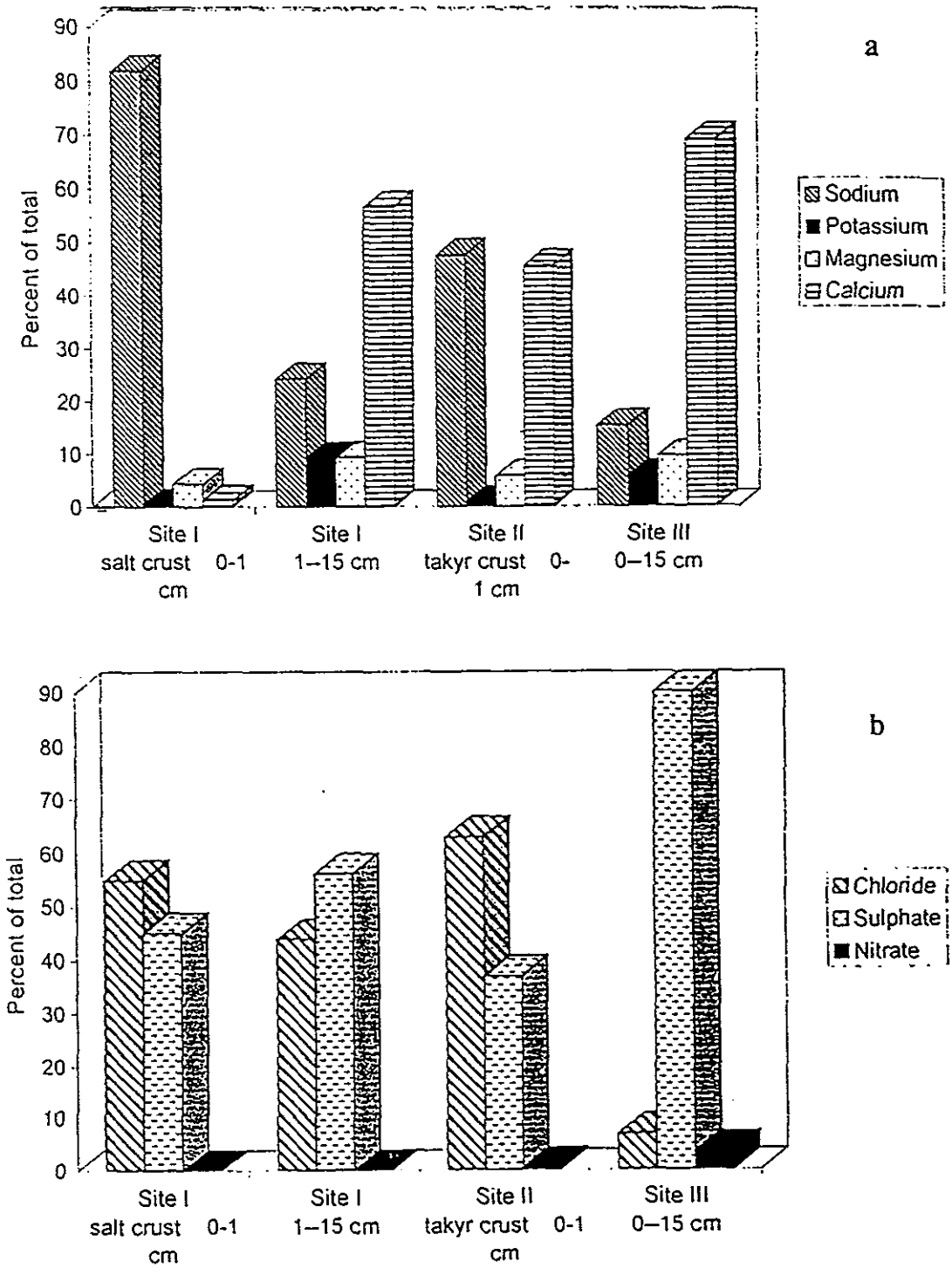

Fig. 4.a.,b. Ionic composition of soluble salts of the salt crust on site I. a ions; b cations

These results are corroborated by X-ray diffractograms of untreated (except crushing) bulk material. For the crust material on site I, a strong diffraction at 2.78 Å indicates the presence of halite (NaCl) and possibly of thenardite (Na_2SO_4) (Fig. 3d). A line at 7.50 Å indicates the presence of gypsum ($CaSO_4 \cdot H_2O$). The relatively high concentration of sulfates suggests that thenardite is one of the principal sulfate salts, though the presence of some bloedite ($Na_2Mg\ SO_4 \cdot 4H_2O$) or konyaite [$Na_2Mg(SO_4) \cdot 5H_2O$] cannot be excluded. The line at 4.19 Å suggests

also the presence of epsomite ($MgSO_4 \cdot 7H_2O$). Salt concentrations in the other materials were too low to be detectable by X-ray diffraction.

Micromorphological and Chemical Examinations

Micromorphology and chemical composition of preserved portions of the salt crust were examined using a scanning electron microscope (JEOL 5410 LV), with an EDAX attachment). Natural, undisturbed fragments of the crust were mounted on stubs, and coated under vacuum with either carbon or gold.

The salt crust was observed to consist of one layer, in which salt crystallites were arranged in one dense, interlocking matrix (Fig. 5a). Chemical scan showed the crystallites to be composed of sodium and magnesium sulfates and chlorides (Table 1). Spot analysis of individual crystallites suggested that the crystallites were either sulfates or chlorides, but not mixed salts. By their cubic habit, halite crystallites were easily recognizable (Fig. 5b). The chemical composition of these crystallites (by spot analysis) indicates only Na and Cl, with some small, additional amounts of Mg. Some of the crystallites were pitted by secondary solution channels. The size of the crystallites varied between 5 and 10 μm.

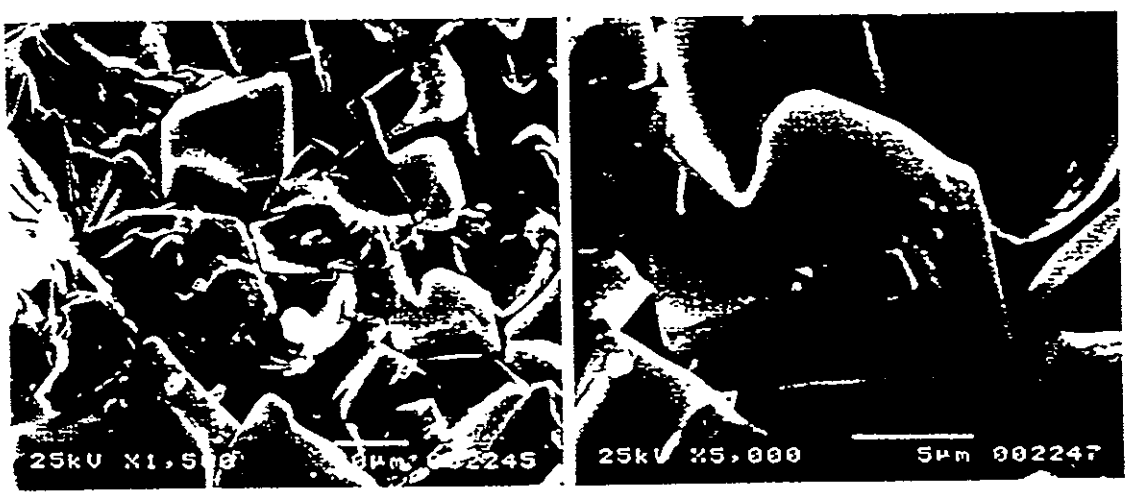

a b

Fig. 5.a.,b. Micromorphology by SEM of portions from the salt crust at site I. a matrix of salt crystallites; b halite crystallites

In the chemical composition of many other crystallites, sulfates could also be identified. The most common cations associated with the sulfates were Na and Mg. By morphology alone, it was impossible to determine whether these salts were orthorombic thenardite (Na_2SO_4), monoclinic mirabilite, or the combined salt bloedite ($Na_2Mg\ SO_4 \cdot 4H_2O$).

Frequently, the dense halite interlocking mosaic layer was overlain by discontinuous gypsum crystallites. The gypsum crystallite appeared to be in a state of decomposition.

In conclusion, SEM+EDAX examination of crystallites support the data obtained by the chemical analysis of the dissolved salts from the salt crust, namely, that the major salt is halite, followed by sulfate salts such as Nasulfate (thenardite) and possibly mixed Na, Mg sulfate salts, such as bloedite and mirabilite. Casulfate salts (gypsum) were observed to form as second-generation salts on top of the halite layer.

The upper surface of the takyr crust, of a thickness varying between 5 and 8 μm, was smooth (between the cracks) and shiny. The upper surface appeared to be dense, but under magnification was seen to contain many fine pores of a diameter varying between 5 and 10 μm (Fig. 6a). The bottom part of the crust was outright vesicular, with the diameter of the vesicles varying between 200 and 300 μm (Fig. 6b). Chemical analysis indicated particles in the surface part of the crust to consist of mica, quartz and Fe, Al silicates.

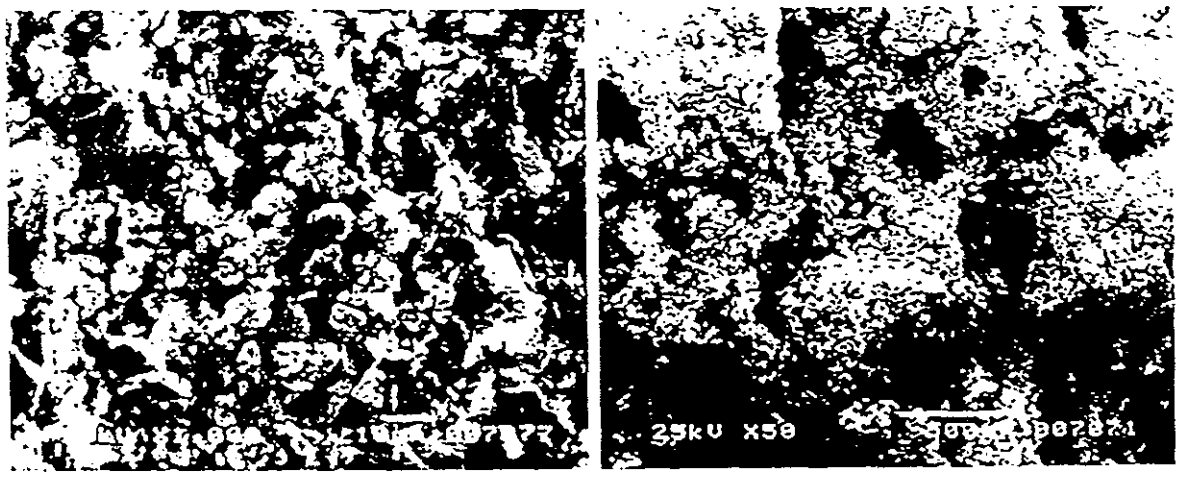

a b

Fig. 6.a.,b. Micromorphology by SEM of portions from the takyr crust at site II. a upper surface of the crust; b bottom part of the crust

Proposed Pathways for the Development of Soils and Crusts from the Aral Sea Bottom Following its Exposure by Desiccation

Salt efflorescences on soils are well-known phenomena in arid and semiarid regions where actual annual evapotranspiration greatly exceeds precipitation. Driessen and Schoorl (1973), for example, described evaporites from Turkish soils subjected to an annual rainfall of 240 mm, and Guzmuzzio et al. (1982) reported the mineral composition of efflorescences in saline soils of Spain. Eghbal et al. (1989) described soils with evaporites from California that have a xeric to aridic (150 mm a^{-1}) moisture regime. The common sources of the salts are seepages of runoff, springs and dry river channels that drain salt-containing rock formations. In less common cases, the origin of the salts was shown to be atmospheric deposition (Singer et al. 1999). In the present case, it is evident that the salts in the

crust had accumulated by the evaporation of groundwater, though a contribution by salt-containing dust is probable also.

Vast areas of the former Aral Sea floor have become desiccated and are in the process of developing into soils. The study of salt distribution in the ADRD may help in predicting into what type of soils the exposed Aral Sea floor will eventually evolve.

Bottom material that is fine-sandy to sandy in texture desiccates to form sand dunes. There will therefore be only limited capillary rise of groundwater and accumulation of salts on the surface. Crust formation will be minimal. The land surface will remain bare, and serve as a source area for short-range aeolian transport of coarse-grained particles. The shifting dunes will be mostly unconnected with groundwater but fed by the, albeit limited, local rainfall. In due time, vegetation can establish itself on these dunes.

If groundwater is close to the surface, with time, active capillary rise and evaporative processes will lead to salt accumulation and crust formation. The time required for the salt crusts to develop is estimated to be approximately 5–10 years. In the presence of the salt crusts, the surface will remain bare (no vegetation) because of the high salinity. This is the common pathway for solonchak soil formation.

Well-developed and cemented crusts, even if totally composed of salts, can be expected to protect the surface from wind erosion. Dust generation will be reduced, because dust entrainment from crusts will be reduced. While it can be expected that salt crusts will be more resistant towards deflation, electron microscopy has shown (see below) that the salt crust is frequently overlain by second generation powdery and fine-grained salt crystallites – not yet very consolidated.

Salt crusts will develop not only in the presence of groundwater close to the surface, but also when periodic flooding takes place. Salt crusts and salt pans develop upon evaporation from various small waterbodies in the Amudarya River Delta. The source of these water bodies is not clear. They possibly represent (1) entrapped sea water or (2) surface runoff of rainwater that had collected in depressions. Mostly likely they are (3) artesian seepage of shallow groundwater fed by drainage water from the irrigated areas of the delta lying to the south.

In the absence of groundwater (or surface water) close to the surface, salt crusts will not form, or will form only to a very minor degree. Clay crusting will take place and ultimately takyr soils will form. The rate of formation of these crusts is much slower than the salt crusts. Dust entrainment from these surfaces will be much more pronounced. After some time, vegetation of shrub-like xerophytes and halophytes (such as tamarisks and jangill) will take root in these areas. As vegetation covers the surface, deflation will decrease. Vegetation recovery apparently can take place relatively rapidly, within 15–20 years of the exposure of the sea bottom. The local rainfall (annual average 100 mm) appears to be sufficient to support this vegetation in non-cultivated areas, stabilizing their surface against further wind erosion. An example of this pathway are the extensive shrub-covered areas east and southeast of Muynak.

Acknowledgements. This research was supported under Grant No. CA16-013 US -Israel Cooperative Development Research Program, Economic Growth, US Agency for International Development.

References

Driessen PH, Schoorl R (1973) Mineralogy and morphology of salt efflorescences on saline soils in the Great Kenya Basin, Turkey. J Soil Sci 24:437–451

Eghbal MK, Southard RJ, Whittig LD (1989) Dynamics of evaporite distribution in soils on a fan-playa transect in the Carizzo Plain, California. Soil Sci Soc Am J 53:898–910

Guzmuzzio J, Battle J, Casas J (1982) Mineralogical composition of salt efflorescences in a typical salorthid, Spain. Geoderma 28:39–55

Singer A, Kirsten WF, Bühmann C (1999) A proposed fog deposition mechanism for the formation of salt efflorescences in the Mpumalanga Highveld, Republic of South Africa. Water Air Soil Pollut 109:313–325

Skarie RL, Richardson JL, McCarthy GJ, Maianu A (1987). Evaporite mineralogy and groundwater chemistry associated with saline soils in eastern North Dakota. Soil Sci Soc Am J 51:1372–1378

Soil Survey Staff (Antizatorova et al.) (1969) Soil map of the Karakalpak Autonomous Region. Scale of 1:200 000. Ministry of Interior, Nukus

Table 1. Particle-size distribution of the (salt-free) soil/crust samples, as obtained by the sedimentation method.

Table 2. Relevant characteristics of the soil/crust samples.

Table 3. Wind speeds during some recent dust storms in the southern Aral Sea Basin.

Table 4. Friction velocity determinations for the soil/crust samples, determined in the wind tunnel at 3 wind velocities.

Table 5. Threshold wind velocity (TWV) for the soil/crust samples, determined in the wind-tunnel at air-dry moisture of the samples.

Table 6. Threshold friction velocity (TFV) for the soil/crust samples, both measured and calculated. TFV is given both for "incipient" detachment and "continuous" detachment.

Tables 7, 8, 9. Effects of three moisture levels on the threshold wind velocity (TWV) for both the "incipient" and the "continuous" detachment. Two repetitions for each level, with the levels not necessarily equal.

Table 10. Effects of the treatments with the chemical soil stabilizer "SOIL SEAL" on the threshold wind velocity (TWV) for both the "incipient" and the "continuous" detachment of 5 soil/crust samples. Results for 2 levels of stabilizer application are given.

Table 11. Threshold wind velocities (TWV) of natural, air-dry soil/crust material, compared to that of the constructed crusts.

Fig. 15. Particle movements as registered by the SENSIT during determination of TWV for the reconstructed crusts.

Fig. 1. Schematic soil map of the Amu Darya river delta with sampling sites: 1 – site 1 with salt crust; 2 – Takyr crust; 3 – Takyr-like soils; 4 – Hydromorphic solonchak;p 5 – Solonchak; 6 – Desiccated Aral Sea bottom; 7 – Desiccated Aral Sea bottom.

Fig. 2. Particle-size distribution (by Laser) of the soil/crust samples (free of salts).

Fig. 3. Particle-size distribution of the (salt-free) soil/crust samples, as obtained by the sedimentation method.

Fig. 4. PM_{850} particles of the soils/crust samples as obtained by dry sieving.

Fig. 5. 0.07- 0.14 mm particles in the soil/crust samples as obtained by dry sieving.

Fig. 6. Aggregate size distribution in the soil/crust samples, as obtained by dry sieving.

Fig. 7. Threshold friction velocity profiles of the soil/crust samples as determined in the wind tunnel.

Fig. 8. Particle movements as registered by the SENSIT during the determination of TWV for the soil/crust samples, treated and untreated, in the wind tunnel.

Figs. 9-14. Photographs of natural and reconstructed soil crusts, including salt crusts and Takyr crusts.

Fig. 15. Particle movements as registered by the SENSIT during determination of TWV for the reconstructed crusts.

Fig. 16. Suction type wind tunnel. SENSIT can be seen in foreground.

	Site	Surface texture	Clay	Silt	F. sand	C. sand
1	Salt crust	Sand	2.80%	6.78%	89.25%	1.16%
	1-15 cm	Sand	1.76%	2.03%	87.60%	8.57%
2	Takyr crust	Loam	19.46%	36.38%	44.18%	0.00%
3	Soil 0-15 cm	Loamy sand	5.14%	10.42%	84.49%	0.00%
4	Wet Solonchak	Sandy loam	5.76%	26.32%	65.54%	2.36%
5	Dry Solonchak	Sandy loam	4.30%	31.64%	62.88%	1.16%
6	Desiccated sea bottom	silt loam	13.44%	59.16%	22.32%	4.94%
7	Desiccated sea bottom	silt loam	9.44%	51.72%	38.60%	0.14%

Table 1: Particle size distribution of the (salt free) soil/crust samples, as obtained by the sedimentation method.

Site		O. C.#	$CaCO_3$	Salts	Air dry Moisture
1	Salt crust	0.83%	8.77%	42.70%	2.283%
	1-15 cm	0.28%	16.09%	3.09%	0.798%
2	Takyr crust	1.56%	8.01%	5.68%	2.873%
3	0-15 cm	0.96%	14.25%	0.30%	0.686%
4	Hydromorphic Solonchak	1.62%	10.24%	19.5%	3.385%
5	Solonchak	0.89%	10.59%	9.80%	0.9845
6	Desiccated sea bottom	0.44%	7.45%	64.80%	5.475%
7	Desiccated sea bottom	0.76%	10.00%	53.60%	5.622%

Table 2: Relevant characteristics of the soil/crust samples.

O.C – Organic Carbon

Wind speeds (av. and maxima) of recent major dust storms in the southern Aral Sea Basin

Meteorological stations

Karakalpakia

Year	*Month*	*Date*	*Duration of dust storm*	*Wind direction (degree)*	*Ave. wind speed*	*Max. Wind speed*
1997	*4*	*8*	*5*	*180*	*4*	*20*
	5	*13*	*14*	*337*	*6*	*17*
	8	*5*	*55*	*157*	*4*	*16*
	11	*23*	*435*	*90*	*9*	*17*
1998	*4*	*21*	*580*	*112*	*10*	*26*
		22	*10*	*90*	*4*	*18*
	7	*20*	*20*	*292*	*4*	*14*
	7	*23*	*52*	*67*	*5*	*13*
	9	*3*	*82*	*292*	*6*	*15*
	10		*67*	*270*	*5*	*12*
		29	*322*	*112*	*7*	*19*
1999	*4*	*4*	*11*	*292*	*7*	*20*
			7	*292*	*7*	*20*
	7	*5*	*5*	*292*	*4*	*11*
		10	*8*	*337*	*4*	*13*
		12	*37*	*292*	*4*	*15*
		29	*8*	*67*	*3*	*14*
	8	*6*	*20*	*202*	*3*	*17*
			10	*202*	*3*	*17*
			30	*157*	*3*	*16*

Kungrad

Year	*Month*	*Date*	*Duration of dust storm (min)*	*Wind's direction (degree)*	*Ave. wind speed (m/sec)*	*Max. Wind speed (m/sec)*
1998	*5*	*11*	*45*	*340*	*6*	*15*
2000		*9*	*25*	*270*	*19*	*34*
2001	*4*	*7*	*285*	*360*	*15*	*18*

Table 3

Chimbay

1997	4	30	125	225	12	15
			60	225	12	15
	5	20	180	360	9	13
			300	315	8	12
	6	3	205	225	8	15
		4	155	360	6	8
	7		60	270	12	15
		5	160	135	3	5
		8	75	290	13	15
		31	120	315	12	14
	8	21	305	360	10	12
		22	174	360	5	9
1998	4	16	40	225	4	6
	5	18	190	20	14	17
		19	180	45	7	17
1998	5	19	160	180	14	17
		23	95	315	20	25
	6	9	15	45	20	25
	11		100	225	13	17
		10	150	225	6	8
1999	4	6	170	315	15	20
	5	8	598	360	15	20
		15	240	180	15	20
	6	6	38	45	4	20
		10	25	360	12	15
		16	40	250	15	20
		17	165	360	7	20
	7	12	30	315	15	20
		13	130	315	7	11
2000	3	12	130	270	13	17
		13	360	90	3	17
			20	270	11	17
		19	410	135	16	18
		20	355	135	5	17
	4	10	10	110	17	23
			260	110	17	23
	5		63	180	15	25
			45	180	15	25
			95	180	15	25
		14	10	360	10	13
	7	21	15	340	13	18
		22	145	360	9	18
	8	16	260	250	13	18
2001	3	4	130	250	13	18
2001	4	22	120	110	11	17

Site	Sediment source	Friction velocity (m/sec)		
		V 1	V 2	V 3
1	Salt crust	0.225	0.252	0.234
	1-15 cm	0.163	0.161	0.191
2	Takyr crust	0.189	0.217	0.213
3	Soil, 0-15 cm	0.171	0.200	0.187
4	Hydromorphic Solonchak	0.176	0.202	0.234
5	Solonchak	0.184	0.191	0.188
6	Desiccated sea bottom crust	0.177	0.224	0.239
7	Desiccated sea bottom crust	0.168	0.213	0.230

Table 4: Friction velocity determinations for the soil/crust samples, determined in the wind tunnel at 3 wind velocities.

site	Sediment source	TWV of first detachment (m/sec)	average (m/sec)	std (m/sec)	TWV of continuously detachme	average (m/sec)	std (m/sec)	Air Dry Moisture (%)
1	salt crust	7.33 6.09 7.23 8.26 7.85 7.29	7.34	0.67	7.59 6.23 7.23 8.79 8.50 7.29	7.61	0.85	2.283%
	1-15 cm	5.92 6.03 5.92	5.95	0.05	6.07 6.03 5.92	6.00	0.06	0.798%
2	Takyr crust	5.93 6.28 5.83	6.01	0.19	6.07 6.29 6.15	6.17	0.09	2.873%
3	soil 0-15 cm	6.59 6.68 6.61	6.63	0.04	6.95 6.68 6.61	6.75	0.15	0.686%
4	Hydromorphic Solonchak	6.31 6.74 6.80	6.62	0.22	7.34 7.87 6.80	7.34	0.43	3.385%
5	Solonchak	7.28 7.37 7.67	7.44	0.17	7.85 7.84 7.60	7.76	0.11	0.984%
6	Desiccated sea bottom	6.84 7.33 6.64	6.94	0.29	6.84 8.22 7.45	7.50	0.56	5.475%
7	Desiccated sea bottom	6.40 6.40 7.22	6.67	0.39	6.92 6.78 7.22	6.97	0.18	5.622%

Table 5: Threshold wind velocity (TWV) for the soil/crust samples, determined in the wind tunnel at air-dry moisture of the samples.

site	sediment source	Measured TFV (m/sec)	Calculated TFV of first detachment (m/sec)	std	Calculated TFV of continuously detachment (m/sec)	std
1	Salt crust	0.308	0.361 0.300 0.356 0.407 0.387 0.359	0.033	0.374 0.307 0.356 0.433 0.419 0.359	0.042
	1-15 cm	0.224	0.252 0.257 0.253	0.002	0.259 0.257 0.253	0.003
2	Takyr crust	0.291	0.281 0.298 0.277	0.009	0.288 0.298 0.292	0.004
3	Takyr like	0.279	0.281 0.285 0.282	0.002	0.281 0.285 0.282	0.002
4	Hydomorphic Solonchak	0.313	0.273 0.291 0.294	0.009	0.317 0.340 0.294	0.019
5	Solonchak	0.344	0.324 0.328 0.341	0.008	0.349 0.349 0.338	0.005
6	Desiccated sea bottom	0.363	0.275 0.295 0.267	0.012	0.275 0.331 0.300	0.023
7	Desiccated sea bottom	0.363	0.307 0.307 0.347	0.019	0.332 0.325 0.347	0.009

Table 6: Threshold friction velocities (TFV) for the soil/crust samples, both measured and calculated. TFV is given both for "incipient" detachment and "continuous" detachment.

Sediment source	TWV of first detachment (m/sec)	TWV of continuously detachment (m/sec)	Soil moisture (%)	Air Humidity	Barometric pressure (mb)	Temp (celsius)		
Salt crust	13.11	16.52	4.797	54.40%	982	24.32	level 1	Exp 1
	15.02	16.16	7.127	50.11%		25.01	level 2	
	16.75	16.75	11.974	51.79%		24.78	level 3	
	11.98	12.59	5.844	No data	No data	No data	level 1	Exp 2
	11.80	14.39	7.552	No data		No data	level 2	
	15.05	15.09	8.942	No data		No data	level 3	
1-15 cm	11.59	12.00	4.749	74.80%	982	21.43	level 1	Exp 1
	13.03	14.19	3.590	68.09%		22.41	level 2	
	17.20	17.20	5.903	65.26%		22.72	level 3	
	11.02	11.95	2.955	No data	No data	No data	level 1	Exp 2
	12.55	15.12	4.894	No data		No data	level 2	
	14.47	15.52	5.707	No data		No data	level 3	

Sediment source	TWV of first detachment (m/sec)	TWV of continuous detachment (m/sec)	Soil moisture (%)	Air Humidity	Barometric pressure (mb)	Temp (celsius)		
Takyr crust	6.15	6.91	7.310	62.00%	983	23.18	level 1	Exp 1
	9.07	9.37	10.852	61.44%		23.21	level 2	
	12.21	13.59	12.702	57.67%		23.80	level 3	
	6.63	6.63	5.741	No data	No data	No data	level 1	Exp 2
	11.42	11.97	No data	No data		No data	level 2	
	13.84	14.12	12.086	No data		No data	level 3	
	9.65	no continuous detachment	8.291	60.81%	979	23.91	level 1	Exp 3
	12.35	no continuous detachment	11.785	59.17%		24.11	level 2	
	14.23	14.23	15.225	59.17%		24.11	level 3	

Table 7

Sediment source	TWV of first detachment (m/sec)	TWV of continuous detachment (m/sec)	Soil moisture (%)	Air Humidity	Barometric pressure (mb)	Temp (celsius)		
Takyr like (0-15 cm)	8.46	8.55	4.985	51.76%	981	24.69	level 1	Exp 1
	11.92	12.67	4.960	48.82%		25.03	level 2	
	14.90	16.80	7.011	50.50%		25.37	level 3	
	6.94	12.07	9.759	60.99%	986	19.80	level 1	Exp 2
	15.27	15.88	11.523	64.44%		19.77	level 2	
	16.31	16.35	11.475	63.83%		20.47	level 3	
	11.80	12.34	5.252	66.23%	978	23.49	level 1	Exp 3
	Not measurable	Not measurable	7.497	66.46%		23.12	level 2	
	Not measurable	Not measurable	10.861	66.29%		23.08	level 3	

Sediment source	TWV of first detachment (m/sec)	TWV of continuously detachment (m/sec)	Soil moisture (%)	Air Humidity	Barometric pressure (mb)	Temp (celsius)		
Hydromorphic Solonchak	8.14	9.11	14.273	89.00%	986	13.88	level 1	Exp 1
	11.21	11.21	19.311	89.50%		13.88	level 2	
	10.96	11.32	25.294	89.50%		13.98	level 3	
	10.29	10.29	8.775	47.97%	987	16.52	level 1	Exp 2
	11.90	no continuously detachment	12.847	44.03%		16.75	level 2	
	13.01	no continuously detachment	19.459	43.43%		17.06	level 3	
	9.84	9.84	11.370	97.10%	983	7.66	level 1	Exp 3
	11.71	no continuously detachment	16.133	98.20%		7.60	level 2	
	13.25	13.25	21.479	99.10%		7.60	level 3	

Sediment source	TWV of first detachment (m/sec)	TWV of continuous detachment (m/sec)	Soil moisture (%)	Air Humidity	Barometric pressure (mb)	Temp (celsius)		
Solonchak	10.45	10.95	5.140	37.40%	986	18.23	level 1	Exp 1
	13.34	13.40	6.760	37.00%		18.36	level 2	
	13.51	no continuous detachment	10.776	35.47%		18.52	level 3	
	11.25	11.94	6.991	98.30%	983	8.18	level 1	Exp 2
	13.58	no continuous detachment	8.464	100.00%		9.84	level 2	
	13.36	13.52	11.946	99.60%		8.49	level 3	
	13.60	Not measurable	No data	57.64%	981	19.37	level 1	Exp 3
	Not measurable	Not measurable	No data	52.61%		19.71	level 2	
	Not measurable	Not measurable	No data	51.89%		19.43	level 3	

Table 8

Sediment source	TWV of first detachment (m/sec)	TWV of continuous detachment (m/sec)	Soil moisture (%)	Air Humidity	Barometric pressure (mb)	Temp (celsius)		
Desiccated sea bottom	Not measurable	Not measurable	12.079	61.59%	978	24.16	level 1	Exp 1
	Not measurable	Not measurable	18.410	62.40%		23.98	level 2	
	Not measurable	Not measurable	No data	No data	No data	No data	level 1	Exp 2
	15.72	אין	16.532	60.90%	979	24.40	level 1	Exp 3
	Not measurable	Not measurable	26.949	62.22%		24.46	level 3	

Sediment source	TWV of first detachment (m/sec)	TWV of continuously detachment (m/sec)	Soil moisture (%)	Air Humidity	Barometric pressure (mb)	Temp (celsius)		
Desiccated sea bottom	14.27	no continuously detachment	14.520	38.81%	986	18.69	level 1	Exp 1
	14.33	no continuously detachment	17.282	38.86%		18.74	level 2	
	14.38	no continuously detachment	24.662	39.04%		18.98	level 3	
	Not measurable	Not measurable	No data	49.49%	981	19.64	level 1	Exp 2
	Not measurable	Not measurable	No data	47.90%		19.84	level 2	
	Not measurable	Not measurable	14.576	29.92%	981	21.32	level 1	Exp 3
	Not measurable	Not measurable	26.402	27.82%		22.22	level 3	

Table 9

Tables 7, 8, 9: Effects of three moisture levels on the threshold wind velocity (TWV) for both "incipient" and the "continuous" detachment. Two repetitions for each level, with the levels not necessarily equal.

site	Sample source	SSPCO. Concentration	TWV of first detachment (m/sec)	TWV of continuous detachment (m/sec)	Soil Seal effect	
					First detachment	Continous detachment
1	Soil, 1-15 cm	untreated soil	5.954	6.07	=====	
		50 GPA	7.816	7.82	31.28%	30.17%
		65 GPA	9.579	10.77	60.89%	79.29%
2	Takyr crust	untreated soil	6.015	6.07	=====	
		50 GPA	8.716	8.716	44.91%	41.27%
		65 GPA	6.889	8.175	14.54%	11.66%
3	Takyr like	untreated soil	6.628	6.952	=====	
		50 GPA	8.971	9.487	35.36%	40.60%
		65 GPA	12.162	12.267	83.50%	81.80%
4	Hydromorphic Solonchak	untreated soil	6.617	7.338	=====	
		50 GPA	9.039	10.621	36.60%	44.80%
		65 GPA	10.210	10.771	54.30%	46.84%
5	Solonchak	untreated soil	7.438	7.849	=====	
		50 GPA	7.969	9.305	7.14%	19.86%
		65 GPA	8.708	9.517	17.08%	22.59%

Table 10: Effects of the treatments with the chemical soil stabilizer "SOIL SEAL" on the threshold wind velocity (TWV) for both the "incipient" and the "continuous" detachment of 5 soil/crust samples. Results for 2 levels of stabilizer application are given.

site	Sediment source	Treatment	TWV of First Detachment (m/sec)	TWV of continuously detachment (m/sec)	crust effect	
					First Detachment	Continously detachment
1	salt crust	*Dry soil*	7.33	7.59		
			6.09	6.23		
			7.23	7.23		
			8.26	8.79		
			7.85	8.50		
			7.29	7.29		
		crust	15.80	16.59	115.21%	118.20%
2	Takyr crust	*Dry soil*	5.93	6.07		
			6.28	6.29		
			5.83	6.15		
		crust	12.57	13.56	108.99%	119.78%
			12.09	not measurable	100.98%	=======
6	Desiccated sea bottom	*Dry soil*	6.84	6.840		
			7.33	8.218		
			6.64	7.454		
		crust	13.16	not measurable	89.70%	=======

Table 11: Threshold wind velocities (TWV) of natural, air-dry soil/crust material. Compared to that of the constructed crusts.

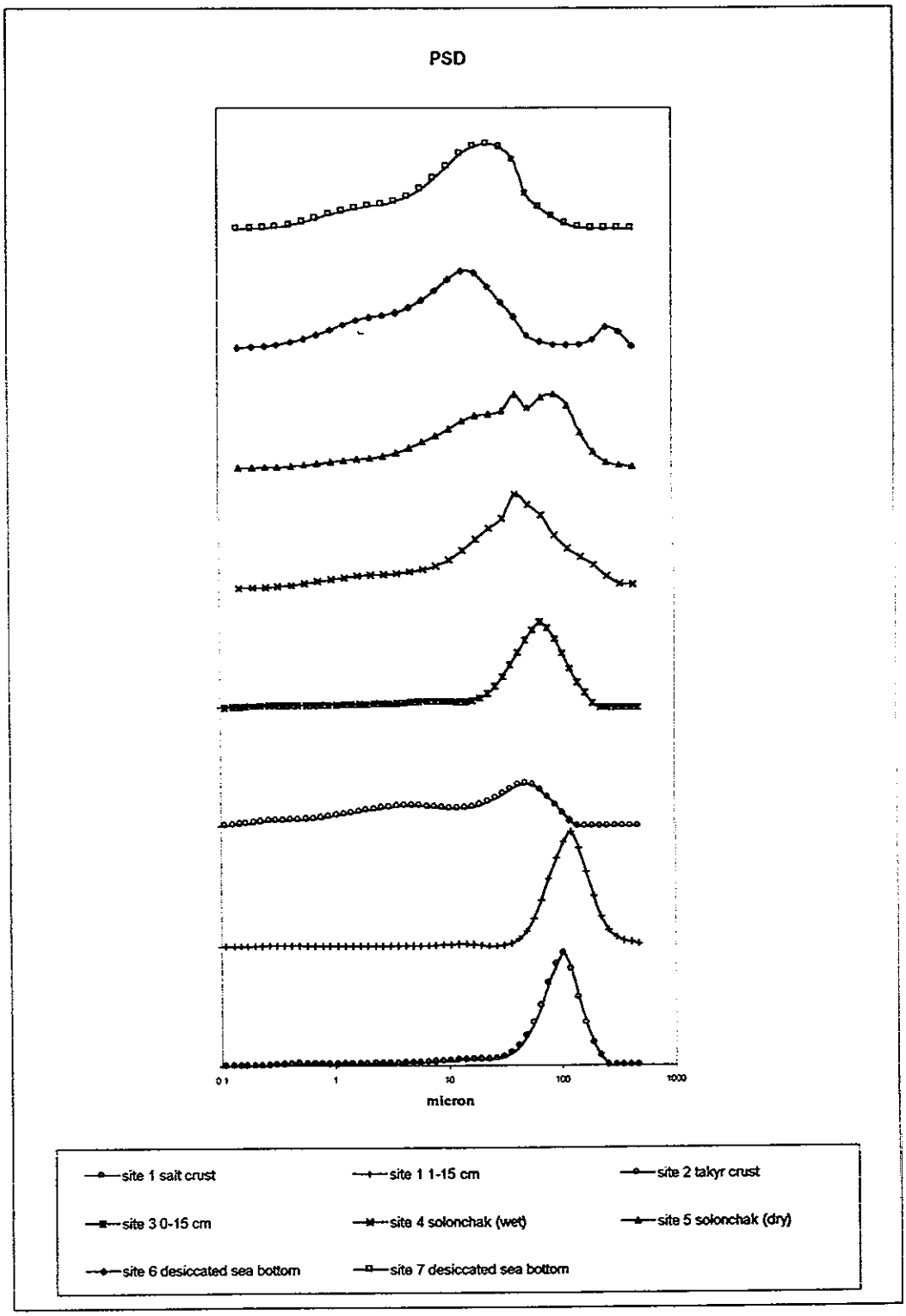

Figure 2: Particle size distribution (by laser) of the soil/crust samples (free of salts).

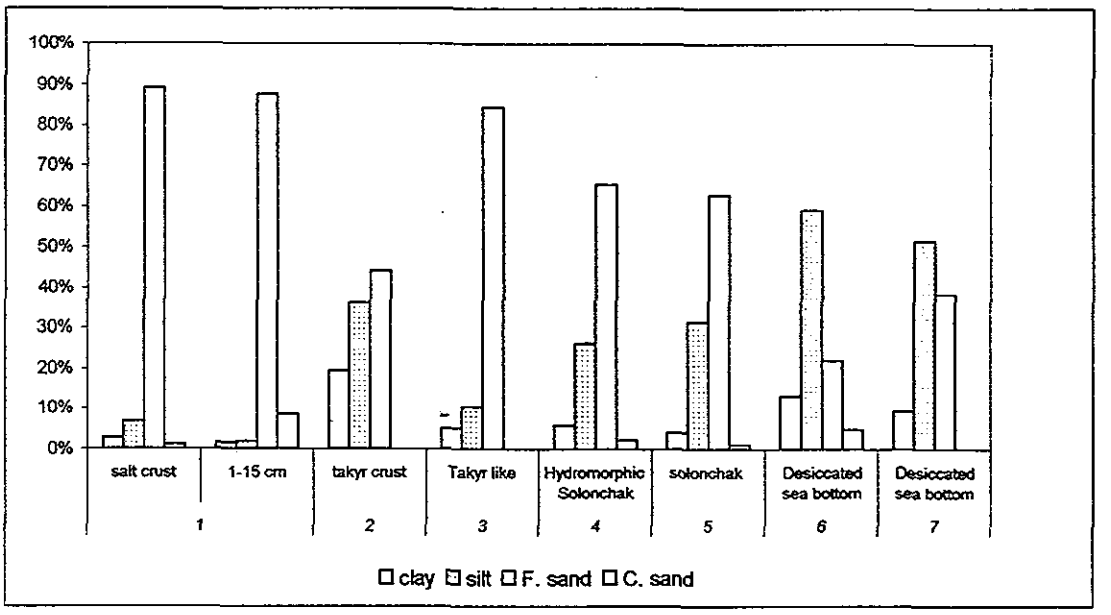

Figure 3: Particle size distribution of the (salt free) soil/crust samples, as obtained by the sedimentation method.

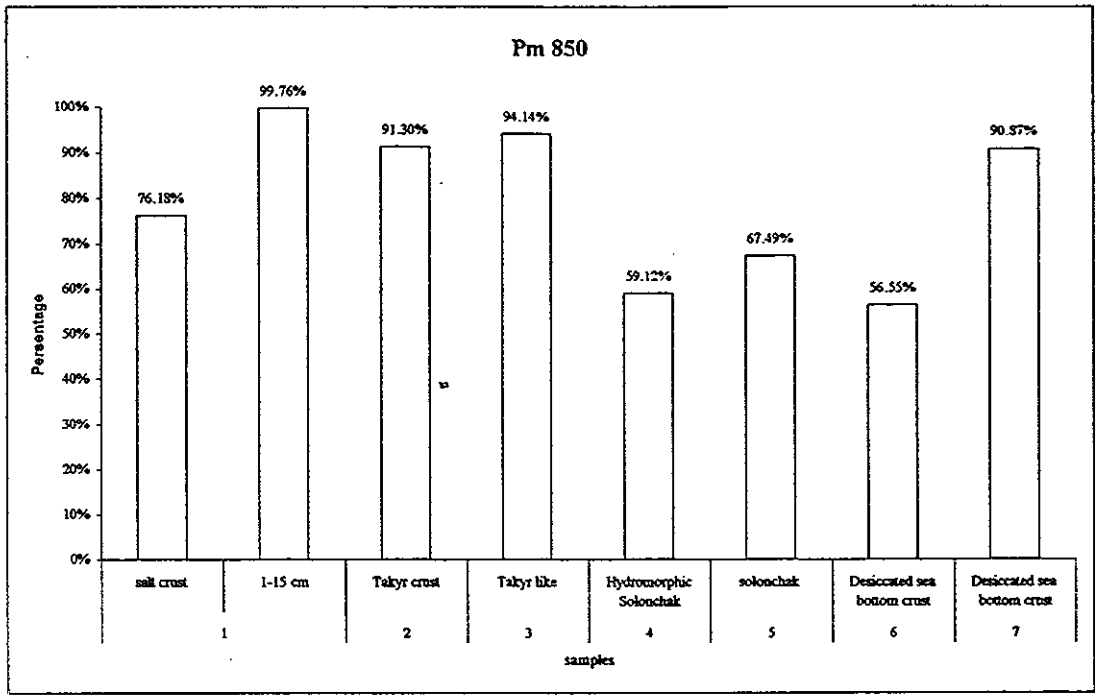

Figure 4 : PM_{850} particles of the soil/crust samples as obtained by the sedimentation method.

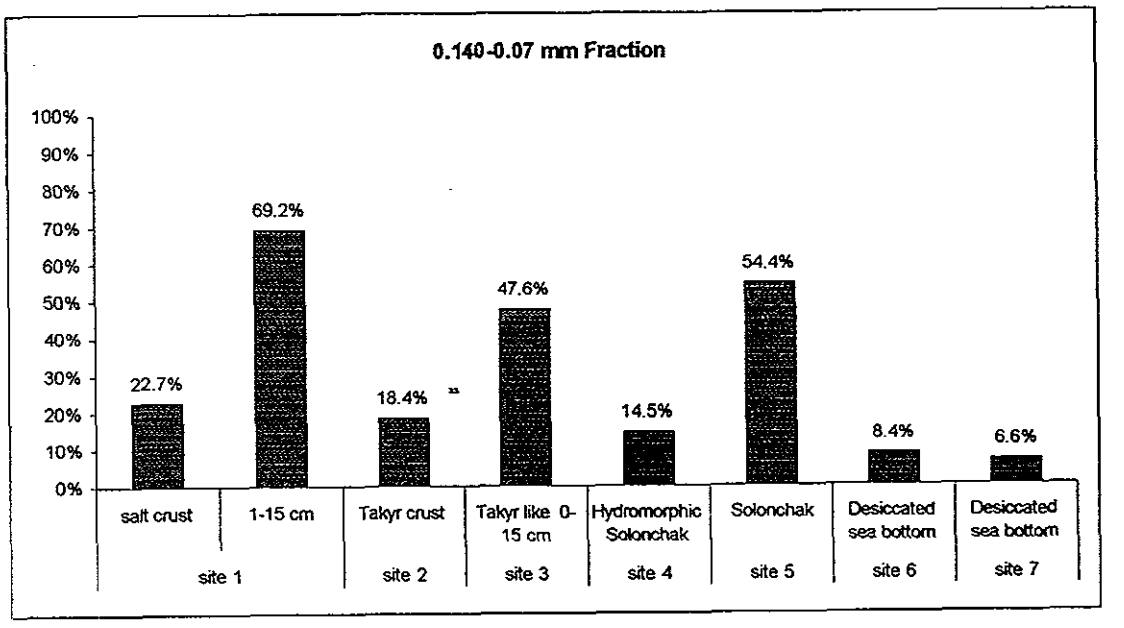

Figure 5: 0.07-0.14 mm particles in the soil/crust samples as obtained by dry sieving.

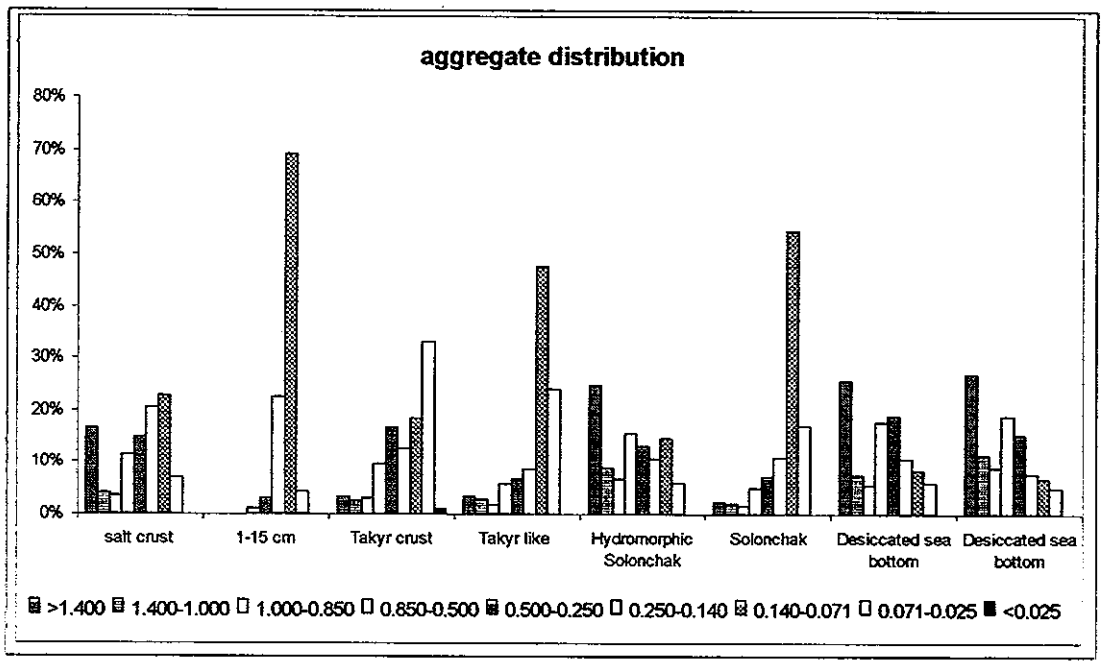

Figure 6: Aggregate size distribution in the soil/crust samples, as obtained by dry sieving.

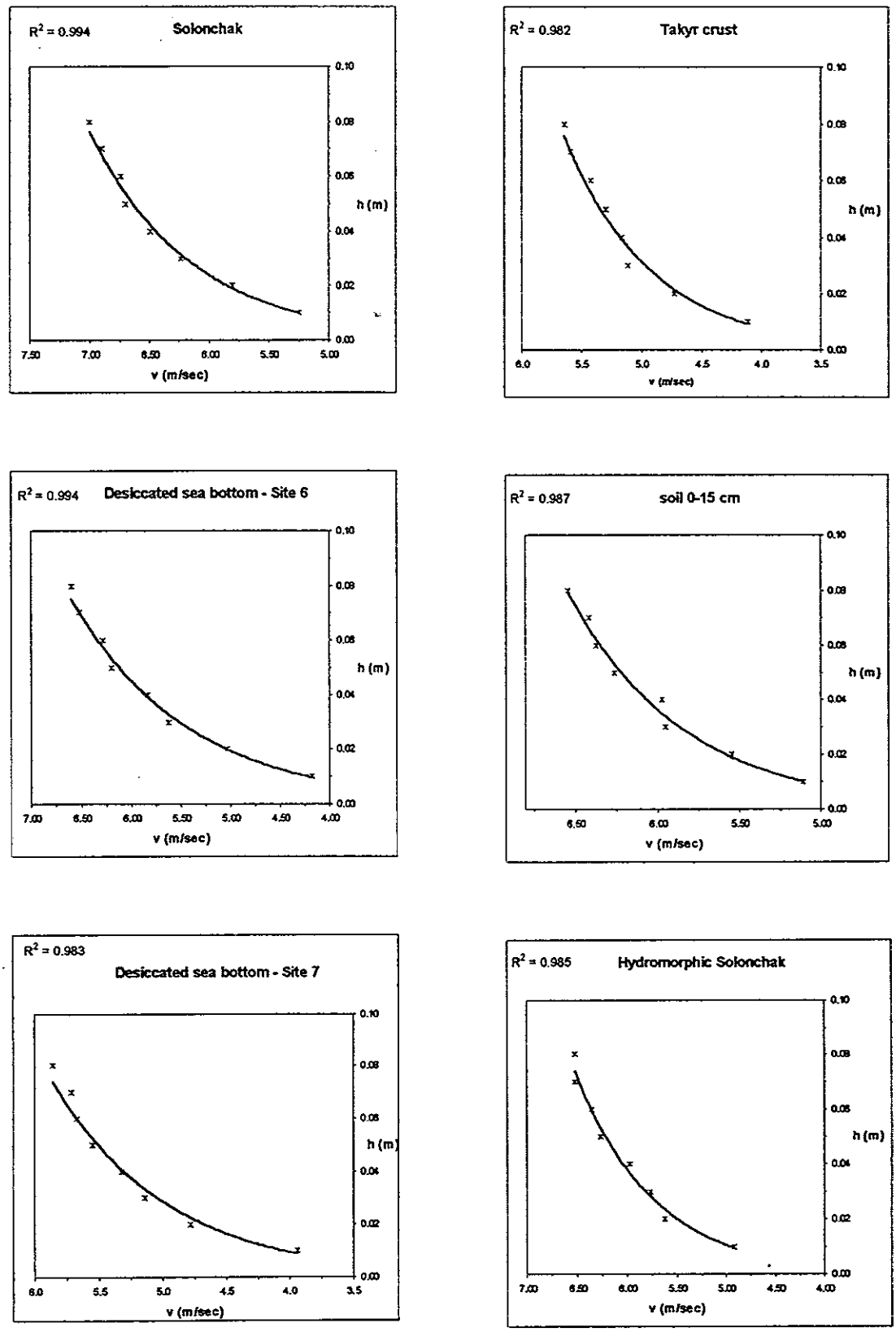

Figure 7: Threshold friction velocity profiles of the soil/crust samples as determined in the wind tunnel.

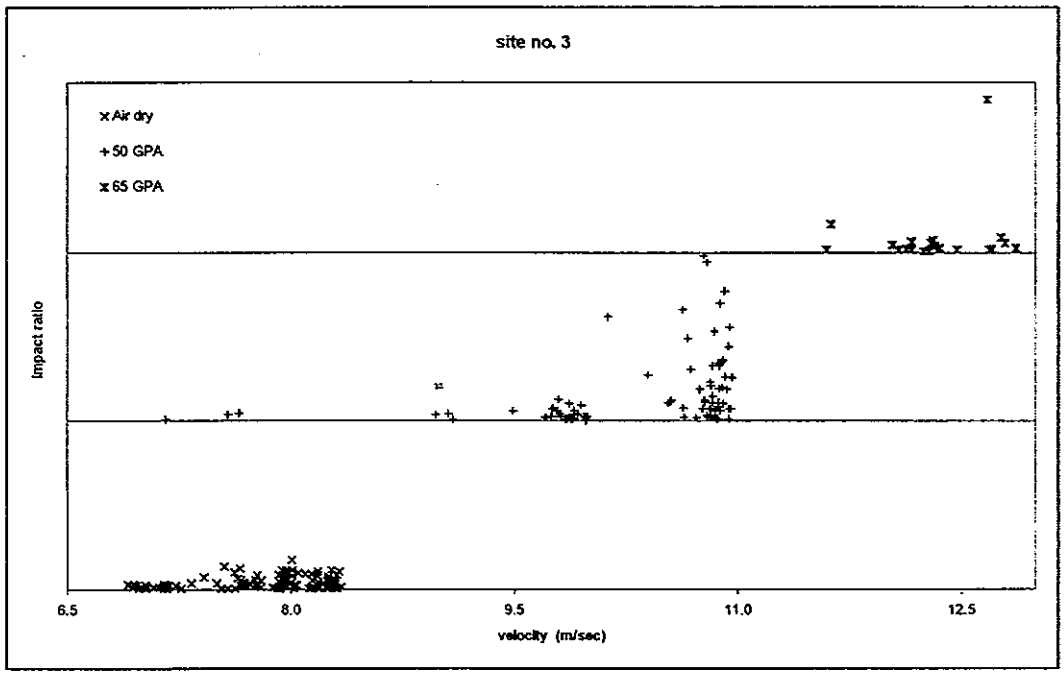

Figure 8: particle movement as registered by the SENSIT during the determination of TWV for the soil/crust samples, treated and untreated, in the wind tunnel

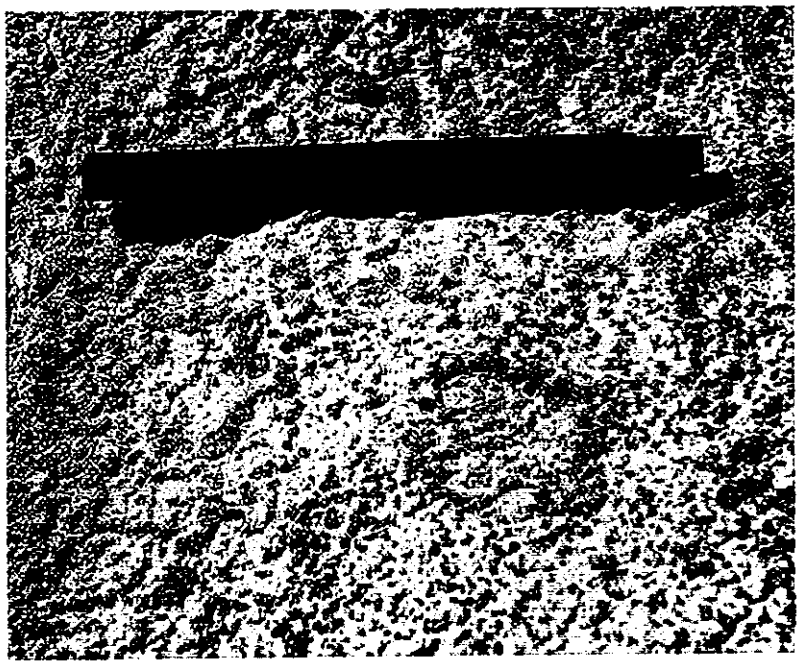

Figure 9 : reconstructed soil crust, site 1 - salt crust.

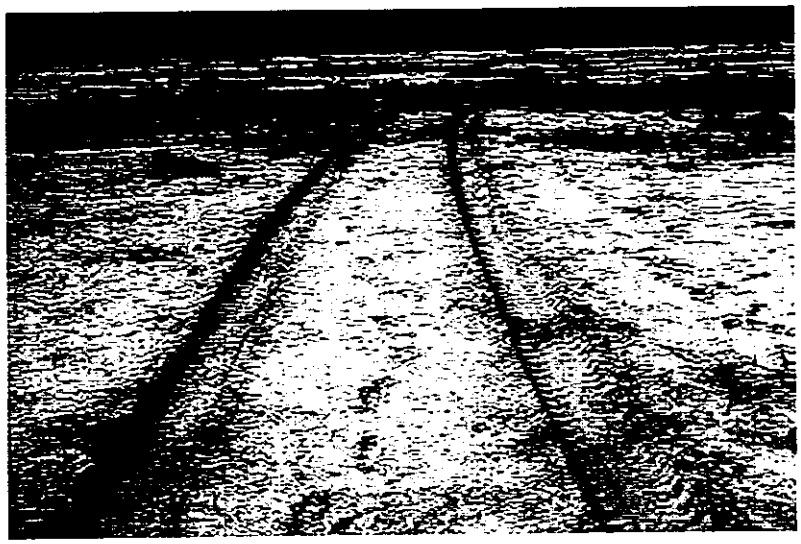

Figure 10 : Natural salt crust.

Figure 11 : Reconstructed soil crust, site 2 - Takyr crust.

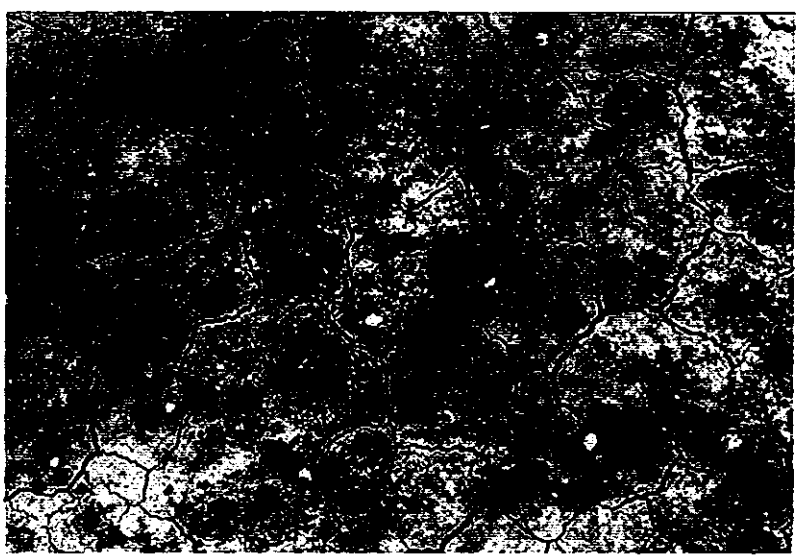

Figure 12 : natural Takyr crust.

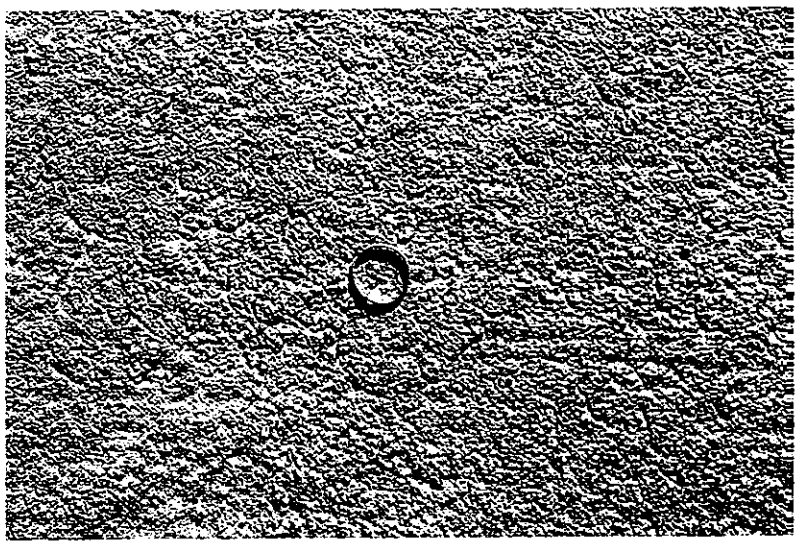

Figure 13: Reconstructed sediment crust, site 6.

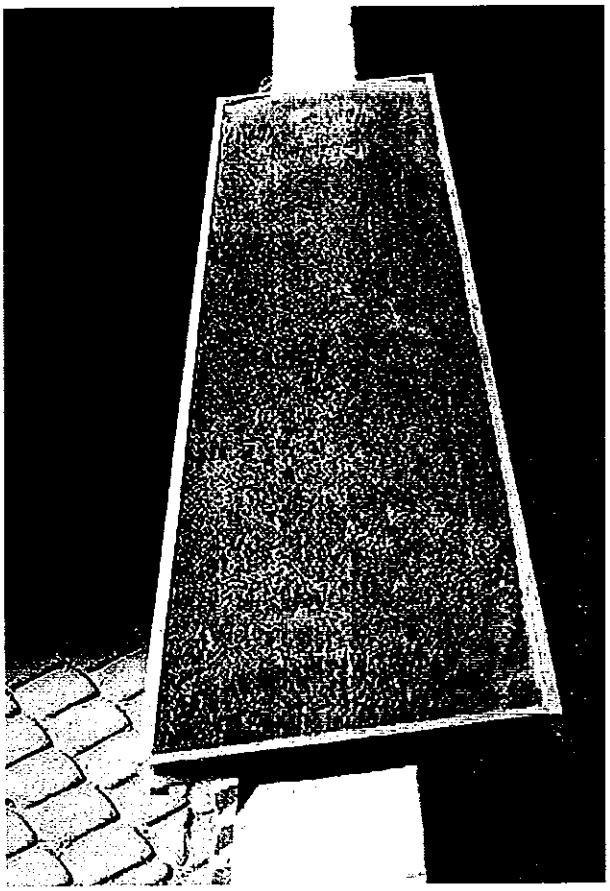

Figure 14 : Reconstructed sediment crust, site 6.

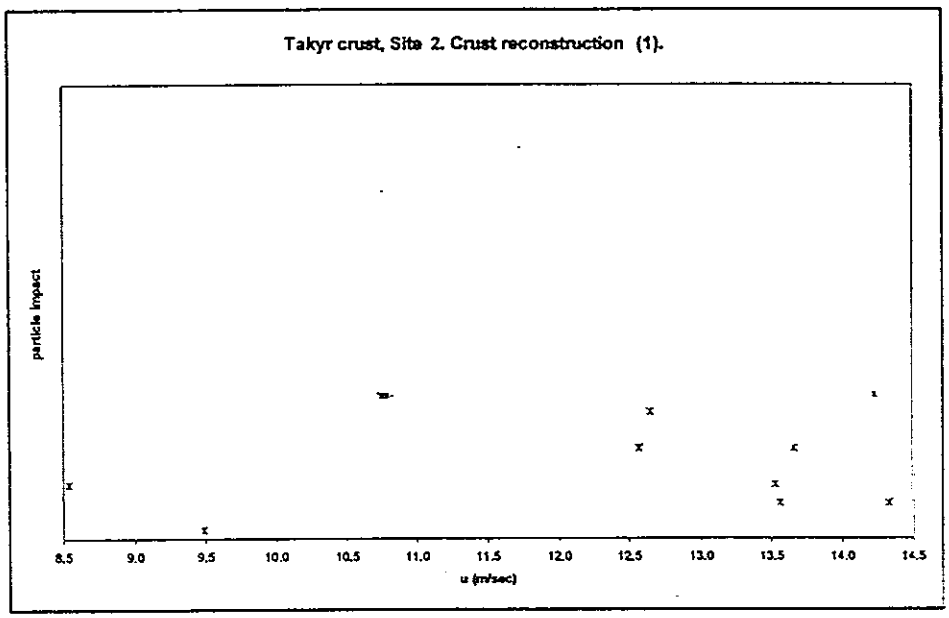

Figure 15: Particle movement as registered by the SENSIT during determination of TWV for the reconstruction crusts.

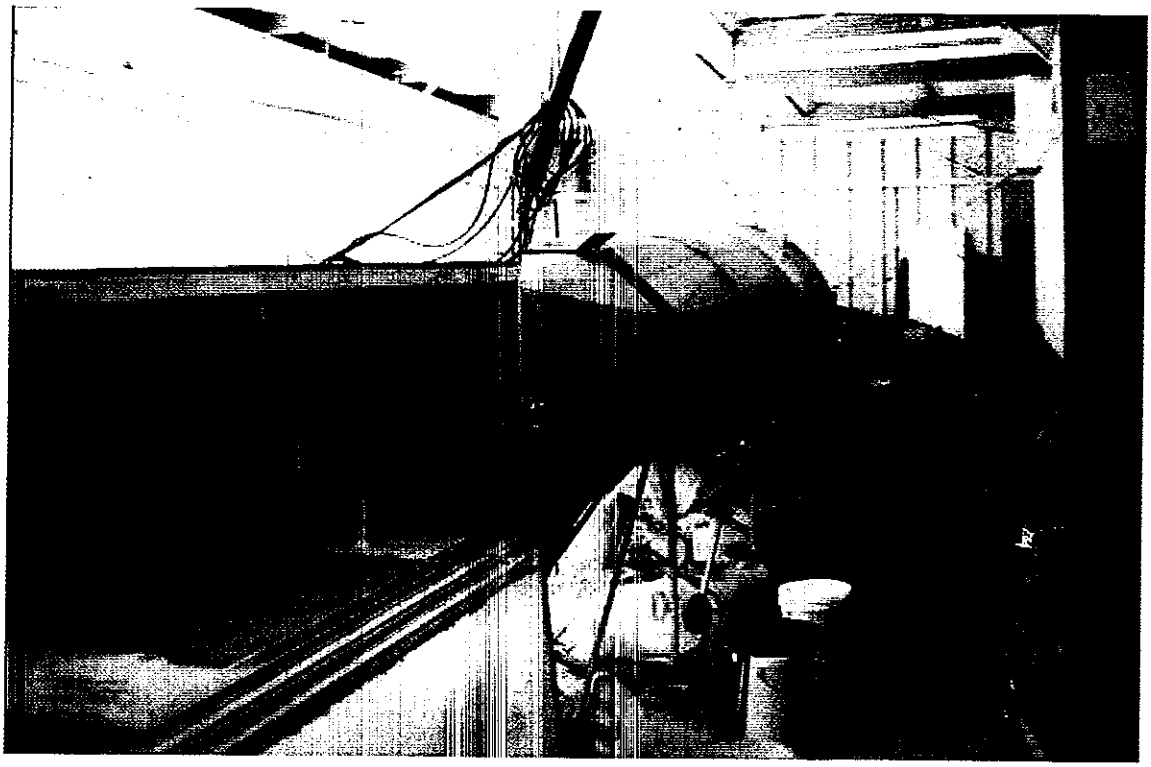

Fig. 16. Suction type wind tunnel, with SENSIT in foreground.

JOURNAL OF
ARID
ENVIRONMENTS

Executive Editors
Professor Charles Hutchinson
Professor Walt Whitford

Elsevier Science Editorial Office
Block A2, Westbrook Centre
Milton Rd., Cambridge CB4 1YG,
England
Telephone: +44 (0)1223 446000
Fax: +44 (0)1223 460236
email: jae@harcourt.com

Dr Arieh Singer
Seagram Center for Soil and Water Sciences
Hebrew University of Jerusalem
Rehovot
76100
Israel

17 January 2002

Dear Dr Singer

Re: Manuscript Reference Number: JAE 01/256

Title: The Dust Generation Potential of Soils/Sediments in the Southern Aral Sea Basin, Uzbekistan

Authors: A Singer, T Zobeck, L Poberezsky, E Argaman

Further to Professor Whitford's email of 16 January 2002:

"JAE 01/256 "Dust generation potential of soils.....Aral Sea Basin, Uzbekistan"

Your manuscript may be acceptable for publication in the Journal of Arid Environments if you are able to address all of the concerns of the referees. It is essential that you undertake a major revision that sharpens the focus and reduces the length of the manuscript. It will be necessary to eliminate all of the extraneous material that does not apply directly to dust generation potential of soils. The detailed referees reports and marked manuscript will be mailed from the Cambridge Office. When you have completed your revisions, please send one copy of the revised ms. directly to me at the address below and the original copy and diskette to the Cambridge Office."

Please find attached the 2 referees' reports and a copy of the manuscript with annotations by referee 1.

Yours sincerely

Olwyn Spurr
(on behalf of Professor Whitford)

The Dust Generation Potential of Soils/Sediments in the Southern Aral Sea Basin, Uzbekistan

A. Singer*, T. Zobeck**, L. Poberezsky*** and E. Argaman*

*Seagram Center for Soil and Water Sciences, Hebrew University of Jerusalem, Rehovot 76100, Israel

**USDA, Agricultural Research Service, Wind Erosion and Water Conservation Research Unit, Lubbock, Texas.

***"Vodproject", Tashkent 70000, Uzbekistan.

Abstract

Resulting from the extensive desiccation of the Aral Sea in Central Asia and exposure of large portions of the former sea bed, enormous dust storms have become common in the area and are having disastrous ecological consequences. The major dust plumes stretch as far as 500 km downwind and hundreds of thousands of tons of dust are deposited annually in areas to the S and SW of the Sea. The dust is, above all, constituting a major threat to the health of the population. Since the dust contains large amounts of salts, it is, in addition, causing severe salinization of waterbodies and huge tracts of agricultural lands, some of them intensely cultivated. The area most afflicted by this catastrophy is the Southern Aral Sea Basin in Uzbekistan.

The objective of this study was to assess the contribution of the major soil/sediment surfaces in the Southern Aral Sea Basin to the dust generation potential of this region. The exposed surfaces include wetlands in the delta close to the Amu Darya River bed, with transitions to Solonchak soils commonly with a salt crust, Takyr and Takyr-like soils exhibiting a fine-grained crust more removed from the river bed, and shallow, stony soils on the more elevated terrain. The desiccated and exposed Aral Sea bed includes a variety of sediments/soils, the most prominent of which are Solonchak-like soils. Eight crusts and soils/sediments from 7 sites, representative of these surfaces, were sampled in the field and their major characteristics (particle size distribution, organic carbon content, carbonate content, salt content and composition) that are related to dust generation, determined. The PM_{10} and $PM_{2.5}$ dust generation potential of the materials was accepted as a general indicator for their dust generation capability, and was determined in the laboratory using the Lubbock

108

Dust Generation, Analysis and Sampling System (LDGASS). The highest amount of PM_{10} dust (579.3 $mg.m^{-3}$) was generated from the Takyr crust material. The lowest by one Solonchak salt crust material (39.6 $mg.m^{-3}$). Salt crusts from the desiccated Aral Sea bottom generated intermediate amounts of dust. Apparently, high potentials for dust generation are related to high proportions of very fine aggregates (<140 μm, obtained by dry sieving), characteristic for Takyr crusts. Salt crusts seem to generate much lower PM_{10} dusts. This is due to the densely interlocking matrix of the salt crystallites forming the crust. It was argued, however, that under field conditions, blowing winds are charged with saltating sand grains that exert abrasive forces on the crusts, breaking interparticle bands and dislodging particles.

The results of these determinations indicate that the Takyrs and Takyr-like soils, roughly of an extent of over 1 million ha in the Southern Aral Sea Basin, constitute the surfaces with the highest potential for being the source for the severe dust storms of the area. Second to the Takyr soils, the Solonchaks and Solonchak-like soils, also with an extent of over 1 million, contribute highly saline dust. To these must be added a large, as yet uncharted, proportion of the approximately 4 million ha of exposed sea bed, that exhibit Solonchak-like characteristics.

Key words: Aral Sea Basin, dust generation, Takyr, Solonchak, soil crusts, PM_{10}, Amu Darya delta, desiccated Aral Sea bed, Lubbock Dust Generator.

Introduction

The Aral Sea, at an altitude of 53 a.s.l., is located in the Central Asian Republics of Uzbekistan and Kazakhstan, with the southern section located in the Autonomous Republic of Karapakalstan. Due to its location in the center of a vast mainland far from oceans, the Aral Sea maintains a continental climate. Temperatures in the region attain 40°C in the summer and in winter temperatures drop to -20°C. Average precipitation, principally in the form of rain, is below 200 $mm.yr^{-1}$ on the average. The Aral Sea is fed by two rivers, the Amu Darya entering the Sea in the south flows northwest from sources in the Pamirs, and the Syr Darya, entering the Sea in the north-east, flowing west from sources in eastern Uzbekistan (Fig. 1).

As a result of intensive irrigation along the two rivers feeding the Aral Sea, the volume of water reaching the sea to replace the enormous evaporation losses (~60 $km^3.yr^{-1}$) has decreased drastically (Fig.2). Once the fourth largest lake on earth, the Aral Sea has been drying up during four decades. By 1995, the Sea had lost ¾ of its original water volume of 1,064 km^3, and its surface of 68,000 km^2 had shrunk by more than half (Fig. 3). Forty-thousand km^2 of the former sea bottom are now exposed (Table 1). Water level in this period fell by 19 m. The shore line had receded in places (the southern part) by 150 km. Salinity of the water had risen from 0.99% in 1965 to 1.5% in 1996.

The lowering of the sea level of the Aral Sea is still continuing. The water level in 1999 was about 33.8 m NN and the surface area of the sea was about 24,400 km^2. It is envisaged that by continuous drying out, the sea will soon be separated into 2 water bodies, into the deeper Western Aral Sea and the shallower Eastern Aral Sea (Fig. 4). The drying up of the Aral Sea, according to the Scientific Board for Global Environmental Changes of the German Federal Republic (WBGV), was declared the greatest environmental disaster which mankind has caused by changing the regional water budget.

Caused by the drying out of the eastern part of the Eastern Aral Sea, the formation of another huge open salt desert has taken place. While the dry sea floor on the areas desiccated from the 1960s and the 1970s have a low salinity, with a sparse plant cover, the areas from the 1980s and the 1990s have already turned into salt deserts (the Aralkum desert) with isolated plants. In continuation of the increase in salt desert areas, salt and dust storms have become frequent.

The Aralkum desert with the remnant water bodies and the recent and older terraces is part of the center of the Aral Sea crisis region. The dry sea floor is a complicated mosaic of Solonchak and sandy ecosystems. On the new dry surface, new sand dunes developed

rapidly, mainly barchan-shaped. One can distinguish two types of dune systems on the dry sea floor: open dune systems with single dunes, covering much less than 50% of the area; and those with a dense pattern of dunes, covering more than 50%.

Since the 1980s, on the dry sea floor almost exclusively Solonchak deserts have formed. The open dry sea floor Solonchak desert is a huge salt flat and a source of salt dust. The Solonchaks have developed on sediments of variable texture, deposited from the Aral Sea water after being introduced by the two major river systems. These are young soils with undeveloped profiles and very slight organic matter accumulation. Their most distinct characteristic is salt accumulation, frequently in the form of a salt crust on the soil surface. The direct influence of aerosols (salt particles, dust) on the adjacent agricultural areas and their salinization as well as on the natural ecosystems and on the health of the people is still under dispute. The huge salt deserts which have developed since the 1980s are characterized by a rather strong deflation and denudation by wind, at a rate of 2 mm yr^{-1} (Semenov, 1990). This means that the upper 4 cm layer has been blown off during the past 20 years, particularly from the saline dry sea floor deserts which date from the 1980s. An increasing drying of the sea floor will create even more and greater saline flats, and thus a more enhanced salt dust regime by storms in the near future. This is a threat to the agricultural areas adjacent and beyond the southern and eastern former coastline. Thus, salt desertification is spreading throughout the whole Aralkum and surrounding areas (Breckle et al., 2001; Rafikov, 1999).

The drying up of the Aral Sea is also negatively affecting the region's climate. Earlier, the Aral Sea acted as a climate regulator for the region: it softened harsh Siberian winds in winter and acted as a conditioner, lowering heat in summer months. The shrinkage of the sea has resulted in drier, shorter and hotter summers, and longer and colder winters.

The environmental and related economic consequences of the Aral Sea desiccation have been wide-ranging and severe. By the early 1980s, the fishery was destroyed, chiefly owing to drying of shallow shore zones where fish bred and fed, and the inability of native species to adapt to the rapidly rising salinity. The ecosystems of the deltas of the Amu Darya and Syr Darya have suffered from desiccation and spreading desertification as a consequence of reduced spring floods, dropping stream and ground water levels, and increasing soil salinity. The area of lakes, wetlands and their associated reed communities in the deltas had been reduced 85 percent by the late 1980s with catastrophic impacts on resident and migratory water flow (Micklin, 1993). Salt and dust from the increasingly large former sea bottom is lifted as high as four kilometers. The major plumes stretch as far as 500 kilometers

111

downwind. Aerosols and particles from them settle on natural vegetation and crops, causing growth retardation or even wilt.

The dust is loaded with toxic materials, residues of the insecticides, pesticides and fertilizers applied to the irrigated areas along the two feeder rivers, Amu Darya and Syr Darya (Ivanov et al., 1996). As a result, the health of the population has been severely affected. Disease rates of anemia, kidney and liver diseases, and asthma have increased dramatically (Micklin, 1996; Orlovsky et al., 2001).

With decrease in their size, and concomitant increase in their specific surface area, the environmentally harmful effects of suspended dust increase. In 1987, as part of the National Ambient Air Quality Standards (NAAWS), the United States Federal Government issued regulations governing PM_{10} (particles with <10 μm aerodynamic diameter) as primary air pollutants. Small airborne particles in the PM_{10} range are capable of being transported long distances by the wind, having potential impacts over a large area and for a long time. Environmental health studies have indicated that PM_{10} is inhaled deeply enough into the human lower respiratory tract that it may adversely impact health (Gordian et al., 1996; Pope et al., 1996). In addition, the potential climatic impact of wind-eroded mineral dusts from disturbed soils has also been recognized (Tegen et al., 1996).

The finest fraction of atmospheric dust, $PM_{2.5}$ μm (particles less than 2.5 μm in diameter) are considered a major environmental and health hazard (Homolya, 1999). According to the Environmental Protection Agency of the USA (EPA) "the three-year average of the annual mean $PM_{2.5}$ concentrations is not to exceed 15 $\mu g\ m^{-3}$, and the 3-year average of the annual 98th percentiles of 24 hour $PM_{2.5}$ concentration is not to exceed 65 $\mu g.m^{-3}$ at any population oriented monitoring Site" (Homolya, 1999).

Different earth materials (soils, sediments) have been shown to emit different amounts of $PM_{10}/PM_{2.5}$ as related to wind velocity (Zobeck et al., 1999). Emission has been shown to be related to source sediment texture, moisture content, surface roughness and local factors such as soil crusts. Field studies of aeolian dust produced at or near the source of intense dust storms are difficult to conduct. As a result of efforts to develop methods for the study of PM_{10} generation of earth materials under controlled laboratory conditions, a new system has been proposed by Zobeck and Amante-Orozco (2001). This equipment has been used for the examination of 8 earth materials from the Southern Aral Sea Basin, with the purpose of determining the PM_{10} and $PM_{2.5}$ dust generation potential of these materials, that represent a large proportion of the surfaces in the area. The objective of this study was to assess the

contribution of the major soil/sediment surfaces in the SASB to the dust generation potential of the area.

Soils and the desiccated Aral Sea bed

Most of the soils of the Amu Darya River Delta (ADRD) had formed on river alluvium, that is frequently layered and with variable texture, close to the present (or former) river bed. Some, on more elevated areas, removed from the river bed, had formed on eroded Tertiary and Early Quaternary rocks.

The soils can roughly be divided into soils associated with and affected by the floodplain (former and present) of the river. These include wetlands consisting of hydromorphic meadow and bog soils with a relatively high clay content, that are slightly to moderately saline (Fig. 5). These soils, that were closest to the river and form most of the river delta to the north, were subjected to annual spring flooding and were therefore only in limited agricultural use; their extent is approximately 800,000 ha. Other soils, south-east of Nukus, in a narrow strip along the river, are hydromorphic meadow and bog soils formed on alluvium, that are non-saline or only slightly saline. Being fertile, they have been under agricultural use (with irrigation) for a very long time; their extent is about 148,000 ha. Finally, to this group of soils also belong hydromorphic meadow soils that are mildly to strongly saline and can therefore be termed Solonchaks; many of these soils are covered by a 1-2 cm thick salt crust; their extent is over 460,000 ha.

A second group of soils, more removed from the riverbed or even the floodplain, are Takyr soils. Takyr soils are soils of the desert zone, distinguished by their hard, polygonally-cracked surface. They exhibit a light-gray, 1-2 cm thick surface crust, compact on its upper surface, highly porous on its lower surface. The crust is very hard when dry, sticky when wet, slightly to moderately calcareous. Takyrs commonly are devoid of plant cover. The Amu Darya Takyrs are mildly to moderately saline, and also partly sodic.[1] Their extent is over 1 million ha; associated with them are gray-brown, sandy to loamy soils that are slightly saline; their extent is 306,000 ha. Finally, more removed from the river bed and on more elevated terrain to the west, on the Usturt plateau, are shallow, stony soils that are saline to varying degrees, from slightly saline when they are sandy, to more developed gypsic soils; their extent is 740,000 ha (Soviet Soil Survey Staff, 1969).

[1]Saline soils: Soils that contain large amounts of soluble salts, appreciably more soluble than calcium sulfate (Singer and Munns, 1999).
Sodic soils: Soils that contain Na^+ as a significant proportion of their total exchangeable cations (>10%).

This distribution of the ADRD suggests that with time and development, the river sediments develop either into strongly saline Solonchak types of soils, or into less saline Takyr types of soils (Singer et al., 2001). The most salient features of most Solonchaks and Takyrs are their crusts.

For the characteristics of the desiccated, exposed former Aral Sea bed, the depth to groundwater, the particle-size distribution and salinity are of major importance. The areas adjacent to the coastline are subject to inundations. The pattern of sedimentation, as well as the former geological history of the Aral Sea determine the particle size distribution and sedimentation layers of the new soils of the dry sea floor. The geomorphological structure of the Aral Sea basin is complicated. Plains predominate in the eastern part of the depression with an inclination of 0.2° to 0.6°. Therefore, the present coast line is situated up to 100 km away from the former eastern coastline. On the west coast, between the Usturt plateau and the islands Barsa-Kelmes and Vozrozhdenie, the inclination of the plain is steeper and amounts to 2°-5°. Correspondingly, the dry sea floor belt is only 4-10 km wide.

The new lacustrine deposits of the retreating Aral Sea form a 1-6m cover over old layers. The salinization of the substrate varies to a great extent, causing a wide variety of saline soil types to emerge: sandy soils, degraded coastal Solonchaks, Takyr soils, Takyr Solonchaks, Solonchaks slightly covered by sand, crusty and puffy Solonchaks, and marshy Solonchaks. From the former coastline to the present one, a typical sequence can be observed: the sediment becomes finer and the salinity increases. This sequence is also of primary importance for the type of soil development and the succession of plant colonization. On sandy sediments following evolutionary soil sequence can be observed: sandy soils (Psamments in the USDA classification. Soil Survey Staff, 1996) → degraded coastal Solonchak → Coastal Solonchak → marshy Solonchaks. The main vegetation types are shrubs, semi-shrubs, perennials and annuals, mainly halophyts, psammophyts, tugai and salt meadow communities (Wucherer and Breckle, 2001). The cover percentage is often rather high, 10-100%. The typical pattern of landscapes, vegetation types and soils is striated. This banded pattern is most characteristically seen along the East Coast of the Aral Sea.

Dust generation and transport in the Southern Aral Sea Basin

The desiccation of the Aral Sea has resulted in a dramatic increase in wind erosion processes. The number of dust storms has increased considerably. Up to 10 major dust storms are now registered annually in the region. In the past, the original large sea water

surface, with the associated wet sea atmosphere, reduced the strong northerly and north-easterly wind activity (Fig. 6). With the drastic reduction in the sea surface, this protective action has now been reduced significantly. Together with the strong reduction in plant cover, resulting from salinization and anthropogenic activities, this has led to deflation of huge dimensions in some areas, deposition of deflated materials in others.

Satellite observations showed that, with north and north-easterly winds prevailing, deflated material is transported and deposited mainly to the south and south-west areas of the S.A.S.B. (Fig.7). The distance traveled depends on the particle size of the deflated material and wind force. Sand fractions that move by saltation, are deposited close to source areas. One dune studied in the area moved 30 m from north to south during the period June 1981 to June 1982, and its volume increased from 4650 to 9562 m^3 (Tolkacheva, 1995; Tolkacheva et al., 1995). Clay and silt-sized material is transported for hundreds of kilometers. Dust from the A.S.B. has been identified as far away as in the fertile Ferghana Valley, 1000 km to the east, in Georgia and even along the arctic shore of the former Soviet Union (Micklin, 1988). The main source areas of the dust are the East Coast of the Aral Sea, the old delta of the Syr Darya river and the former Akk-Petka archipelago. Most of the finer material is deposited to the southwest in the Amu Darya River delta (about 60%), smaller amounts (about 25%) to the Usturt plateau to the west, and less than 11% to the south-east (Fig.7). About 85% of the deflated material travels over the Aral Sea. Therefore, a large proportion of the coarser grained material is deposited over the sea bed, and the material reaching the areas to the south west and west is relatively fine grained (Grigoryev, 1991).

There are differing estimates of the volume of material removed, transported and deposited. The average rate of removal from the dried sea floor has been calculated at 2 $mm.yr^{-1}$. This has been corroborated by measurements which showed that during the past 3 decades, a 6-9 cm thick layer of soil/sediments has been removed by wind from the newly dry surfaces (Semenov, 1990). According to Razakov and Kosnazarov (1996) however, the removal rate during 1982-1989 was much higher, 40-135 $mm.yr^{-1}$. The Institute of Geology and Geophysics of the Academy of Uzbekistan give a removal rate of 22.8 $ton.ha^{-1}yr^{-1}$, and a total figure for the years 1960-1983 of 43 million tons (Razakov and Kosnazarov, 1996). The dust includes large concentrations of salt. The salt input from the dried bottom of the sea to the atmosphere is 60-100 $ton.ha^{-1}.yr^{-1}$ (Kosnazarov, 1985).

There are differing estimates of the volume of material deposited. According to some calculations, in the Amu Darya Delta region, on an area of 10,000 km^2, on the average 90,000-100,000 tons of material are deposited annually (90-100 $kg.ha^{-1}$). On 13,000 km^2 of

the Usturt Plateau, about 40,000-50,000 tons (31-39 kg $ha^{-1}.yr^{-1}$) have been deposited (Orlovsky et al., 2001). Though, as mentioned before, some deposition occurs in the Aral Sea bed (particularly in the portions that are not yet dried up), the overall balance is that of deflation and the desiccated and exposed sea bottom is considered as one of the major dust sources. Huge loads of deflated material are deposited in some localities both on the dried sea bottom and in the Amu Darya river delta. According to estimates, 280-540 $kg.ha^{-1}$ yr^{-1} dust is deposited in some areas of the ASB, and of these 150 $kg.ha^{-1}$ yr^{-1} are soluble salts. Eleven kg of soluble salts are deflated annually from 1 m^2 of dried sea bottom. The salt input from the dried bottom of the sea to the atmosphere is 60-100 ton ha^{-1} yr^{-1} (Kosnazarov, 1985). According to observations by Razakov and Kosnazarov (1996), deposition rates in the S.A.S.B. vary between 1.5-6.0 ton $ha^{-1}.yr^{-1}$.

The maximal concentration of dust in dust plumes was found at heights of up to 50 m above ground (Kosnazarov, 1985). At heights of 600-800 m, the dust concentration decreased by 40-50%, at 1000 m by 70%, and at 2000 by 80%. The dominant particle size in the center of the dust plumes is between 10-50 μm (Fig. 8).

The gravest ecological consequence of the dust transfer in the southern Aral Sea Basin is the salinization of lands. The dust includes large concentrations of salt. In summer, the salt content in the dust is in the range of 30-40%, but in winter it may pass 90% (Hydrometeorological Centert of Uzbekistan). As a result, huge amounts of salt are transferred from the dust source areas (principally the dried Aral Sea bottom) and distributed over the soils of the Amu Dary River Delta (Fig. 9). The principal sources for saline dusts are the Solonchak soil areas. Between 12-20 ton $ha^{-1}yr^{-1}$ of salt are deflated from Solonchak soils (Kosnazarov, 1985). This figure indicates that up to nearly 500 $kg.ha^{-1}$ of salt were deposited in some areas of the delta during 1986 (Tolkacheva, 1995). According to Tsitasov (1990), from 0.2 to 5 ton $ha^{-1}.yr^{-1}$ of salt are deposited in some places in the Amu Darya river delta by atmospheric deposition. Values vary between 111-802 $kg.ha^{-1}.yr^{-1}$ for the exposed Aral Sea bottom and 41-384 $kg.ha^{-1}.yr^{-1}$ for Amu Darya River delta soils. Some of the atmospherically transported salt reaches the intensively irrigated and cultivated soils far to the south, hundreds of kilometers from the source areas.

Sampling Sites (see Fig. 5)

Sampling Site 1

Salt crust. Location 43°30'/59°56'. The surface is covered by a nearly continuous whitish, 2-3-mm-thick salt crust. Small patches of reeds intervene between the salt covered surfaces. A core was taken down to 1 m depth. The profile is uniform, fairly wet, of a gray (10 YR 6/1, Munsell) color. Groundwater was encountered at 90 cm depth. The texture was silty at the surface, becoming more sandy (fine sand) with soil depth. The salt crust, as well as the soil beneath it, were sampled.

Sampling Site II

Kasakhdaria. Takyr crust. Location: 43°25'/59°35'. Cultivated fields are mainly on the northern side of the village. A sample was taken from an uncultivated area to the south of the village. Part of the surfaces was wet after some light rains. The dry surface portions were cracked into polygons, of roughly 5-10-cm diameter. The surface, partly occupied by bushes, was covered with a not very firm, undeveloped crust about 0.5 cm thick. Only the crust was sampled. The texture of the soil was silty clay.

Sampling Site III

Muynak. Location: coord. 43°50'/59°05'. Stabilized Takyr-like soil surfaces, with a fairly dense cover of planted tamarisk-jangill. The sample was taken from an uncultivated field about 25 m east of a 10-12-m-wide ditch filled with water, that emptied a (storage) lake near to Muynak into the Aral Sea. The sample of surface soil (up to 25 cm depth) was wet and had a sandy silt texture. No crusting could be observed. The wetness of the soil was due to rains that fell during the preceding night.

Sampling Site IV

Kungrad area. Location coord. 43°28'/58°22' near former Sudoche Lake. Wet, hydromorphic (marsh) Solonchak soil. Sparse cover of short shrubs. The upper 2-3 cm of soil was sampled.

Sampling Site V

Kungrad area. Location coord. 43°50'/58°35'. Dry Solonchak soil (coastal), drained, formed on bottom sediments of former Adjubay Gulf. Very sparse cover of grasses. The upper 2-3 cm of soil, including a fine salt crust, were sampled.

Sampling Site VI

Recently (~10 years) desiccated and exposed Aral Sea bottom sediment. Location coord. 44°15'/58°23', near to the southern coast of (former) Vozrojdenia Island; completely level, bare, no plant cover. The 1-1.5 cm thick salt crust was sampled.

Sampling Site VII

Recently (~15 years) desiccated and exposed Aral Sea bottom sediment. Location coord. 43°58'/59°02', near to the Muynak Settlement; completely level, very sparse shrubs; The 1-1.5 cm thick salt crust was sampled.

Methods of Examination

Crust samples were collected manually, soil samples using a shovel. The micromorphology and chemical composition of crust materials was examined using a model JSM-5410LV scanning electron microscope to which an energy-dispersive x-ray spectrometer (EDSA) was attached. Particle size distribution was determined by the sedimentation method, supplemented by wet sieving and also by a Malvern Mastersizer Laser. Aggregate size distribution was determined by dry sieving. Carbonates were determined by acidifying the material and measuring the amount of CO_2 evolved (Bundy and Bremner, 1972). Organic C was determined using a CNS analyzer. Soluble salts were extracted and analyzed by ICP and ion chromatography.

Dust was generated from approximately 10 g samples tumbled in the Lubbock Dust Generation, Analysis and Sampling System (LDGASS) (Fig. 10). An earlier version of the LDGASS used a 1-m long dust generating tube in which the sample was rotated and dropped the length of the tube (Zobeck and Amante-Orozco, 2001). A shorter 0.5 m long tube was used in this study to accommodate smaller samples. In this system, kinetic energy is applied by gravity to the samples to generate dust. The sediment sample is placed in the dust generating tube (A in Fig. 10). An electric motor connected to the center of the tube rotates the tube 180 degrees from a vertical position 27 times per minute (13.5 revolution per minute). The samples adhere to the end of the tube during rotation and fall after ortation ceases to generate dust. The dust is drawn out of the chamber by air flowing through a 1.5-diameter orifice located at the center of the tube. The dust is conveyed to a settling chamber (B in Fig. 10) where dust sampling heads are located. A vacuum situated at the end of the system originates the air flow. Air enters the system in the dust generating tube through one of two 2.54-cm diameter valves (C in Fig. 10). A simple valve mechanism using a marble ensures that air enters only from the upper end of tube.

The airtight settling chamber is 45-cm tall with a 30-cm square base (D in Fig. 10). Dusty air enters the settling chamber at its top and is sampled at a constant flow rate by various dust monitoring sampling heads. In this study, a MiniVol (Air-Metrics, Inc.) impactor-type instrument was used for collecting gravimetric samples of particulate matter ≤10 cm aerodynamic diameter (PM_{10}).

Most of the coarse particles suspended and transported by the airflow deposit in the settling chamber. After passing through the settling chamber, airflow passes through a cyclone separator (E in Fig. 10) which collects must of the remaining dust particles leaving the settling chamber. Two replications of each sediment were rotated for 10 minutes.

RESULTS

Soil/sediment and crust characteristics

Particle-size distribution

The salt-free particle-size distribution of the soil salt crust and the underlying soil (Site I), of the desiccated Aral Sea bottom sediment salt crust (Sites VI and VII), of the Takyr soil crust (Site II) and of the Solonchak soils (Sites IV, V) are given in Table 2. Fine sand dominates in all materials except the desiccated sea bottom crust. Coarse sand is negligible; medium sand is present in minor quantities only. The Takyr crust from Site II contains a sizable silt fraction. The Takyr-like soil at Site III has a similar grain-size distribution. The soil at Site I below the salt crust has a grain-size distribution similar to that of the salt crust. In the Solonchak soils from Sites IV and V, fine sand and silt dominate. The amounts of clay and coarse sand are very low.

Aggregate size distribution is shown in Table 4. The Takyr crust from Site II had the highest proportion of very fine aggregates, the salt crusts from Sites VI and VII the highest proportions of very coarse aggregates. Also, the hydromorphic Solonchak from Site IV and the salt crust from Site I had high proportions of very coarse aggregates.

Fig. 11A presents the salt-free particle size distribution of the salt crust from Site 1 as determined by laser. Particles of 100 μm equivalent diameter absolutely dominate. Coarse and medium sand and clay are negligible; silt is present in minor quantities only. SEM observations however showed that the size of the salt crystallites varied between 5-10 μm. They were arranged in one dense, interlocking matrix (Singer et al., 2001). A second generation of smaller, apparently less crystalline particles was sometimes located on top.

The soil below the crust and the Takyr-like soil from Site 3 have similar particle size distributions. In the Takyr crust from Site 2, on the other hand, the maxima had shifted to lower sizes, with a major peak at about 65 μm and a smaller peak at 8 μm. This corresponds to finer sand and a sizeable silt fraction.

The laser particle size distribution curves of the Solonchaks from Sites IV and V (Kungrad area) and of the Aral Sea bottom sediments (Sites VI and VII) is shown in Fig. 11B. In the Aral Sea bottom sediments, ~20 μm particles dominate, in distinct contrast to the salt crust from Site I, where 100 μm particles dominate. In the Kungrad Solonchak soils from Sites IV and V, peaks at 60-80 μm indicate the dominance of fine sand.

All materials contain moderate amounts of carbonates (Table 2). The Solonchak soil below the salt crust of Site I contains the highest amount of carbonates, the dried sea bottom crust from Site VI, the lowest (7.45%). The only carbonate present is calcite, except in the Solonchak from Site IV, where some dolomite is present too.

Organic carbon is present in all materials in low amounts only (Table 2). The highest amount (1.62% org. C) was found in the hydromorphic Solonchak of Site IV, the lowest amount (0.28% org. C) in the soil below the salt crust of Site I.

All soils contain salts (Table 2). The highest amounts (64.8 and 53.6%) are present in the salt crusts of the dried sea bottom soils from Sites VI and VII. The salt crust of the Solonchak soil from Site I contains 42.7% salt. The lowest amounts were determined in the Takyr-like soil of Site III. In the hydromorphic Solonchak from Site IV and in the Takyr-like soil from Site III, sulfates dominate over chlorides. In all other materials, chlorides and sulfates are represented in about equal proportions. Nitrates in very minor amounts were identified in the Takyr crust from Site II, in the Solonchaks from the dried sea bottom and in the hydromorphic Solonchak from Site IV. Trace to minor amounts of fluorides were identified in the materials from Sites IV-VII. The dried sea bottom Solonchaks also contained traces of bromine. Among the cations, calcium dominated, except in the crusts, where sodium was the dominant cation. Potassium in significant amounts was present in the soil below the salt crust of Site I. Sodium is the dominant cation in the soils/sediments of Sites V-VII. It is followed by magnesium in the salt crusts of Sites VI and VII, and by calcium in the Solonchak soils of Sites V and VI. Significant amounts of potassium were present in the salt crusts too. Minor amounts of strontium were identified in the extracts of all materials. For the mineralogy of some of the soils/sediments see Singer et al. (2001).

PM_{10} and PM_{25} generation

Fig. 12 shows the particle size distribution of the generated PM_{10} dust. Only very little PM_{10} dust (39.6 $mg.m^{-3}$) had been produced by the salt crust of Site 1, but a relatively large proportion of that dust, 48.2% is $PM_{2.5}$ (Table 3). The dust produced from the salt crust on Site 1 has a distinctly bimodal distribution curve, with one major maxima at about 1.5 μm and a second at 5 μm (Fig. 12a). Since there is no aluminosilicate clay and very little silt (Table 2, Fig. 10) in the crust, most of this dust must have been composed by salt particles. Also very little PM_{10} dust (81.6 $mg.m^{-3}$) was produced by the subcrust soil from Site 1. About 1/5 of that dust was $PM_{2.5}$. The dust produced from that soil has a nearly uni-modal distribution, peaking at 9 μm (Fig. 12a).

In strong contrast to the salt crust, the Takyr crust generated a very large amount of PM_{10} dust (579.3 $mg.m^{-3}$), about 7 times more. The proportion of $PM_{2.5}$ in this dust, however, was similar to that in the salt crust (45.1%). The distribution curve obtained from this PM_{10} dust was distinctly uni-modal, peaking at 3 μm (Fig. 12a). It should be noted that the Takyr crust contains relatively large amounts of silt (Table 2).

The amount of PM_{10} dust generated from the Takyr-like soil at Site 3 was, with 379.5 $mg.m^{-3}$, still large but smaller than from the Takyr soil crust. The $PM_{2.5}$ proportion in this dust was also smaller than in the dust from the Takyr crust, 34%. The PDC from this soil was also uni-modal, but displayed two bulges, one in the clay sized particle range, the other at about 15 μm. The maxima of the curve was at 4 μm.

From the Solonchak from Site IV, little PM_{10} dust was generated, only 115.5 $mg.m^{-3}$, and only about one-fifth of that dust was $PM_{2.5}$ (22.2%). Very much larger (520.5 $mg.m^{-3}$ amounts of PM_{10} were produced from the Solonchak at Site V, and a larger proportion (32.2%) of that dust was $PM_{2.5}$. The PDC curves of Solonchaks IV and IV dust were distinctly uni-modal, with the maxima at 6 μm for Site IV and 3 μm for Site V.

Different amounts of PM_{10} dust were generated from the Aral Sea bottom crusts. From one crust (Site VI), the amount of dust obtained was 252.3 $mg.m^{-3}$, from the other crust (Site VII) it was much lower, 111.6 $mg.m^{-3}$. The corresponding proportions of $PM_{2.5}$ were 33.7% (Site VI) and 22.8% (Site VII). The shape of the PDC for Site VI was uni-modal, with the maxima at 4.5 μm. The PDC curve for sample VII was bi-modal, with maxima at 0.6, 6 and 18 μm.

DISCUSSION

The highest amount of PM_{10} dust was generated by the Takyr crust from Site II. This suggests that Takyr crust material potentially has a very high PM_{10} dust generation capability. It should be noted, however, that this material in vivo is organized in the form of a crust. On the effects of this crust, below. The $PM_{2.5}$ dust generation of this material too is very high, 45.1% of the PM_{10} dust (Table 3). This material contains relatively large amounts of clay and silt, and is only mildly saline and calcareous. Noteworthy is the dominant proportion of small aggregates (<140 μm). Zobeck et al. (1999) found for a large group of soils from Lubbock, Texas, that PM_{10} concentration by texture group varied from 35 $mg.m^{-3}$ for clay soils to 500 $mg.m^{-3}$ for sandy clay soils. In general, PM_{10} concentration increased with increasing clay content with the exception of the clay soil samples. For the examination of the effects of texture on dust emission, the technique of particle size determination, i.e. dry sieving or dispersed particle sizing is important. Chandler et al. (1998) found strong trends between the soil dustiness index (D) and both clay and silt contents in soils analyzed by mechanical sieves and aerodynamic sizing. Similar trends did not exist between D and soil texture classes as determined by dispersed particle sizing. This intuitively suggests that dust generation of soils is a measure of the dust freely available in a natural-aggregated condition. This is confirmed by the SASB soils and sediments, where the highest PM_{10} dust concentrations were generated by the Takyr soil crust material which also had the highest proportion of very fine aggregates (<71 μm) (Table 4). In contrast, PM_{10} dust generated by the hydromorphic Solonchak from Site IV, which also has a fairly high clay and silt content, was much lower. This should be explained by the fact that this material had a much lower proportion of very fine aggregates. On the other hand, the Solonchak from Site V, which had low amounts of clay and silt, but large amounts of fine aggregates, generated large amounts of PM_{10}. The subcrust material from Site I (1-15 cm), which also has predominantly fine aggregates, generated only low concentrations of PM_{10} dust. This possibly is due to the relatively high content in $CaCO_3$ in this material. $CaCO_3$ in soils often acts as a cementing agent. This is not supported by Zobeck et al. (1999) who obtained an increase in PM_{10} dust concentration with increasing $CaCO_3$ content of a variety of samples from near Lubbock, Texas. Organic carbon contents in the examined SASB materials are low. The effect of organic carbon on PM_{10} generation is questionable. Zobeck et al. (1999) found a positive correlation between organic carbon content and PM_{10} generation.

The Solonchak from Site IV generated a relatively low concentration of PM_{10} dust, though its silt content is relatively high (Table 2). This may be due to the carbonates and organic carbon contents in this material, but is probably mainly the result of the salts in this soil. Particularly low PM_{10} dust emissions are from soils with high salt contents. The salt crust from Site I had the lowest PM_{10} dust emission. Also the materials from the desiccated sea bottom (Sites VI and VII), that were covered with salt crusts, emitted relatively low PM_{10} dust concentrations.

Apparently salts diminish PM_{10} dust generation. The materials from the Sites with the highest dust generation (Sites II, III, V) had also the lowest salt contents. The differences in dust generation between the Solonchak materials from Sites IV and V and between the desiccated sea floor materials from Sites VI and VII are associated with differences in salt content. Most salt crust crystallites are in the size group of fine silt, 5-10 μm (Singer et al., 2001). This size-group should be susceptible to suspension as dust. But apparently these salt crystallites are aggregated into much larger units, which appear to be stable. In the salt crust from Site I, the crystallites can be seen to have formed a tightly interfitting mosaic (Singer et al., 2001). From Table 4 the salt crust materials can be seen to have disintegrated into a high proportion of large (>1,400 μm) aggregates, and into a low proportion of fine (<140 μm) aggregates). In contrast, the materials with the lowest contents in salts, have low proportions in very large aggregates. It must be concluded that high salt contents (of evaporitic origin) in surface crusts of soils/sediments, reduce their PM_{10} dust emission potential. Salt crusts from the SASB, examined in a wind tunnel, had very high threshold shear velocities (Argaman and Singer, in preparation).

Yet according to Razakov and Kosnazarov (1996), the salt crust in sandy and sandy-loam soils from the exposed bed of the Aral Sea, was destroyed and removed by even light winds (velocity of 2.5-5.0 $m.sec^{-1}$). On loam and clay soils, the salt crust was destroyed by winds exceeding a velocity of 7 $m.sec^{-1}$. This suggests a high susceptibility of the salt crusts to wind erosion. The very high salt contents in atmospheric dusts collected from over the SASB also suggest salt crusts as potential sources for dust generation (Fig. 9). The question then is: Do the salt crusts have a high PM_{10} dust emission potential?

In this context it should be pointed out that the mechanical composition of the materials given in Table 2 is on a salt-free basis. Since, as mentioned before, the salt crystallites in the salt crusts are mostly in the fine-silt size fraction, the amounts of silt (including the salt) in the salt crusts of Sites I, VI and VII are actually much higher, and this should have resulted in a higher PM_{10} emission potential.

Using a portable field wind tunnel, Hunser and Nickling (2001) found that, despite disturbances to the surface, the emission of PM_{10} from clay crusts decays rapidly without abrasion. Only in the presence of saltating grains was PM_{10} continuously liberated from the surface, such that the emission rate varied linearly with the saltation transport rate. This suggests that PM_{10} emission from crusts depends on saltation abrasion. Crusted surfaces are only significant continuous sources of PM_{10} when the interparticle bonds of the crust are broken, as by the abrasive action of saltating grains. This might offer an explanation for the relatively low amounts of PM_{10} generated by the LDGASS from the salt crust material. Even when in a highly disturbed state, in the absence of saltating grains the strong cohesive forces between the salt crystallites could not be overcome by the mechanical energy applied, and little PM_{10} dust was released. In the field, it can be surmised that the situation would be different. Numerous surfaces in the SASB are composed of sand dunes, and the winds would be loaded with saltating sand particles. The abrasive forces produced would break the interparticle bonds between the salt crystallites, and PM_{10} dust composed largely of salt crystallites would be generated. This would result in the highly saline dusts reported from the area (Fig. 8).

From their high PM_{10} dust generating capability, it can be concluded that the Takyr and Takyr-like soils from the SASB constitute the surfaces with the highest potential for being the source for the severe dust storms of the area. These are the fine-grained, slightly to moderately saline Takyr soils (cambic gypsiorthids) on the left and right hand of the Amu Darya river bed, somewhat removed from the bed (Fig. 5). Their extent is over 0.5 million ha. Some Takyrs are in association with solonchaks and sands. The extent of their soil association, to the east and even more removed from the river bed, is over 600,000 ha. On the Usturt Plateau, to the west of the Amu Darya River Delta, are soil associations that include Takyr and Takyr-like soils too. This indicates that huge areas, of over 1 million ha, have a prime potential for generating PM_{10} dust. In addition to the Takyr soils, Solonchak soils too have a PM_{10} dust generating capability, some directly, as shown in this study for the Solonchak from Site V, and others if the abrading action of saltating sand grains is taken into account. Including the Solonchak soils as potential sources for PM_{10} dust, would add at least 1 million ha in the Amu Darya River Delta, as well as a sizeable portion of the 4 million ha of desiccated Aral Sea bed.

References

Breckle, S., Scheffer A. & Wucherer, W. (2001) Halophytes on the dry sea floor of the Aral Sea. p. 139-146. In: W. Breckle, M. Veste and W. Wucherer (Eds.) Sustainable Land Use in Deserts. Springer.

Bundy, L.G. & Bremner, J.M. (1972) A simple titrimetric method for determination of inorganic carbon in soils. Soil Sci. Soc. Am. Proc. 36:273-275.

Chandler, D.G., Horning, L., Stetler, L. & Saxton, E. (1998) Relating empirical parameters of a dust emission model to loess soil properties. p. 42-44. In: Dust Aerosols, Loess Soils and Global Change (A. Busacca, ed.). Washington State University, Publication No. MISCO 190.

Gordian, M.E., Ozkaynak, H., Xue, J. Morris, S.S. & Spengler, J.D. (1996) Particulate air pollution and respiratory disease in Anchorage, Alaska. Env. Health Perspectives 104:290-297.

Grigoryev, A. (1991) Ecological lessons of the past and present. Nauka, Leningrad, 251 pp. Cited in: Orlovsky, N., Glantz, M., Orlovsky, L., 2001. Irrigation and Land Degradation in the Aral Sea Basin. In: W. Breckle, M. Veste and W. Wucherer (eds.) Sustainable Land Use in Deserts. Springer, p. 115-125.

Homolya, J. (1999) Particulate matter ($PM_{2.5}$) Speciation Guidance Document. January 21, 1999. DRAFT 131 U.S. EPA.

Hunser, C. & Nickling, W. (2001) The emission and vertical flux of particulate matter <10 μm from a disturbed clay-crusted surface. Sedimentology 48:255-267.

Hydrometeorological Center of Uzbekistan. Data for 1986-1995. Unpublished.

Ivanov, N., Chub, E., Subbotina, O., Tolkacheva, G. & Toryannikova, R. (1996) Review of the Scientific and Environmental Issues of the Aral Sea Basin. p. 9-21. In: The Aral Sea Basin (P. Micklin amd W. Williams (Eds.)). Nato Asi Series 2, Environment – Vol. 12. Springer.

Kosnazarov, K.A. (1985) Study of wind transport of dust and salt from dry bottom of the Aral Sea. Report on scientific research work, SANIIRI, Tashkent, p. 2-45.

Micklin, P. (1988) Desiccation of the Aral Sea, a water management disaster in the Soviet Union. Science (4870) 241:1170-1176.

Micklin, P. (1993) The shrinking Aral Sea. Geotimes, April 1993, p. 14-18.

Micklin, P. (1996) Introductory remarks on the Aral issue. p. 3-8. In: The Aral Sea Basin (P. Micklin amd W. Williams (Eds.)). Nato Asi Series 2, Environment – Vol. 12. Springer.

Orlovsky, N., Glantz, M. & Orlovsky, L. (2001) Irrigation and land degradation in the Aral Sea Basin. p. 115-125. In: W. Breckle, M. Veste and W. Wucherer (Eds.) Sustainable Land Use in Deserts. Springer.

Pope, C.A.III, Bates, D.V. & Raizenne, M.E. (1996) Health effects of particulate air pollution: time for reassessment? Env. Health Perspectives 103:472-480.

Rafikov, A. (1999) Regional desertification in the Aral Sea Basin. In: M.H. Glantz (Ed.) Creeping Environmental Problems and Sustainable Development in the Aral Sea Basin. Cambridge University Press, Cambridge.

Razakov, R. & Kosnazarov, K. (1991) The processes of salt formation and aeolian transfer in the Aral Sea zone. FAN, Nucus, 190 p. (in Russian).

Razakov, R. & Kosnazarov, K. (1996) Dust and salt transfer from the exposed bed of the Aral Sea and measures to decrease its environmental impact. p. 95-102. In: The Aral Sea Basin (P. Micklin amd W. Williams (Eds.)). Nato Asi Series 2, Environment – Vol. 12. Springer.

Ressl, R. (1996) Monitoring of recent area and volume changes of the Aral Sea and development of an optimized land and water use model for the Amu Darya Delta. p.149-160. In: The Aral Sea Basin (P. Micklin amd W. Williams (Eds.)). Nato Asi Series 2, Environment – Vol. 12. Springer.

Semenov, O. (1990) Assessment of the amounts of salt and sand transfer from the draining area of a dune In: Gidrometeorologischeskie problemy Priaralya (Hydrometeorological problems of Ural region). Gidrometizdat, Leningrad, pp. 200-216 (in Russian).

Singer, M. & Munns, D. (1999) Soils, an Introduction. Fourth Edition. Prentice Hall.

Singer, A., Banin, A., Poberezsky, L. & Gilenko, M. (2001) Soil crusts in the Amudarya River Delta: Properties and formation. p. 103-114. In: W. Breckle, M. Veste and W. Wucherer (Eds.) Sustainable Land Use in Deserts. Springer.

Soil Survey Staff. (1996) Keys to Soil Taxonomy. 7th Edition, USDA. Natural Resources Conservation Service, Washington.

Soviet Soil Survey Staff (Antizatorova et al.) (1969) Soil Map of the Karakalpak Autonomous Region. Ministry of Interior, Nukus.

Tegen, I., Lacis, A.A. & Fung, I. (1996) The influence on climate forcing of mineral aerosols from disturbed soils. Nature 380:419-422.

Tolkacheva, G.A. (1995) On the assessment of the possible extent of salt transport carried along by wind from the dried coast and sea bottom part and water surface of Aral Sea. Proceeding of SANIGMI, Tashkent, p. 13-18.

Tolkacheva, G.A., Kovalevskaya, J.I., Askenova, L.A., & Gorelkin, N.E. (1995) Study of thechemical composition of the Aral Sea area soils and their contribution to the processes of aerosol formation. Proceeding of SANIGMI, Tashkent, p. 55-64.

Tsitsasov, G.N. (ed.) (1990) Hydrometeorological problems of the Aral region. Gidrometeozdat. Leningrad. 277 pp.

Wucherer, W. & Breckle, S.W. (2001) Vegetation dynamics on the dry sea floor of the Aral Sea. p. 53-68. In: W. Breckle, M. Veste and W. Wucherer (Eds.) Sustainable Land Use in Deserts. Springer.

Zobeck, T.M., Gill, T. & Popham, T. (1999) A two-parameter Weibull function to describe airborne dust particle size distributions. Earth Surf. Process. Landforms 24:943-955.

Zobeck, T.M. & Amante-Orozco, A. (2001) Effect of Dust Source Clay and Carbonate Content on Fugitive Dust Emissions. Proceedings of the 10th International Emission Inventory Conference, Denver, CO.

Acknowledgements. This research was supported in part under Grant No. CA16-013 US-Israel Cooperative Development Research Program, Economic Growth, US Agency for International Development. Mr. Dean Holder from the USDA is thanked for his devoted sample and data processing work.

Table 1. Development of the environmental crisis in the Aral Sea Basin (from: http://www.grida.no/aral/aralsea/english/arsea/arsea.htm)

	1966	1976	1996	2000
Exposed dried sea bed km^2	-	13,200	38,000	42,000
Mass of potential dust/salt 10^6t	-	550	2,300	3,300
Area affected by dust storms 10^3km^2	-	100-150	250-300	400-450
Dust transported $kg \cdot ha^{-1}yr^{-1}$	-	100-200	500-700	700-1,100
Population in the area affected 10^3	-	500-600	3,000-3,500	3,500-7,000

(from: Aral Sea crisis. Communique on the results of the international technical meeting on the Aral Sea Basin problems, Tashkent, 1997).

Table 2. Some physical and chemical characteristics of soil crusts and soil sediments in the southern Aral Sea Basin.

Site	Sediment source	Mechanical composition (%)* (on a salt-free basis)					O.C.	$CaCO_3$	Salts
		Clay <0.002mm	Silt 0.002-0.05mm	f.sand 0.05-0.20mm	m.sand 0.20-0.5mm	c.sand 0.5-2.00mm	%	%	%
I	Salt Crust	0	4.5	80.1	14.3	1.05	0.8	8.8	42.7
	1-15 cm	0	0.6	80.0	18.4	1.00	0.3	16.1	3.1
II	Takyr crust	12.9	32.8	52.4	0.8	1.10	1.6	8.0	5.7
III	Soil 0-25 cm	5.4	26.5	66.8	1.1	0.26	1.0	14.2	0.3
IV	Wet Solonchak	9.1	31.8	55.7	1.6	1.8	1.62	10.24	19.5
V	Dry Solonchak	3.6	16.4	76.4	2.7	0.9	0.9	10.6	9.8
VI	Desiccated sea bottom crust	1.7	50.7	38.9	1.97	6.7	0.4	7.4	64.8
VII	Desiccated sea bottom crust	0.2	48.9	42.9	1.8	6.2	0.8	10.0	53.6

*on a salt-free basis.

Table 3. PM_{10} and $PM_{2.5}$ dust generation by the Lubbock dust generator from the South Aral Sea Basin soils/sediments.

Site	Sediment source	Dust (PM_{10}) conc. $mg.m^{-3}$	Dust ($PM_{2.5}$) conc. $mg.m^{-3}$	Relative $PM_{2.5}$ conc. %
I	Salt crust	39.6	19.1	48.2
	1-15 cm	81.6	16.5	20.2
II	Takyr crust	579.3	261.1	45.1
III	Soil, 0-25 cm	379.5	135.0	34.0
IV	Solonchak (wet)	115.3	25.6	22.2
V	Solonchak (dry)	520.5	167.7	32.2
VI	Desiccated sea bottom crust	252.3	85.1	33.7
VII	Desiccated sea bottom crust	111.6	25.4	22.8

132

Table 4. Aggregate size distribution of the Southern Aral Sea Basin samples, obtained by dry sieving.

	Site I		Site II	Site III	Site IV	Site V	Site VI	Site VII
Sieve (mm)	Salt crust	1-15 cm	Takyr crust	Takyr-like 0-25 cm	Hydromorphic Solonchak	Dry Solonchak	Desiccated Sea bottom	Desiccated Sea bottom
>1.400	16.44%	0.04%	3.14%	3.30%	24.51%	2.24%	25.52%	26.84%
1.400-1.000	4.02%	0.09%	2.51%	2.62%	8.96%	1.85%	7.31%	11.29%
1.000-0.850	3.36%	0.11%	3.05%	1.68%	6.66%	1.56%	5.36%	8.78%
0.850-0.500	11.30%	0.97%	9.72%	5.59%	15.56%	5.03%	17.75%	18.84%
0.500-0.250	14.76%	3.04%	16.84%	6.64%	13.13%	7.13%	19.08%	15.17%
0.250-0.140	20.54%	22.36%	12.47%	8.54%	10.68%	10.92%	10.68%	7.53%
0.140-0.071	22.69%	69.17%	18.36%	47.57%	14.46%	54.36%	8.35%	6.62%
0.071-0.025	6.85%	4.15%	32.99%	23.97%	6.01%	16.87%	5.93%	4.92%
<0.025	0.04%	0.07%	0.93%	0.08%	0.02%	0.05%	0.03%	0.00%
sum	100.00%	100.00%	100.00%	100.00%	100.00%	100.00%	100.00%	100.00%

Figure Captions

Fig. 1. Satellite map of the Aral Sea area (in: http://karakalpakstan.freenet.uz).

Fig. 2. Shrinkage of the Aral Sea (after Micklin, 1993).

Fig. 3. Hydrological changes of the Aral Sea (after Breckle et al., 2001).

Fig. 4. Shrinkage of the Aral Sea surface (from Ressl, 1996, in: The Aral Sea Basin (Micklin and Williams, eds.).

Fig. 5. Schematic soil map of the southern Aral Sea Basin (after Soviet Soil Survey Staff, 1969). Scale 1:2,500.000. Sampling sites are marked by nos. 1-7.

I. Hydromorphic meadow soils (Aquents, Fluvents) with a well-developed upper Ap horizon, developed on alluvium. Only slightly saline, highly fertile soils, that have been under cultivation for a long time.

II. Slightly hydromorphic meadow soils (Aquents, Arents, Fluvents) developed on alluvium; transition to Solonchaks. Moderately to highly saline. With light to moderate drainage. Partly cultivated; delta of the Amu Darya river.

III. Hydromorphic, low-lying bog and meadow soils with a clay texture, with poor drainage. Prone to flooding, slightly saline; mostly uncultivated.

IV. Fine-grained Takyr soils (cambic gypsiorthids) slightly to moderately saline, transitional to Solonchaks (Salorthids).

V. Takyr soils, in complexes with Solonchaks and sands (Psamments). Ancient floodplain of Amu Darya river; in patches irrigated, mostly pasture.

VI. Grayish-brown soils, sandy to loamy, slightly sodic; moderately saline, stony, on hilly topography; mostly pasture.

VII. Usturt Plateau, grayish-brown soils, in complexes with Takyr soils, Solonchaks and sand fields; mostly shallow, occasionally gravelly, with gypsic horizons; (Gypsids); not suitable for irrigation; mostly pasture.

VIII. Kizyl Kum desert, sand fields, in complexes with desert soils and Solonchaks; low-grade pasture.

IX. Water.

Fig. 6. Average wind direction distribution in the Southern Aral Sea Basin (after R. Razakov and K. Kosnazarov, 1991).

Fig. 7. Distribution of dry aerosol deposits in the Southern Aral Sea Basin for 1986, in tons $ha^{-1}.yr^{-1}$ (after R. Razakov and K. Kosnazarov, 1991). Sea shore line is for 1986; shaded areas are low-lying marshes.

Fig. 8. Grain-size distribution of aerosol (dust) over the Southern Aral Sea Basin (after R. Razakov and K. Kosnazarov, 1991).

Fig. 9. Distribution of dust-derived salt deposition in the Southern Aral Sea Basin for 1986, in $kg.ha^{-1}.yr^{-1}$ (after R. Razakov and K. Kosnazarov, 1991). Sea shore line is for 1986; shaded areas are low-lying marshes.

Fig. 10. The Lubbock Dust Generation, Analysis and Sampling System (LDGASS).

Fig. 11A. Particle size distribution (salt free) as determined by Malvern Mastersizer Laser of materials from Sites I, II, III (after Singer et al., 2001). a – I, salt crust; b – I, 1-25 cm; c – II, Takyr crust; d – III, 0-25 cm soil.

Fig. 11B. Particle size distribution (salt free) as determined by Malvern Mastersizer Laser of materials from Sites IV, V, VI and VII. a – IV, hydromorphic Solonchak; b – V, Solonchak; c – VI, desiccated sea bottom crust; d – VII, desiccated bottom crust.

Fig. 12. Particle size distribution curves of PM_{10} dust generated by the Lubbock dust generator from southern Aral Sea basin soils/sediments. (A) – Site I, salt crust; (B) – Site I, 1-25 cm; (C) – Site II, Takyr crust; (D) – Site III, 0-25 cm soil; (E) – Site VI, desiccated sea bottom crust; (F) – Site VII, desiccated sea bottom crust; (G) – Site IV, hydromorphic Solonchak; (H) – Site V, Solonchak.

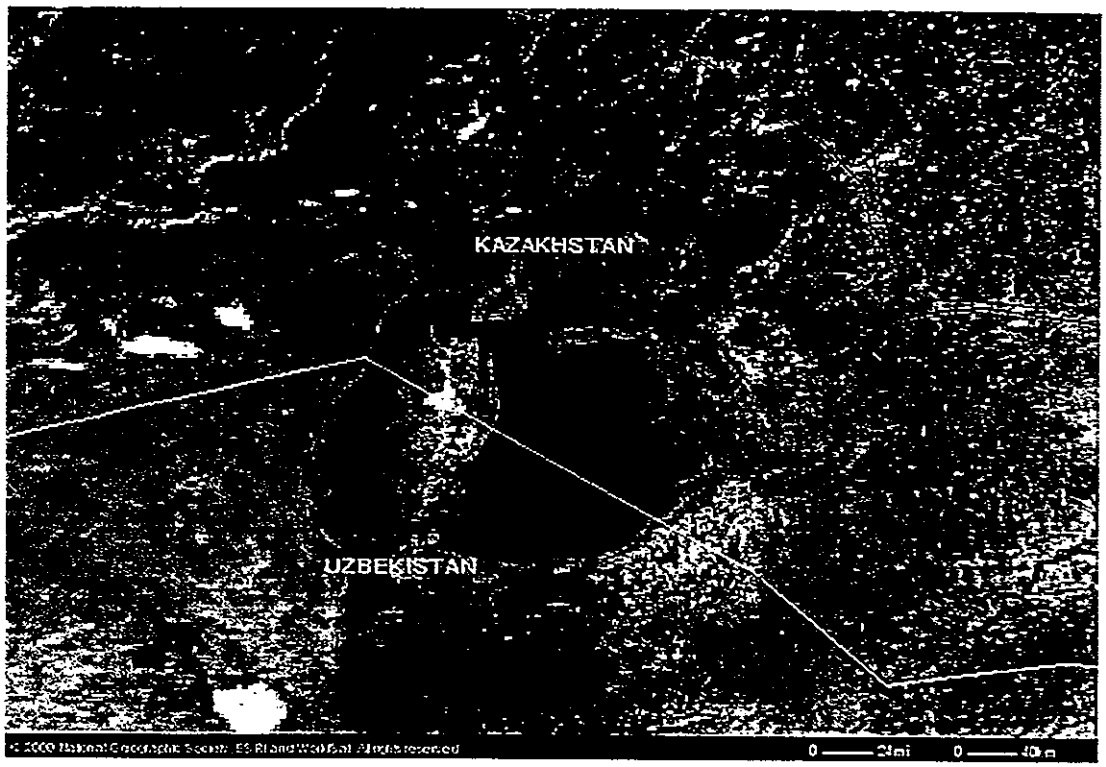

Fig. 1

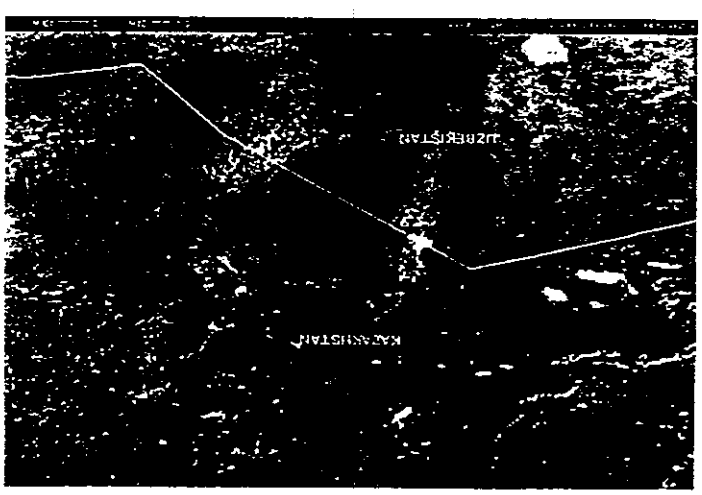

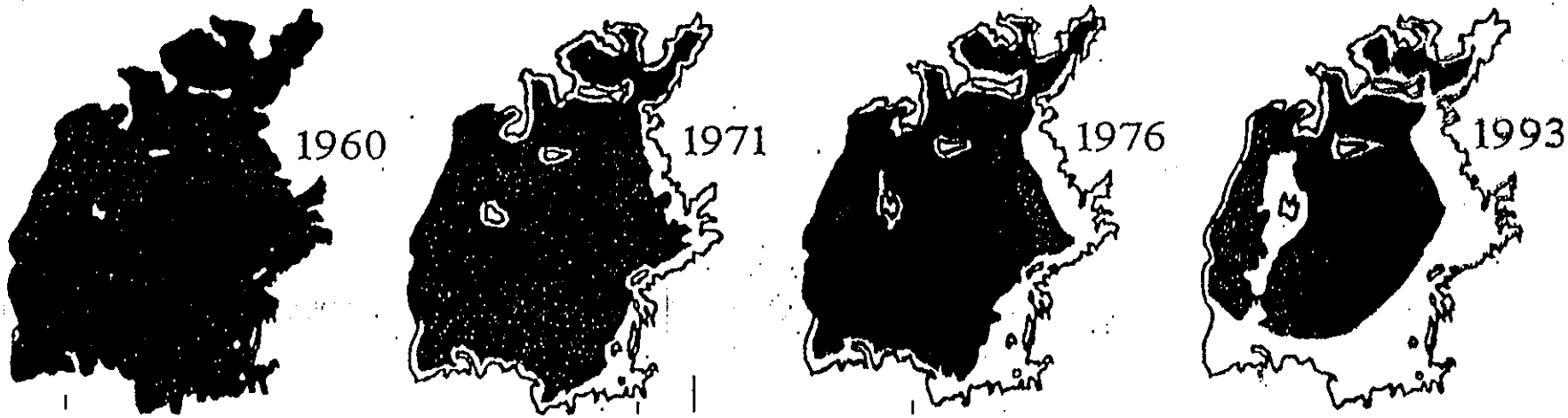

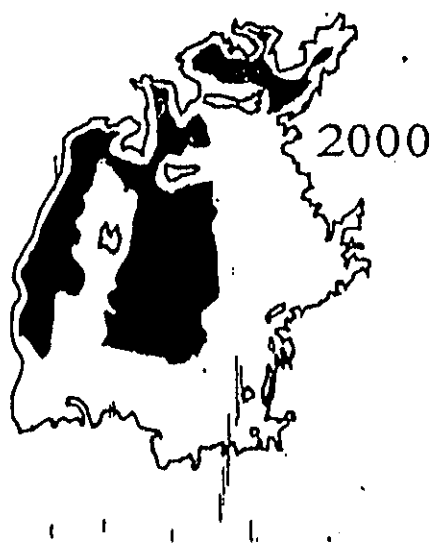

YEAR	AVERAGE LEVEL (meters)	AVERAGE AREA (sq.-km)	AVERAGE VOLUME (cu.-km)	AVERAGE SALINITY (grams/liter)
1960	53.41	66,900	1090	10
1971	51.05	60,200	925	11
1976	48.28	55,700	763	14
1993 (January 1)		33,642	300	
large sea	36.89	30,953	279	~37
small sea	39.91	2,689	21	~30
2000 (January 1)		24,154	175	
large sea	32.38	21,003	159	65-70
small sea	40.97	3,152	24	~25

P. M. 1993

PHILIP P. MICKLIN, WESTERN MICHIGAN UNIVERSITY

Fig. 2

137

Hydrological changes of the Aral Sea

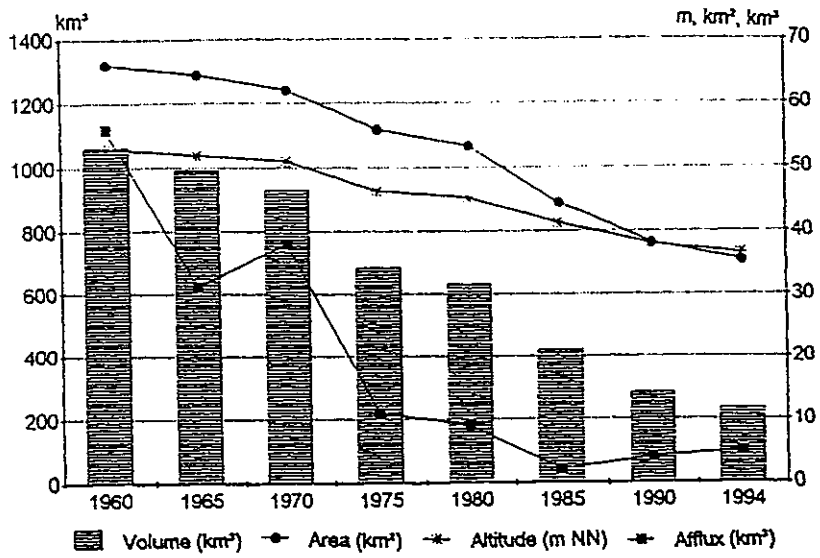

Fig. 3

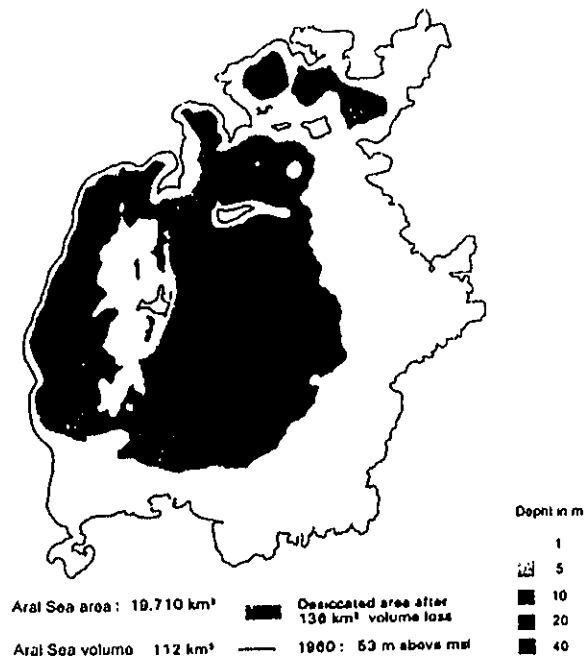
Depht in m
1
5
10
20
40
Aral Sea area : 19.710 km²
Desiccated area after 136 km³ volume loss
Aral Sea volume 112 km³
1960 : 53 m above msl

Fig. 4

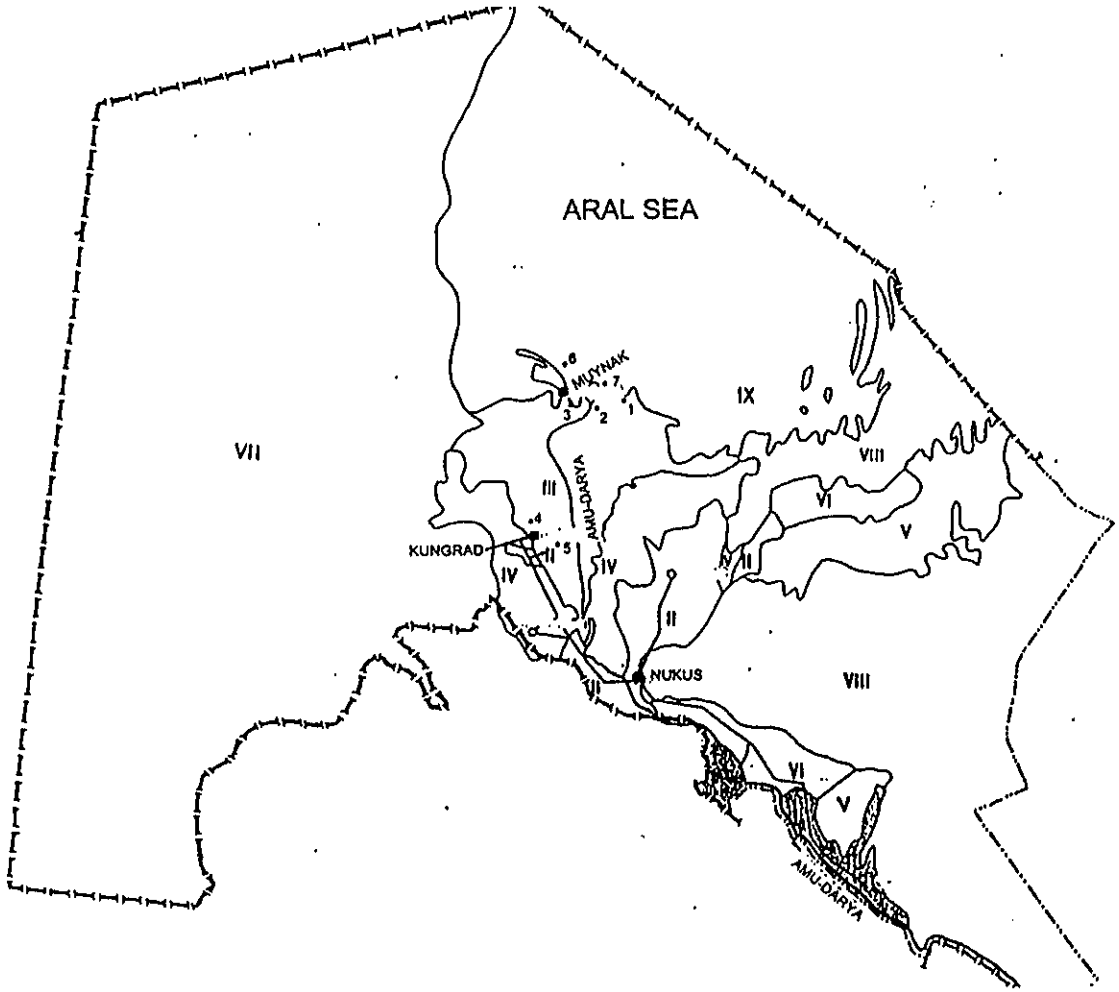
ARAL SEA
MUYNAK
KUNGRAD
NUKUS
AMU-DARYA
AMU-DARYA
VII
III
IV
II
IX
VIII
VI
V
VIII
VI
V

Fig. 5

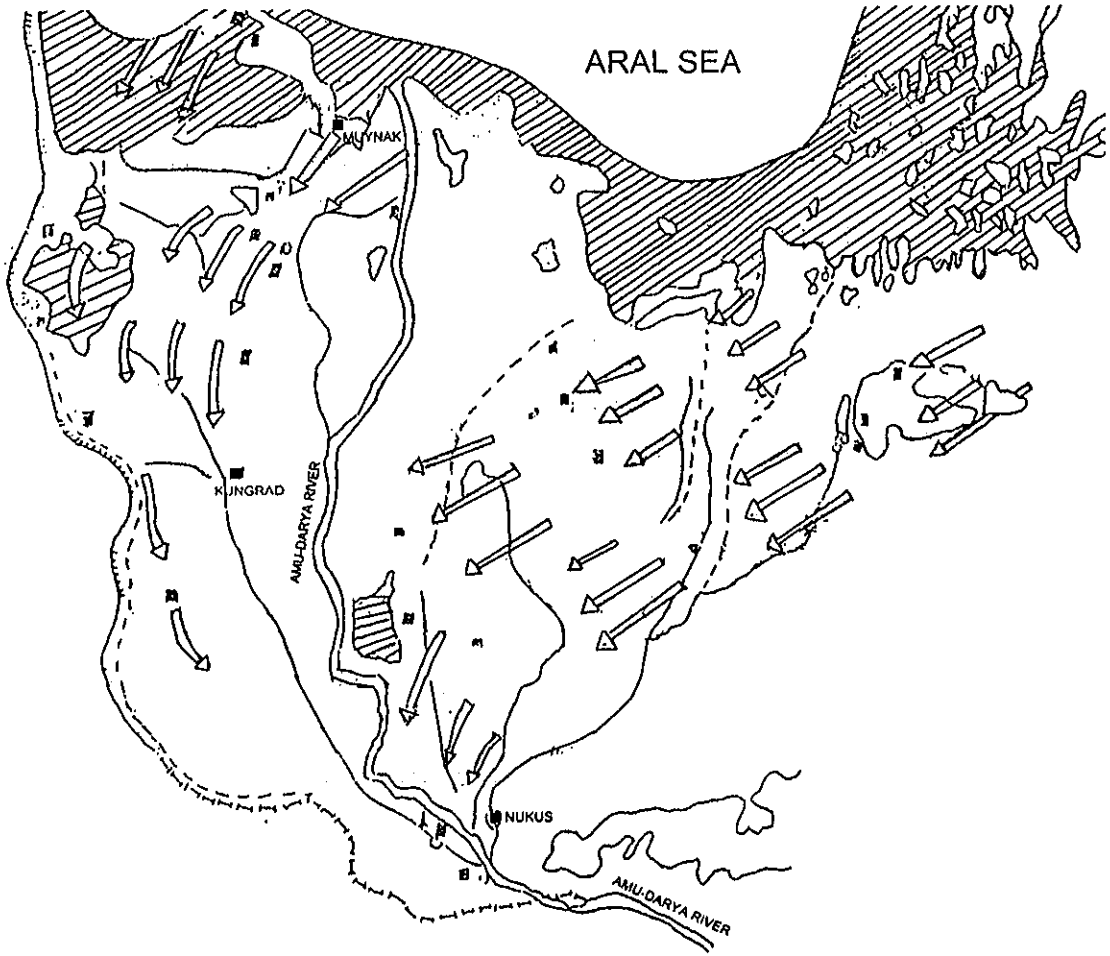
ARAL SEA
MUYNAK
KUNGRAD
AMU-DARYA RIVER
NUKUS
AMU-DARYA RIVER

Fig. 6

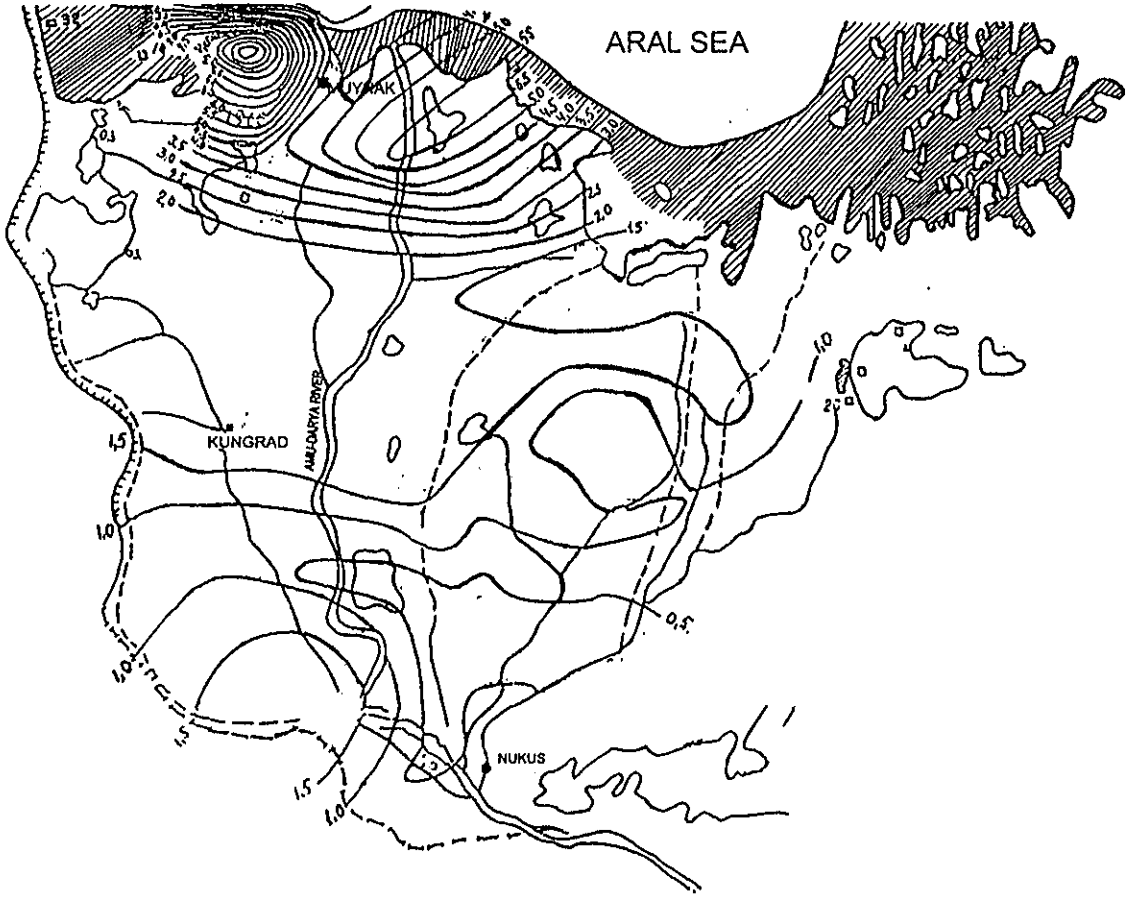

Fig. 7

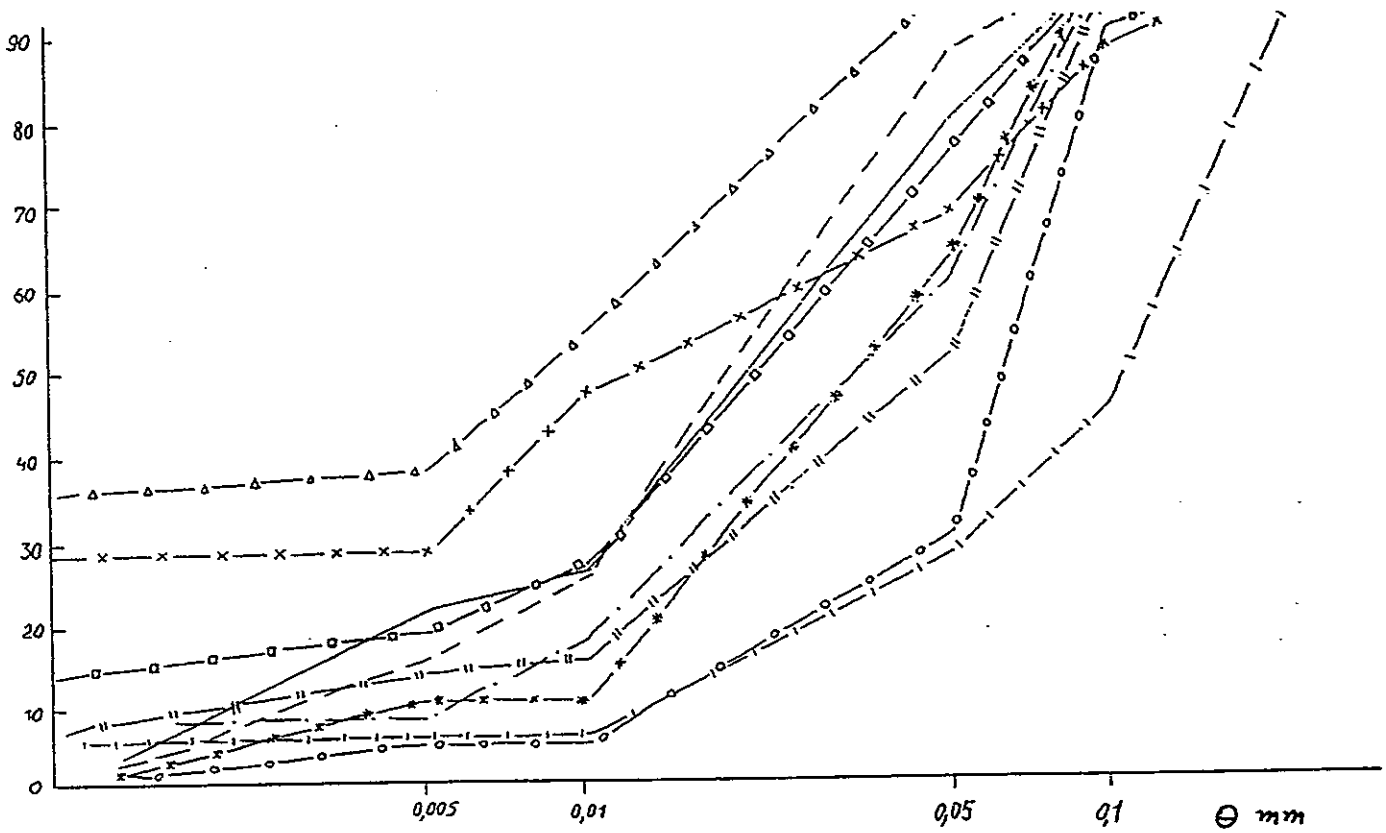

Fig. 8

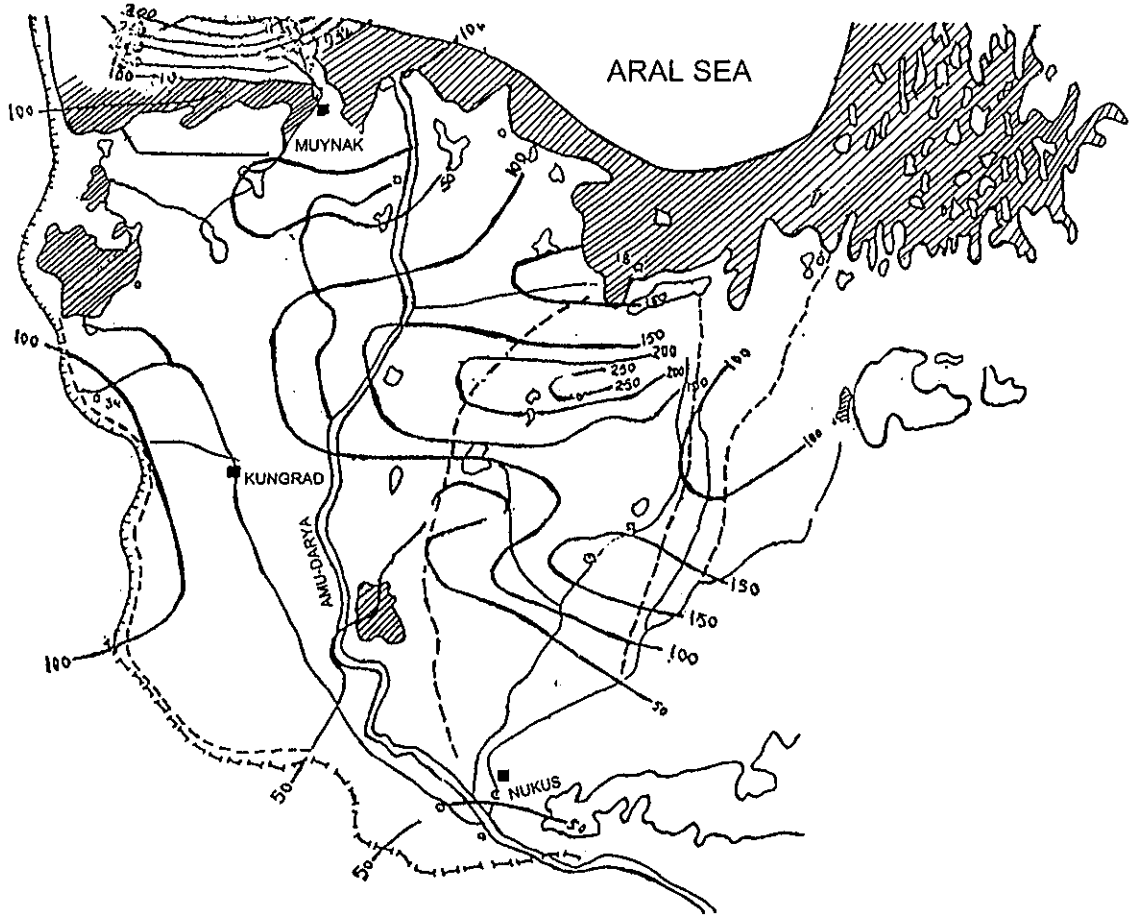

Fig. 9

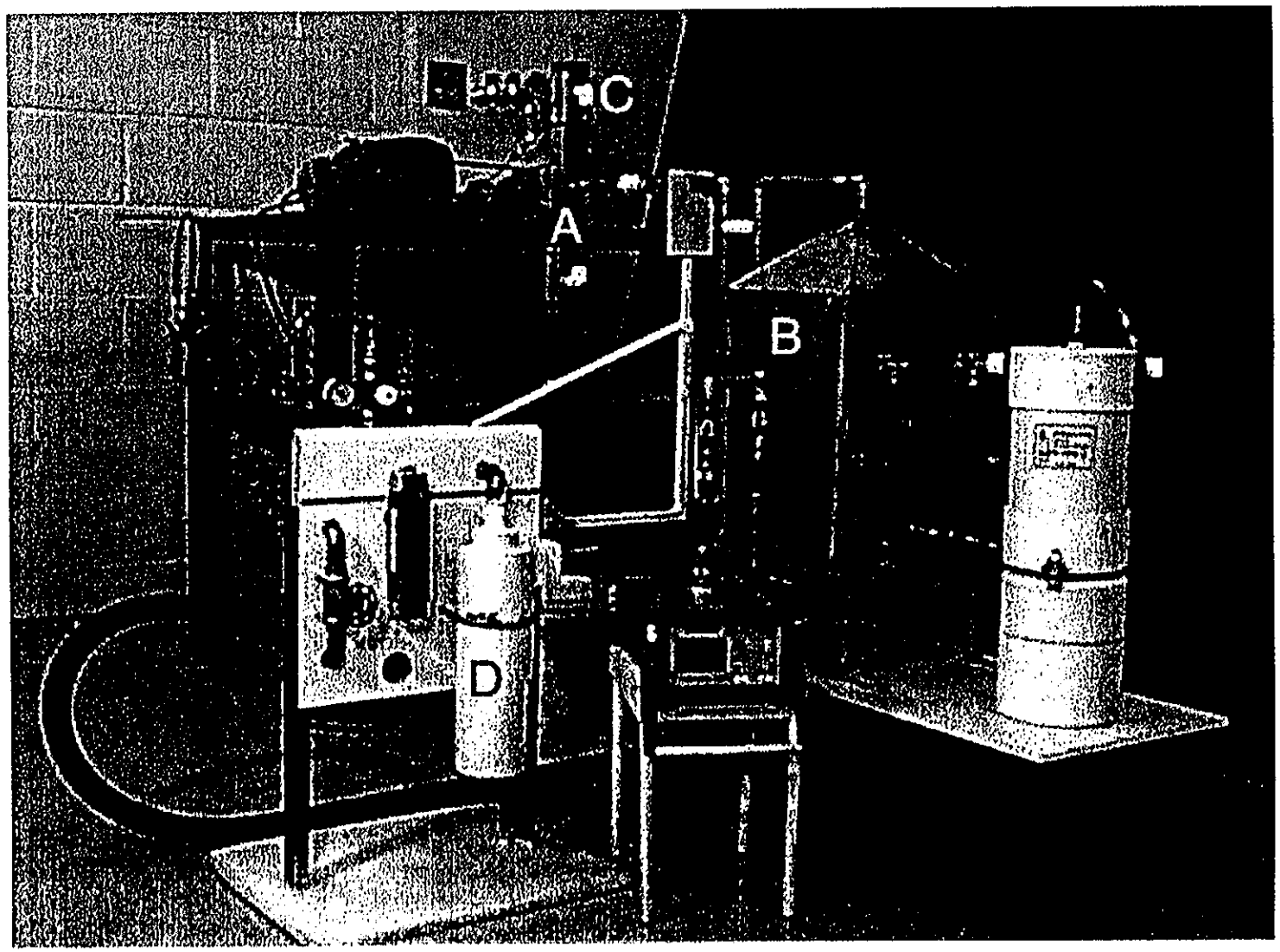

Fig. 10

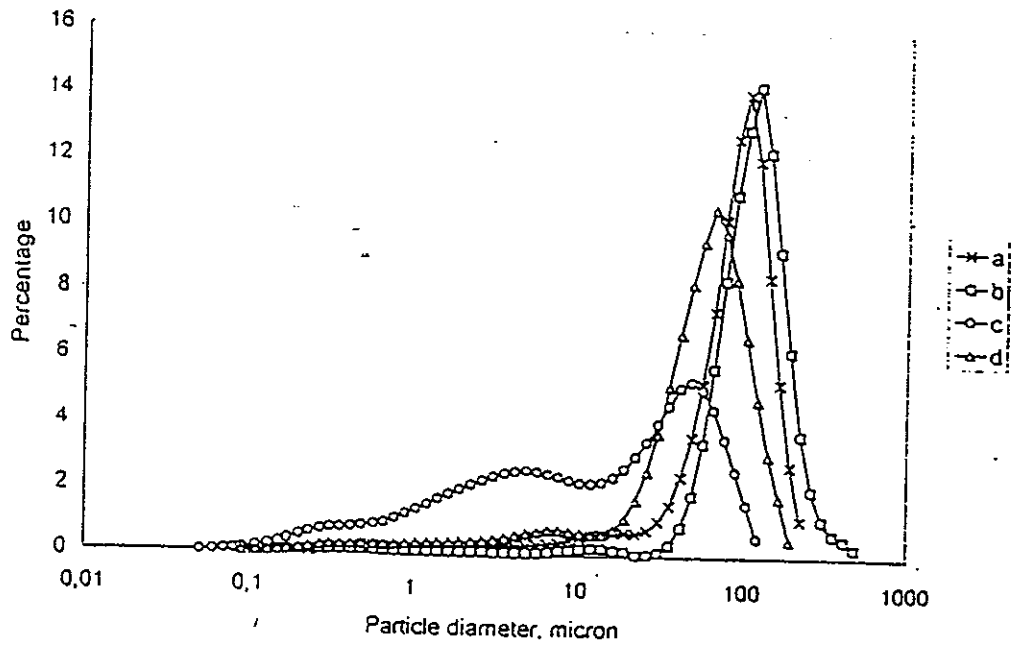

Fig. 11 A

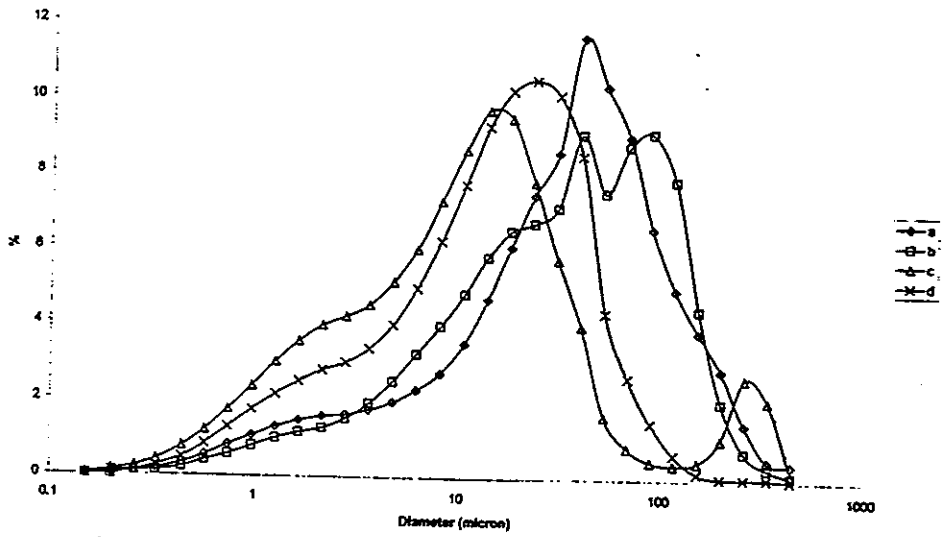

Fig. 11 B

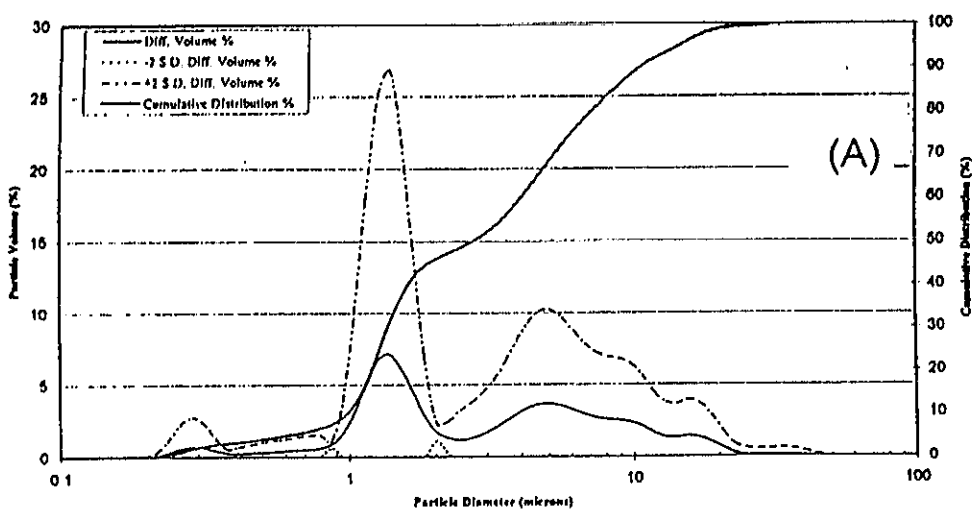
Diff. Volume %
-2 S.D. Diff. Volume %
+2 S.D. Diff. Volume %
Cumulative Distribution %
(A)
Particle Volume (%)
Cumulative Distribution (%)
Particle Diameter (microns)

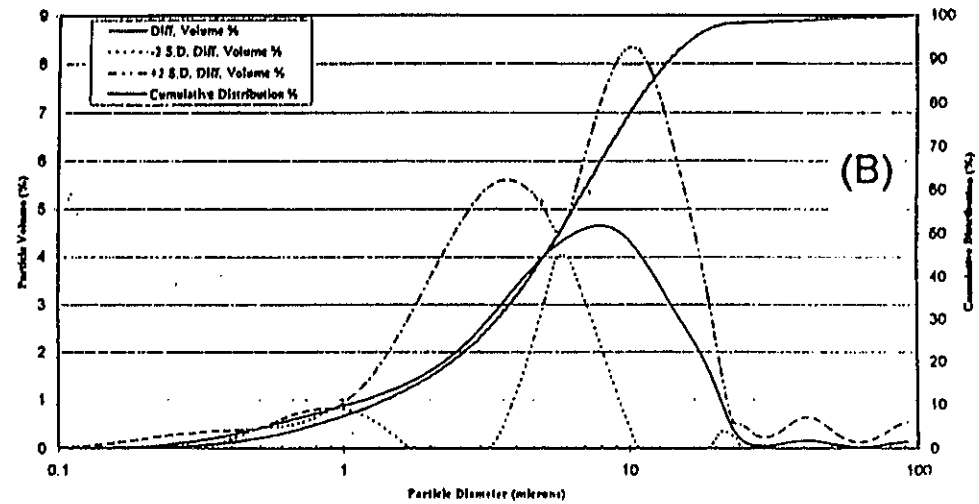
Diff. Volume %
-2 S.D. Diff. Volume %
+2 S.D. Diff. Volume %
Cumulative Distribution %
(B)
Particle Volume (%)
Cumulative Distribution (%)
Particle Diameter (microns)

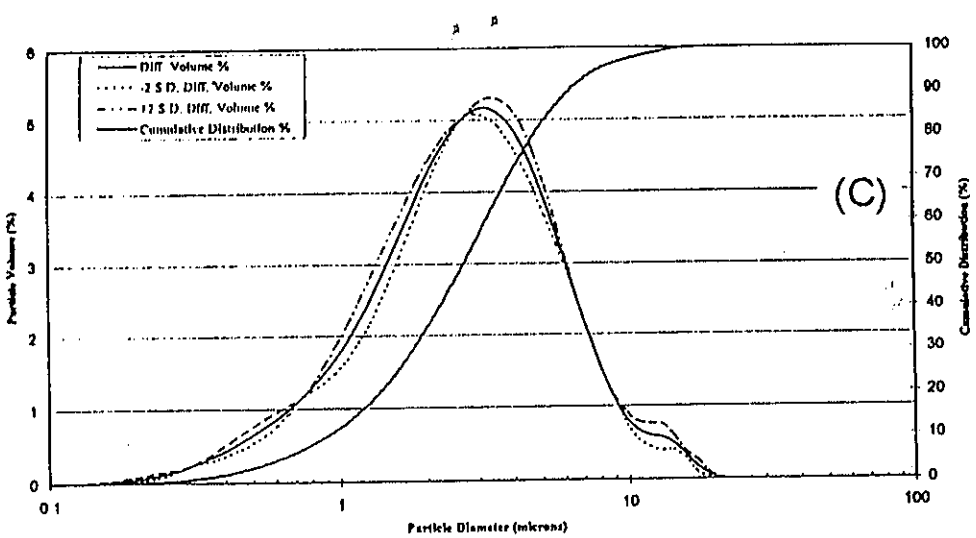
Diff. Volume %
-2 S.D. Diff. Volume %
+2 S.D. Diff. Volume %
Cumulative Distribution %
(C)
Particle Volume (%)
Cumulative Distribution (%)
Particle Diameter (microns)

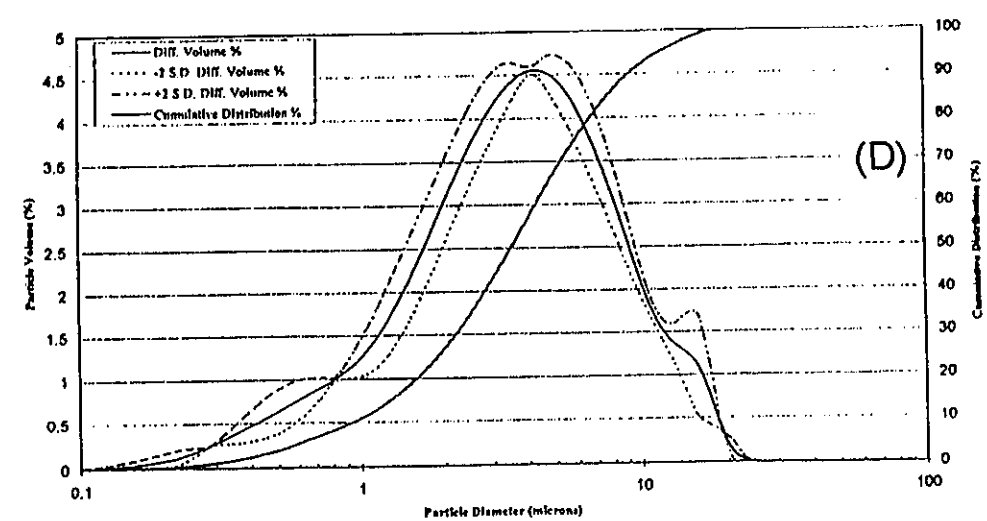
Diff. Volume %
-2 S.D. Diff. Volume %
+2 S.D. Diff. Volume %
Cumulative Distribution %
(D)
Particle Volume (%)
Cumulative Distribution (%)
Particle Diameter (microns)

Fig 17 a.

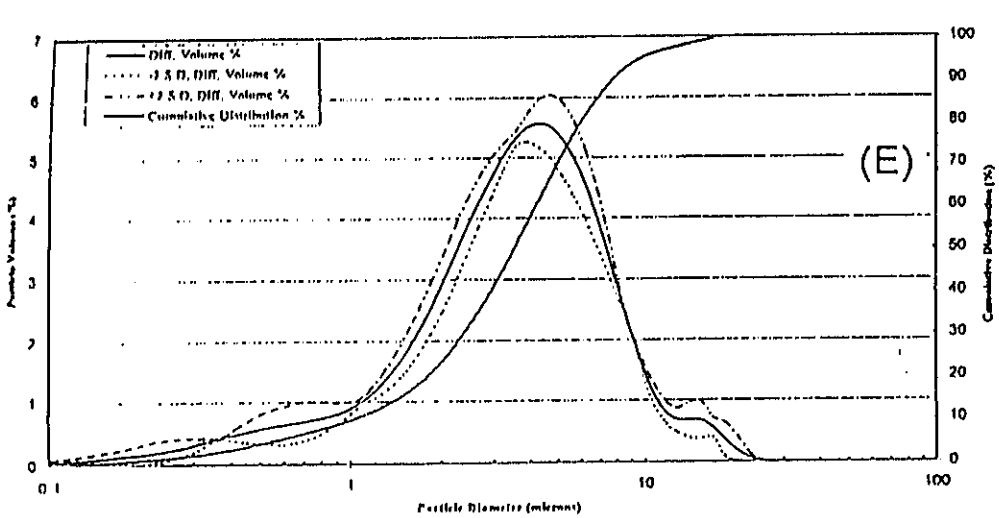
Diff. Volume %
-1 S.D. Diff. Volume %
+1 S.D. Diff. Volume %
Cumulative Distribution %
(E)
Particle Volume (%)
Cumulative Distribution (%)
Particle Diameter (microns)

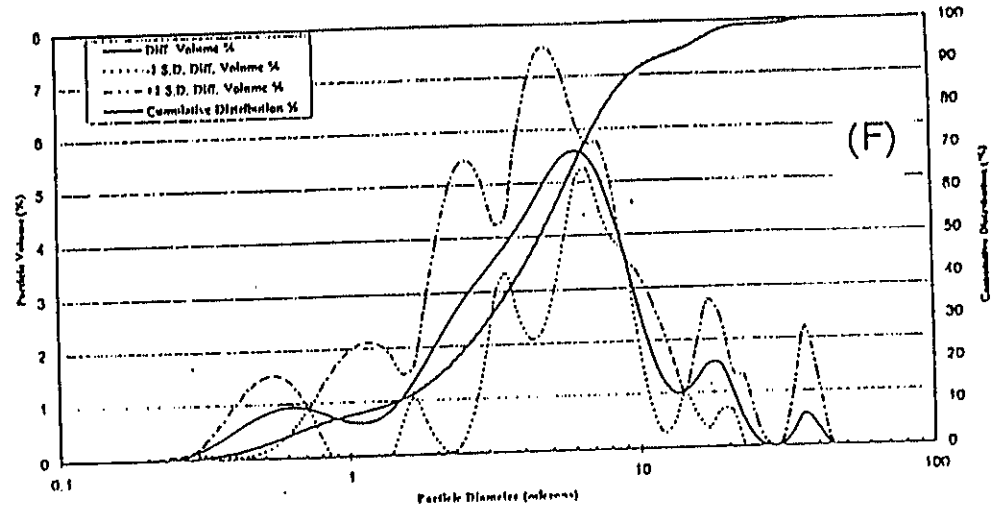
Diff. Volume %
-1 S.D. Diff. Volume %
+1 S.D. Diff. Volume %
Cumulative Distribution %
(F)
Particle Volume (%)
Particle Diameter (microns)

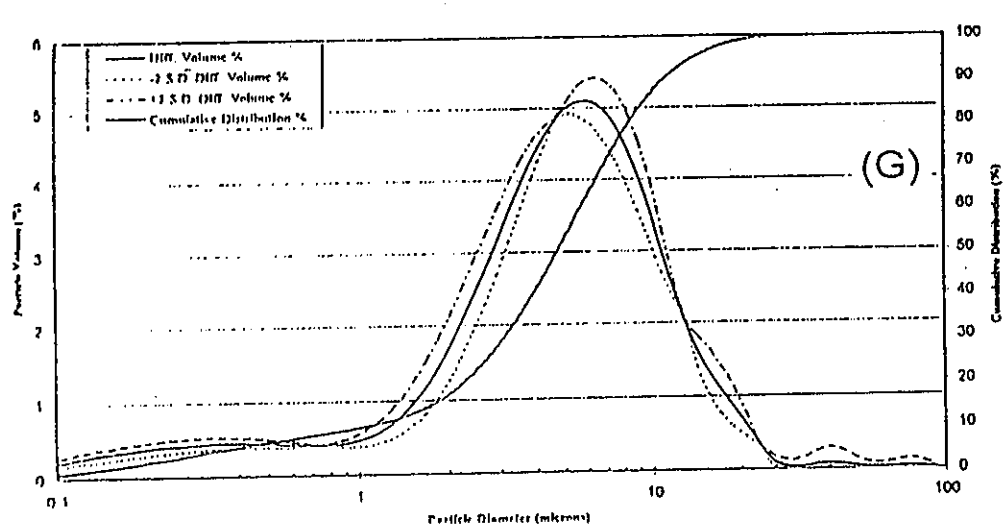
Diff. Volume %
-1 S.D. Diff. Volume %
+1 S.D. Diff. Volume %
Cumulative Distribution %
(G)
Particle Volume (%)
Cumulative Distribution (%)
Particle Diameter (microns)

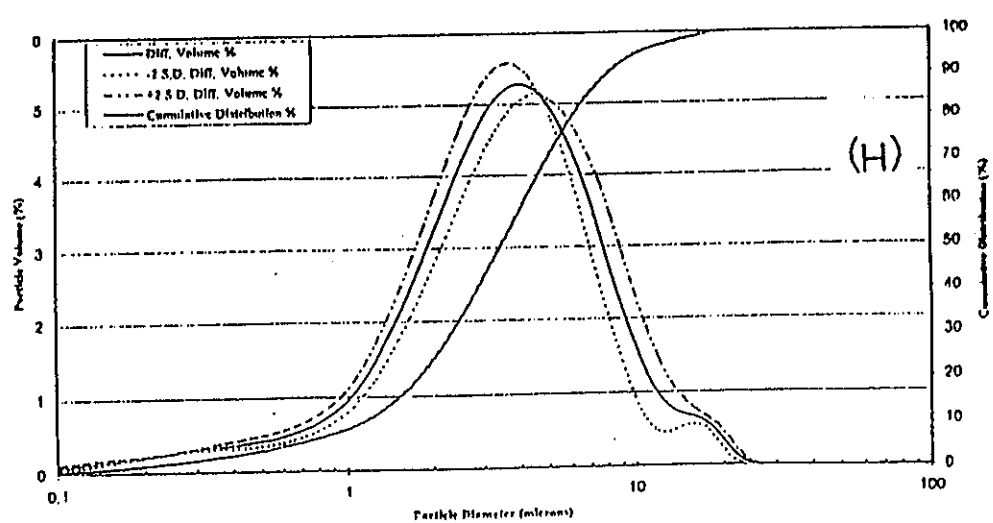
Diff. Volume %
-1 S.D. Diff. Volume %
+1 S.D. Diff. Volume %
Cumulative Distribution %
(H)
Particle Volume (%)
Particle Diameter (microns)

Fig. 12 b

Impact Relevance and Technology Transfer

The findings produced by the project may contribute significantly towards an alleviation of the Aral Sea crisis. This contribution is to be viewed from two different angles: (1) Transfer of knowledge to the Uzbek partner and (2) Analytical results, conducive towards crisis management measures.

(1) Accepting that dust generation, movement and deposition are among the major factors responsible for the crisis, the processing of data relating to the dust problem is of cardinal importance. A major instrument in this processing step is the use of the Geographical Information System (GIS). A wealth of cartographic ground data relating to the Aral Sea Basin have been processed in Rehovot and have been made available to the Uzbek partners institute via an extended traineeship of two Uzbek technicians in Israel, using appropriate software programs. GIS is now routinely used in the partner institute in Tashkent. Technology transfer relating to trapping of dust by high volume impactors, as well as techniques of using wind tunnels for evaluating wind erodibility of soils, has also been exercised vis-à-vis the Uzbek partners. This technique transfer has been made in the course of the frequent visits of the research partners in Israel. Another sphere of technology transfer was with regard to the modeling of dust transfer. The effects of water bodies (one of the contemplated measures to contain dust generation) were examined in Rehovot, using advanced modeling programs. These programs were transferred to Tashkent, together with the required hard and software.

(2) Important analytical results were obtained with regard to the wind erodibility of the Southern Aral Sea Basin soils and sediments. In a collaboration work with the USDA wind erosion laboratory in Lubbock, these soils/sediments were evaluated and graded according to the wind erosion hazards they present. This evaluation potentially will have a great impact on measures planned to be taken in order to decrease erosion and dust generation. Not less important were the results obtained using the wind tunnel. These results suggest that maintaining these surface materials at a high moisture level drastically reduces their erodibility. Similar results can be obtained with commercial soil stabilizers which, however, might economically be irrelevant. For the first time, the stability of salt crusts was determined. It should be stressed that these results are significant not merely for the Aral Sea Basin, but for many other areas in Central Asia, with similar surface materials.

7. Project Activities/Outputs

Meetings attended

Dr. A. Singer, the PI from Israel, attended an international meeting organized by the University of Bielefeld, Germany, in May 1999 on "Sustainable Land Use in Deserts", with the emphasis on the Aral Sea crisis, and presented a paper that was later published by Springer. Dr. Singer also repeatedly lectured in different forums, such as the Weizmann Institute of Science and the A&M University in Texas, on various aspects of the Aral Sea crisis. In July this year, he will deliver a paper on this subject at the 2002 International Conference on Wind Erosion and Aeolian Processes, to be held in Lubbock, Texas.

Dr. I. Mahrer, Co-Investigator from Israel, presented a paper entitled: "Dust propagation following desiccation of the Aral Sea" at the International Workshop on "Mineral Dust" held in Boulder, Colorado during June 1999.

Training

Two technicians from the "Waterproject Institute" in Tashkent trained in Rehovot for 4 weeks during 1998.

Publications

An article, entitled: "Soil crusts in the Amu Darya River delta: properties and formation" was published in 2001 by Springer in the book: "Sustainable Land Use in Deserts" (Breckle, Veste, Wucherer, eds.). A second article, entitled: "The dust generation potential of soils/sediments in the Southern Aral Sea Basin, Uzbekistan" has been accepted for publication in the Journal of Arid Environment.

8. Project Productivity

Not all the project objectives were accomplished. Most notably, no field trials to verify the results obtained experimentally in the wind tunnel in Israel were carried out. Field trials were not carried out because of the logistic difficulties of handling sophisticated equipment in the area. Hygienic conditions on ground are very poor and do not permit extended stays. Unattended equipment will be stolen or vandalized. Trained personnel for the servicing of this equipment is not available in situ. Therefore the rate of mineral matter deflation and deposition could not be assessed, and a salt balance for the region could not be established.

9. Future Work

The results obtained in this project will have to be extended and expanded in order to achieve their full effectiveness towards enhancing management practices aimed at containing the dust generation problem in the Aral Sea Basin and in Central Asia in general. These results can thus be viewed as "seed" data for future work. Emphasis of future work will have to shift to data collection, experimentation and data processing in the affected countries themselves, Uzbekistan, Turkmenistan and Kazahstan.